

Topological walking bipeds with and without cargo

Von der Universität Bayreuth
zur Erlangung des akademischen Grades eines
Doktors der Naturwissenschaften (Dr. rer. nat.)
genehmigte Abhandlung

von

Mahla Mirzaee Kakhki

aus Mashhad

1. Gutachter: Prof. Dr. Thomas Fischer
2. Gutachter: Prof. Dr. Werner Köhler

Tag der Einreichung: 09.11.2020

Tag des Kolloquiums: 08.02.2021

Topological walking bipeds with and without cargo

Von der Universität Bayreuth
zur Erlangung des akademischen Grades eines
Doktors der Naturwissenschaften (Dr. rer. nat.)
genehmigte Abhandlung

von

Mahla Mirzaee Kakhki

aus Mashhad

1. Gutachter: Prof. Dr. Thomas Fischer
2. Gutachter: Prof. Dr. Werner Köhler

Tag der Einreichung: 09.11.2020

Tag des Kolloquiums: 08.02.2021

Abstract

This cumulative thesis is dedicated to the experimental study of the adiabatic and non-adiabatic transport of colloidal bipeds that walk on top of periodic magnetic patterns. It builds on work on the transport of single colloidal particles on top of the same magnetic patterns. Colloidal bipeds are rods self assembled from single colloidal particles. We may theoretically view such bipeds as single particles obtained from a single isotropic colloidal particle by deforming it from the isotropic shape towards the length of the experimental colloidal biped. The rod lengths is a continuous parameter. I address the question how a continuous change of the biped lengths effects the topological nature of the biped transport that occurs if I periodically modulate a homogeneous external magnetic field as a function of time. I will sort bipeds of certain length ranges into different topological classes that are transported differently but commensurate with the period of the magnetic pattern. I will show, how to invert the relation between the external modulation loop and the resulting transport directions. The inversion allows to a priori know the parallel polyglot commands in form of the external field loops given the desired transport directions of the different topological classes of bipeds. I will use the so developed polyglot language to program polymerization addition reactions between bipeds and I will program the simultaneous writing of different letters to form a word. I will extend a gauge theory on transport in low Reynolds number fluids to the situation of bipeds on a pattern and explain what we can learn about the physics of walking bipeds by analyzing their motion in two different gauges. I will explain what happens if we leave the adiabatic regime and how hydrodynamic friction alters the walking character of the bipeds. Finally I will use non-adiabatic modulation to transfer the topological transport from bipeds still able to walk to single colloids that if left separated from the bipeds are no longer able to move.

Kurzdarstellung

Diese kumulative Arbeit widmet sich der experimentellen Untersuchung des adiabatischen und nicht-adiabatischen Transports kolloidaler Zweibeiner, die auf periodischen Magnetmustern laufen. Es baut auf Arbeiten zum Transport einzelner kolloidaler Partikel auf denselben magnetischen Mustern auf. Kolloidale Zweibeiner sind Stäbe, die aus einzelnen kolloidalen Partikeln selbst assembliert sind. Wir können solche Zweibeiner theoretisch als einzelne Partikel betrachten, die aus einem einzelnen isotropen kolloidalen Partikel entstehen, indem wir es von der isotropen Form auf die Länge des experimentellen kolloidalen Zweibeiners strecken. Die Stablänge ist ein kontinuierlicher Parameter. Ich beschäftige mich mit der Frage, wie sich eine kontinuierliche Änderung der Zweibeinerlänge auf die topologische Natur des Zweibeinertransports auswirkt, der auftritt, wenn ich ein homogenes externes Magnetfeld als Funktion der Zeit periodisch moduliere. Ich werde Zweibeiner bestimmter Längenbereiche in verschiedene topologische Klassen sortieren, die unterschiedlich transportiert werden, aber kommensurabel mit der Periode des magnetischen Musters bewegt werden. Ich werde zeigen, wie die Beziehung zwischen der externen Modulationsschleife und den resultierenden Transportrichtungen umgekehrt werden kann. Die Inversion ermöglicht es a priori, die parallelen Polyglot-Befehle in Form der externen Feldschleifen zu kennen, wenn die gewünschten Transportrichtungen der verschiedenen topologischen Klassen von Zweibeinern gegeben sind. Ich werde die so entwickelte polyglotte Sprache verwenden, um Polymerisationsadditionsreaktionen zwischen Zweibeinern zu programmieren, und ich werde das gleichzeitige Schreiben verschiedener Buchstaben programmieren, um ein Wort zu bilden. Ich werde eine Eichtheorie zum Transport in Flüssigkeiten mit niedriger Reynoldszahl auf die Situation von Zweibeinern in einem Muster ausweiten und erklären, was wir über die Physik laufender Zweibeiner lernen können, indem wir ihre Bewegung in zwei verschiedenen Eichungen analysieren. Ich werde erklären, was passiert, wenn wir das adiabatische Regime verlassen und wie hydrodynamische Reibung den Geharakter der Zweibeiner verändert. Schließlich werde ich schnellere nicht-adiabatische Modulationen des externen Magnetfelds verwenden, um den topologischen Transport von Zweibeinern, die noch laufen können, auf einzelne Kolloide zu übertragen, die sich nicht mehr bewegen können, wenn sie von den Zweibeinern getrennt bleiben.

Table of Contents

I	Topological walking bipeds with and without cargo	1
1	Introduction	3
1.1	Walking	3
1.2	Topology	5
1.2.1	Topology in condensed matter	6
1.2.2	Topology and gapped quantum systems	8
1.2.3	Topological insulators	9
1.3	Topology of electronic versus colloidal systems	9
1.3.1	Particle-hole concept against paramagnet-diamagnet concept	10
1.3.2	Crystal electric field against magnetic pattern magnetic field	10
1.3.3	Band structure and dispersion relation against stationary manifold	10
1.3.4	Adiabatic pumping with an electric field against adiabatic pumping with a time dependent external magnetic field	11
1.3.5	Dirac points against gates	11
1.3.6	Virtual states against saddle points	12
1.3.7	Pauli exclusion principle against excluded volume interaction	12
1.3.8	Edge currents against skipping orbits	12
1.3.9	Colloidal bipeds	13
1.4	Gauge theory	14
1.5	Geometry of self-propulsion at low Reynolds number	15
1.6	Parallel computing	17
1.6.1	Polyglots	19
1.7	Hydrodynamic friction, hydrodynamic interactions and dissipation	19
1.7.1	Condensation in active systems	20
1.8	Magnetism and the dipolar interaction	22
1.8.1	Exchange bias films	22
1.8.2	Dipolar interaction	22
2	Materials and Methods	27
2.1	Setup	27
2.2	Elimination of perturbing effects	28
2.2.1	Elimination of non-universal Fourier components of the magnetic field of the pattern	28
2.2.2	Elimination of adhesion	29
2.2.3	Elimination of structural entropy of the initial state	30
2.3	Elimination of errors due to sign conventions	30

II	Publications	35
	Publication 1	
	Simultaneous polydirectional transport of colloidal bipeds	37
	Publication 2	
	Gauge invariant and gauge dependent aspects of topological walking colloidal bipeds	53
	Publication 3	
	Colloidal trains	67
III	Summary	75
3	Summary and Outlook	77
	3.1 Summary	77
IV	References	81

Part I

**Topological walking bipeds
with and without cargo**

Chapter 1

Introduction

1.1 Walking

Walking is an amazingly complex process. My son, Ali, started walking before we came here to Germany. He put forward one foot at a time thereby step by step progressing forward. Starting to walk is a synonym of making progress and I feel very similar to Ali in making my first steps in the realm of colloids during this PhD-thesis. How could I make sufficient progress to accumulating enough insights into colloidal dynamics that would justify me getting a PhD? I try to answer this question by making colloids walk. A colloid is a collective assembly of small often spherical particles and thus their walking is a collective effort. We must assemble them into something that has at least two feet and then we want to simultaneously control the walking of all these different assemblies. Furthermore a walker makes real sense only when carrying something along so we want the walkers to be charged with cargo. I will show in this thesis how to achieve these different goals and understand the underlying physics. In doing so I need to consider a variety of mathematical, computer scientific, and physical issues that might seem quite disconnected from each other and their relevance will become clear only after walking you through those different aspects of colloidal walking.

Ali has two feet, a left one and a right one. They are related to each other by a mirror symmetry and so as like Ali's walking colloidal walking involves a lot of symmetry arguments. An even more important mathematical aspect of colloidal walking arises from the fact that you must walk on something[1]. In my experiments colloidal walkers will walk on a symmetric periodic pattern. The result of a walk is a translation within this periodic pattern, such that mathematically we are interested into the translational group. However, since the pattern is periodic we can reduce the translational group to the quotient group of all translations modulo a lattice translation, which allows us to describe the entire walking process within one unit cell that is connected to itself via the periodic boundary conditions. Such trick renders the unit cell from a topological point of view into a torus, i.e. into a mathematically manifold that is not simply connected. This trick is stolen from solid state physics, where similar tricks[2, 3, 4] have been used to answer such questions as the transport behavior of quantum mechanical electrons in strange new materials such as topological insulators, metals or superconductors. Albeit the electronic transport is quantum mechanical in nature it shares the topological features arising from the periodicity of the lattice with classical systems[5, 6, 7, 8, 9, 10, 11, 12, 13, 14, 15] in

nuclear systems [16] and with our single colloids [17, 18, 19] and our colloidal walkers. It is for this reason that I must talk about topology.

Walking is also a reduced form of swimming and our colloids will of course walk in water, the liquid they are dispersed in. It has been shown by Shapere and Wilczec[20, 21] that the theoretical description of objects that swim in low Reynolds number liquids by periodically changing their shape as a function of time is redundant. There exist many gauges that describe the swimming in an equivalent way. The framework of Shapere and Wilczec's description thus is a gauge theory and involves a gauge potential the integral of which when integrated over a period is a topological invariant. In our experiments the colloids walk because of interactions with the periodic pattern and it will be worthwhile to consider the generalization of Shapere and Wilczec's paper to an object walking on a pattern.

When Ali walks I consider his walking active. The contrary form of motion is that of my fellow student Anna, who introduced me to the Rotmain center shopping mall where we usually take the escalator that passively walks us up to the first floor. The distinction between active and passive motion seems an important one since many recent work[22, 23, 24, 25, 26] is dedicated to active motion and not to passive externally driven motion [27, 28, 29]. As we will show the question whether our colloidal walkers are active or passive has a surprisingly complex answer that is related to questions of topology and to gauge theories.

Our colloidal dispersion is a collective assembly of many particles. The desire to collectively control[1, 30, 31, 32, 33, 34, 35, 36] their walking should seem obvious. Hence we would like to make them collectively walk with one external command but possibly in different ways depending on what is the exact shape of our walker. This brings in the a topic that I must speak about, which is the problem of parallel computation. Parallel computation[37] is a way of simultaneously giving or executing several commands addressed to different parts of a computer program. For this one needs either a hardware or a software where the global command is split in the different subtasks.

Finally we want to charge the walkers with cargo. In order to walk the cargo along with the walker, the walker must interact with its cargo. We will consider quasi-static as well as hydrodynamic interactions between the two that must be used in keeping the cargo on the walker. Since hydrodynamic interactions must be involved our walkers will feel friction and dissipation play a role under such circumstances. The cargo free walking is mainly adiabatic as our driving of the walker is slow. In order to be able to charge the walker with cargo we must leave the realm of adiabatic processes that are merely geometric[38] in nature and that do not depend on the time schedule of how fast or slow we walk. We will have to examine the effect on topologically protected walks when speeding up processes such that dissipation becomes relevant.

In the following sections of chapter 1 I will address those issues in more detail: Section 1.2 is a summary of the topology of surfaces, topological invariants and their relation to differentiable manifolds. In section 1.3 I will compare the topological aspects of colloidal systems with those of topologically non trivial electronic systems. In Section 1.4 I will explain the ideas behind gauge theories and in section 1.5 I will explain how gauge theories are used to describe shape changing swimmers. In Section 1.6 I explain the ideas behind parallel computing and will explain what is a polyglot. In 1.7 I talk about hydrodynamic friction and hydrodynamic interactions as well as about swarm formation of active swimmers. The major quasistatic interactions used are of magnetic nature. Section 1.8 therefore contains the physics of our magnetic patterns and fundamental aspects of dipolar interactions. Chapter 2 contains details of my setup and strategies used to eliminate disturbing physical effects.

Part II of this thesis contains the major results of my experiments that have been published in three papers. Prior to those papers I briefly explain the major question answered by each of the three papers and how this questions rely on the issues discussed in chapter 1. The task of answering those questions have been a collaborative effort and is based on the theoretical footing of my fellow PhD student Adrian Ernst and the experimental footing provided by myself. Prior to each paper I will therefore clearly explain, which tasks of the three papers have been performed by Adrian and which parts have been performed by myself. Finally I summarize the major finding in part III at the end of the thesis.

1.2 Topology

Topology[39] is the mathematical study of the properties that are preserved through deformation, twisting and stretching of objects. Although, we should keep it under our mind that we are not allowed to tear them apart. A sphere can be smoothly deformed into many different shapes, such as the surface of a disk or a bowl. However, a sphere cannot be smoothly deformed into the surface of a doughnut. A sphere and a doughnut are distinguished by an integer topological invariant called the genus, g , which is essentially the number of holes. Since an integer cannot change smoothly, surfaces with different genus into one another and they are topologically distinct. Surfaces that can be deformed into one another are topologically equivalent. If two objects have the same topological properties, they are said to be homeomorphic. There is an important statement about surfaces in differential geometry, known as the Gauss-Bonnet theorem, connecting their geometry in the sense of curvature to their topology in the sense of the Euler characteristic. Firstly, consider a two-dimensional surface, at any point on the surface, there are two radii of curvature r_1 and r_2 . We define Gaussian curvature as,

$$\kappa = \frac{1}{r_1 r_2} \tag{1.1}$$

Most topological invariants in physics arise as integrals of some geometric quantity. This theorem states that the integral of the Gaussian curvature κ over a surface defines an integer topological invariant called the Euler characteristic

$$\chi = \frac{1}{2\pi} \int_S \kappa(\mathbf{r}) d^2 A = 2 - 2g \quad (1.2)$$

More generally, the Euler characteristic is quantized ($\chi \in 2\mathbb{Z}$) and related to the genus by,

$$\chi = 2 - 2g \quad (1.3)$$

In closed surfaces like what we have in Fig. 1.1. The area integral of the curvature over the whole surface is quantized and it is a topological invariant. Where the genus for sphere is zero $g = 0$, for the torus the genus is one $g = 1$, for the n -holed torus is the genus is n ($g = n$).

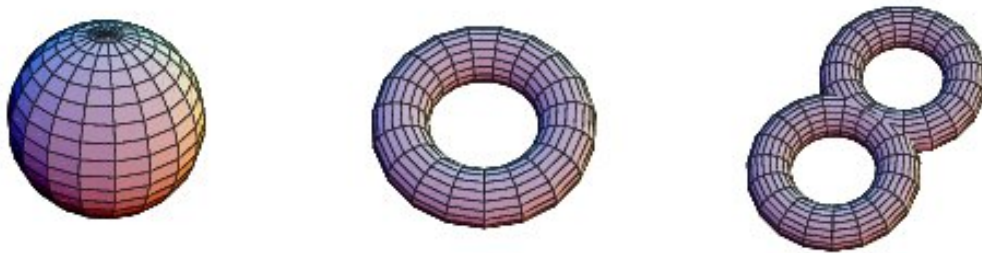


Figure 1.1: A sphere of genus $g = 0$, a torus of genus $g = 1$, and a 2-holed torus of genus $g = 2$

It can easily be checked that $\chi = 2$ for a sphere of radius R , where $\kappa = 1/R^2$. Topology can be used to abstract the inherent connectivity of objects while ignoring their detailed form. For example, the Fig. 1.2 illustrates the connectivity of a number of topologically distinct surfaces. In Fig. 1.2, parallel edges drawn as arrows of the same color join one another with the orientation indicated by the arrows, so corners labeled with the same letter correspond to the same point, and rigged lines show edges that remain free. The surfaces correspond to the disk, the Klein bottle, the Möbius strip, the tube, the sphere, and the torus.

1.2.1 Topology in condensed matter

The whole theory of solid state physics is based on a foundation of quantum mechanics since electrons behave in a manner that is more wave-like than particle-like. One of the

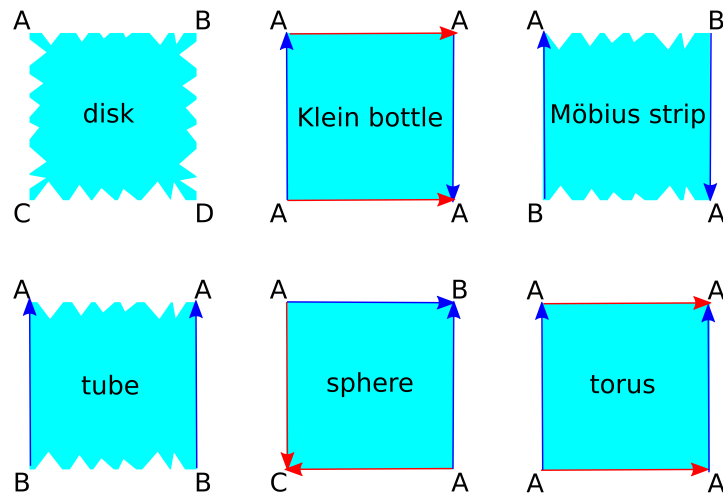


Figure 1.2: Various topologically distinct surfaces. Vertices labeled with the same letter and edges with arrows with the same color are identified with each other. Rigged edges are boundaries of the surface. The Klein bottle, the sphere and the torus are closed surfaces without boundary.

great achievements within condensed matter physics during the 20th century was the formulation of the band theory of solids. This progress gives a more detailed insight into the origin of macroscopically observable material properties. We need to understand the role of topology in the transport of magnetic soft matter systems. The electronic transport properties result in three main categories; metals, semiconductors and insulators. electronic bands are filled up to the Fermi energy ϵ_F . In conductors the Fermi energy falls within an energy band such that only a small amount of energy is needed in order to excite one of the most energetic electrons into a higher energy state. For insulators and semiconductors, on the other hand, the Fermi energy falls into an energy gap between filled and empty states which is so large that it requires a substantial amount of energy to excite an electron across the band gap. In semiconductors the energy gap is smaller than in the insulators and semiconductors have an intrinsic conductivity in between an insulator and a conductor. Fig. 1.3 shows the Fermi energy and band structure of the insulator diamond, the metal aluminum, and the semiconductor silicon.

Band theory derives these bands and band gaps by examining the allowed quantum mechanical wave functions for an electron in a large, periodic lattice of atoms or molecules. The single-electron Schrödinger equation is solved for an electron in a lattice-periodic potential, giving Bloch waves as solutions:

$$\psi_{n,\mathbf{k}} = e^{i\mathbf{k}\cdot\mathbf{r}} u_{n,\mathbf{k}}(\mathbf{r}) \quad (1.4)$$

where \mathbf{k} is called the wavevector. For each value of \mathbf{k} , there are multiple solutions to the Schrödinger equation labelled by n , the band index, which simply numbers the energy

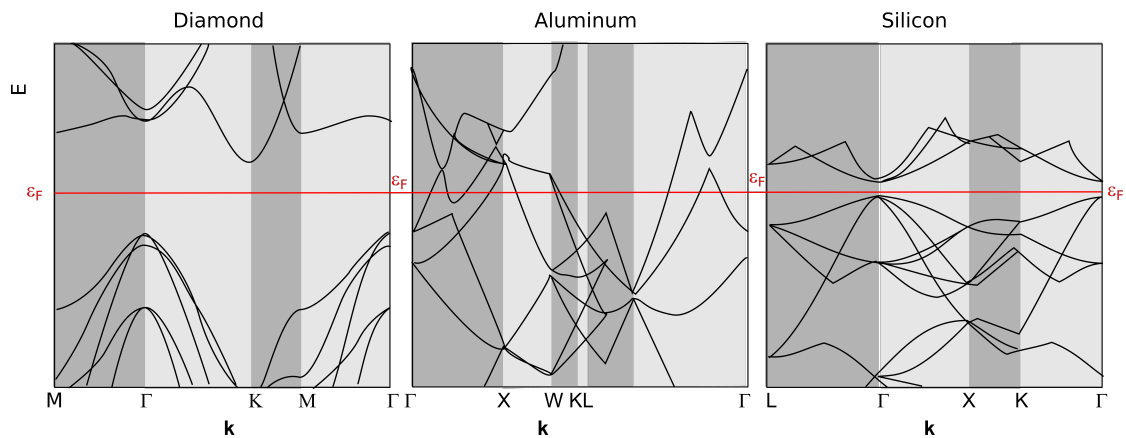


Figure 1.3: Fermi energy and bandstructure of the insulator diamond, the metal aluminum, and the semiconductor silicon

bands. Each of these energy levels evolves smoothly with changes in \mathbf{k} , forming a smooth band of states. For each band we can define a function $E_n(\mathbf{k})$, which is the dispersion relation for electrons in that band.

1.2.2 Topology and gapped quantum systems

I have mentioned before that a different classification scheme has been developed which identifies the topological order of a material. The concept of topology, in the context of band structure, can at first glance appear rather abstract. However, the fact is that studies of band structures enable the identification of topological invariants, quantities or properties which are shared by different objects within the same topological phase but distinct from that of objects belonging to another phase. In geometry, this can more easily be understood since topology here deals with the actual shape of an object. As we said before a sphere is topologically different from a torus since the torus has a hole in it while the sphere does not. The topological invariant in this case is its genus that is the number of holes in the object.

When studying the configuration and appearance of the band structure of materials one is tempted to make a topological distinction between materials based on the presence or absence of an energy gap in the band structure. We can simply observe this issue in figure 1.3.

A question arising in this context is then; are all materials in which there is a finite band gap for example insulators and semiconductors, topologically equivalent? Likewise in condensed matter physics we can also ask whether the Hamiltonians of two quantum systems can be continuously transformed into each other. If that is the case, then we can

say that two systems are topologically equivalent. If the answer is yes, then one would be able to transform the band structure of any material within this class into any of the other in a smooth and continuous changing of material parameters without closing the energy gap. If we considered all Hamiltonians without any constraint, every Hamiltonian could be continuously deformed into every other Hamiltonian, and all quantum systems would be topologically equivalent. This changes drastically if we restrict ourselves to systems with an energy gap. This means that there is a finite energy cost to excite the system above its ground state. If an energy gap is present, then the Hamiltonian of the system has no eigenvalues in a finite interval around zero energy. We can now use the following criterion: we say that two gapped quantum systems are topologically equivalent if their Hamiltonians can be continuously deformed into each other without ever closing the energy gap[4]. If two Hamiltonians have a different topological invariant, they must be separated by such a transition. In other words, it is impossible to go from one to the other without closing the gap.

1.2.3 Topological insulators

In recent years, the study of band structure topology has gained popularity after the discovery of materials which at first glance appear to be traditional band insulators but when examined more closely turn out to be of a topologically different character. For these materials, a simple, continuous deformation of the band structure does not influence the topological invariants and therefore cannot change the band structure into that of a trivial insulator. Due to the resemblance with the normal insulators on one hand but the topological difference on the other, these materials are called topological insulators[3, 4].

1.3 Topology of electronic versus colloidal systems

As previously stated, topology plays a crucial role in electronic systems protecting the transport of charge and spin against dissipative scattering which in topologically trivial systems usually destroys the transport. In recent work we have shown that similar but not identical, behavior can be found in soft matter systems, where driven magnetic colloids replace the electrons and periodic magnetic patterns replace the background solid state. Due to the mesoscopic size of the transported objects the system can be treated by classical instead of quantum physics. If we have a closer look we have all the credible data to compare our colloidal system with the electronic solid state system. In the following we summarize some principle aspects of our comparison.

1.3.1 Particle-hole concept against paramagnet-diamagnet concept

If an electronic state below the Fermi energy is not occupied, we call it a hole, while an occupied state above the Fermi energy is called an electron. A hole is the anti-particle of the electron and they can neutralize each other by emitting the excitation energy of the electron-hole pair in form of other particles. In our system sometimes we can put paramagnetic and diamagnetic colloids on our pattern that exhibit magnetic moments in opposite direction when they are exposed to magnetic field. When the magnetic moments of both colloids have the same magnitude but opposite sign, the energy in a magnetic field shows a particle-hole behavior[17]. Collision of a paramagnetic colloid with a diamagnetic colloid leads to a compound colloidal particle having no magnetic moment.

1.3.2 Crystal electric field against magnetic pattern magnetic field

The behavior of electrons and holes and their dispersion relation is a result of the interaction of free electrons with the crystal electric field from the atomic lattice and the core electrons. The behavior of paramagnetic and diamagnetic colloids and their energy results from the interaction with the magnetic field of the crystalline magnetic pattern and the homogeneous external field.

1.3.3 Band structure and dispersion relation against stationary manifold

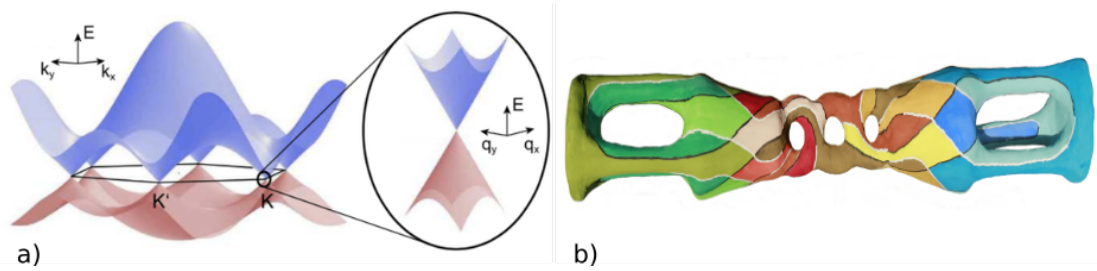


Figure 1.4: Dispersion relation of electrons in graphene. b) Stationary manifold in phase space for magnetic colloids on a six-fold symmetric lattice.

In Fig. 1.4 we have the stationary manifold which describes the set of stationary points in phase space which is the product space $\mathcal{C} \otimes \mathcal{A}$ of action space \mathcal{A} (the two dimensional set of positions of the colloids above our pattern and control space \mathcal{C} (the set of possible orientations of our external magnetic field). We can compare it to the dispersion relation (Fig. 1.4a) which describes the set of stationary electronic states in the Brillouin zone. But only part of the stationary manifold corresponds to stable states in action space which in those area, the potential is minimum and they are demonstrated by green and

blue regions. Saddle points which are brown and red in Fig. 1.4b are unstable, and they intervene between the paramagnetic (green) and diamagnetic (blue) equilibrium states on the stationary manifold. These saddle points can be viewed as dissipative electronic states (with complex energy) in the gap.

1.3.4 Adiabatic pumping with an electric field against adiabatic pumping with a time dependent external magnetic field

When electrons are driven by an external electric field in a conductor, they adiabatically move through the Brillouin zone along the Fermi surface on a path perpendicular to the magnetic field. During this process they acquire a geometric phase. A non-zero geometric phase corresponds to nontrivial electronic transport that changes the charge at the edge of the lattice. When colloids are driven by a modulation loop of the external field they wind around the holes of the stationary manifold. The holes in the stationary manifold are inherited from the direct lattice that topologically is a torus. A full winding around a hole is a nontrivial geometric phase and results in an increase of the magnetic moment at the edge of the lattice.

1.3.5 Dirac points against gates

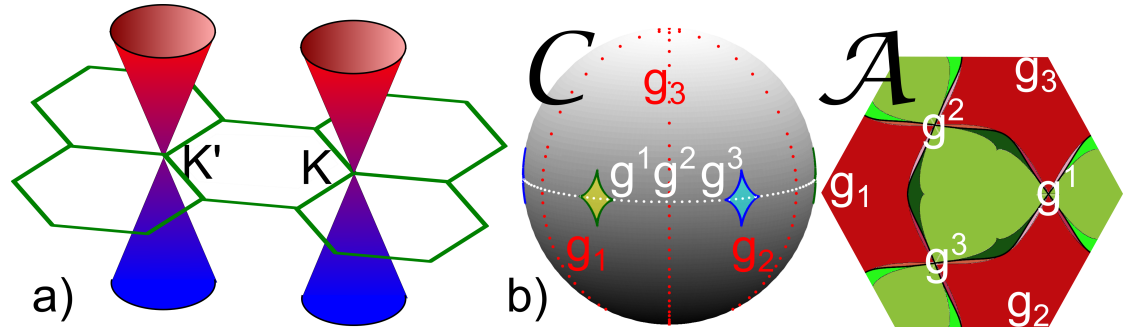


Figure 1.5: a) Dirac cones in the dispersion relation of electrons in graphene. b) Gates in control and action space

If we attach the electronic wave function to the Brillouin zone the result is mathematically a vector bundle. The projection from the vector bundle onto the Brillouin zone is a mapping that removes the vector from the bundle. There are special points in the Brillouin zone where the preimage of this projection is not a point but a higher dimensional object. These points are called Dirac points (Fig. 1.5 a). The stationary manifold (1.4 b) is an object in phase space that is the product space $\mathcal{C} \otimes \mathcal{A}$ of action space and control space. The projection from phase space into action space (Fig. 1.5b right) is obtained by removing the external magnetic field from the point of phase space[19]. There are special

points in action space where the preimage of this projection on the stationary manifold is not a point but a closed line. These points are called the gates, the analogue of Dirac points.

1.3.6 Virtual states against saddle points

We can try to excite a bulk state at a particular point in the Brillouin zone with an energy in the gap. Such a state is not a stationary state because it is not on the dispersion relation, but it is a virtual state that has a specific life time. We can also try to excite a long-lived state in the gap with a fixed real energy. The analogues of virtual states in our system are the saddle points of the stationary manifold. We have shown that saddle points in the vicinity of stable stationary points are important in driven dissipative systems, because they are the starting points for ratchet jumps [40, 41, 42, 43].

1.3.7 Pauli exclusion principle against excluded volume interaction

The Pauli exclusion principle is the quantum mechanical principle which states that two or more identical fermions cannot occupy the same quantum state within a quantum system simultaneously. The quantum nature of an electronic system is mostly due to the Pauli exclusion principle that causes the states at the Fermi energy to be the only ones being able to be driven out of equilibrium and to participate in the adiabatic pumping processes. The analogue of the Pauli exclusion principle is the excluded volume interaction[44] of the colloids which prevents two colloids from overlapping. In the colloidal system on a magnetic lattice. Colloids fill up the magnetic potential valley until the excluded volume potential energy level (Fig. 1.6 a). Only colloids sitting at the excluded volume potential energy level participate in the driven colloidal transport.

1.3.8 Edge currents against skipping orbits

When the topological invariants of the conduction and valence band of a two-dimensional topological insulator differ, there are non-trivial topological edge states that span the gap, allowing for Fermi arc at the edge even though there is no Fermi arc in the bulk. The edge states[45] on these edge Fermi arcs are chiral and convert into open skipping orbits in an external magnetic field in the semi classical limit (Fig. 1.7 B). Bulk states, on the contrary, are closed cyclotron orbits. My predecessor in Thomas' group Johannes Löhr has shown that similar skipping orbits occur at the edges between two magnetic patterns in our colloidal system when the modulation loop induces closed orbits in the bulk (Fig. 1.7 A) [46, 47].

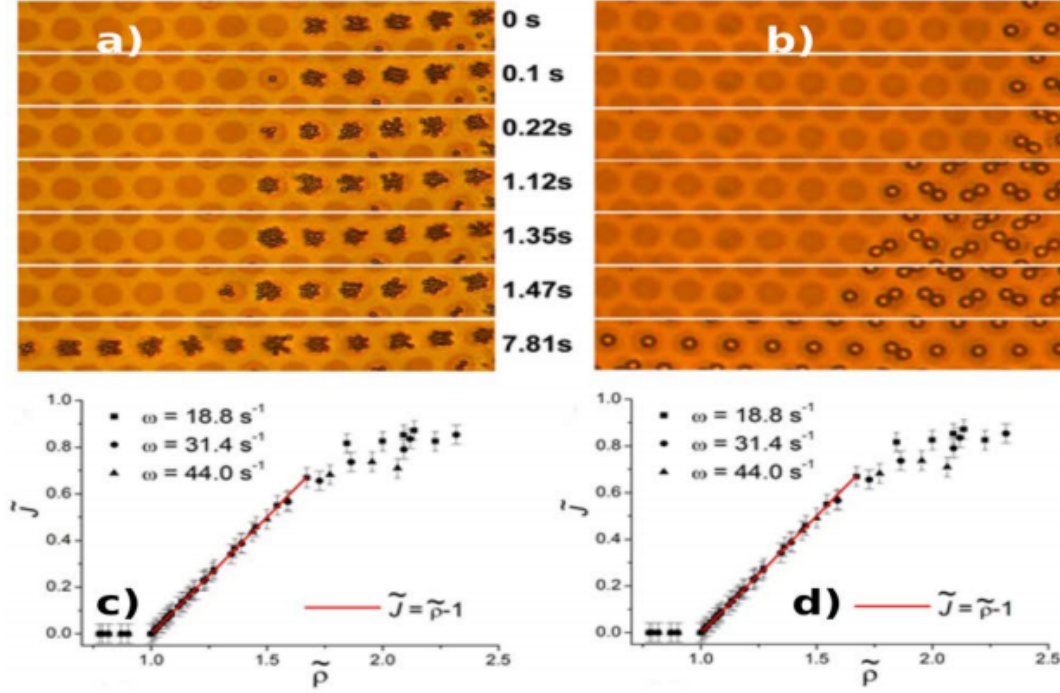


Figure 1.6: a) Microscope image sequence of the transport of 1 μm paramagnetic beads on a garnet film. b) Microscope image sequence of the transport of 2.8 μm paramagnetic beads on a garnet film. Panels c) and d) show the reduced current as a function of the reduced density for the beads in a) and b)

According to previous arguments, we understand the accuracy of resemblance between electronic systems and mentioned colloidal system. Also in the electronic system we have three properties a particle carries: the mass, the charge, and the spin of an electron. We, therefore, may define a mass current, an electronic current and a spin current. In our colloidal system, the colloidal particle has a mass and a magnetic susceptibility. We, therefore, have a mass or particle current and a susceptibility current. We can treat the colloidal particle current as the analogue of the electric current.

1.3.9 Colloidal bipeds

I have shown that there are many similarities between electronic systems and the behavior of single paramagnetic colloidal particles. It is well known that dipolar interactions between paramagnetic particles can lead to the formation of colloidal chains along the external magnetic field. I will explain dipolar interactions in more detail in section 1.13. If dipolar interactions are strong the number of colloidal particles within a chain remains conserved and we can treat the chains as a new form of quasi particle, a colloidal biped,

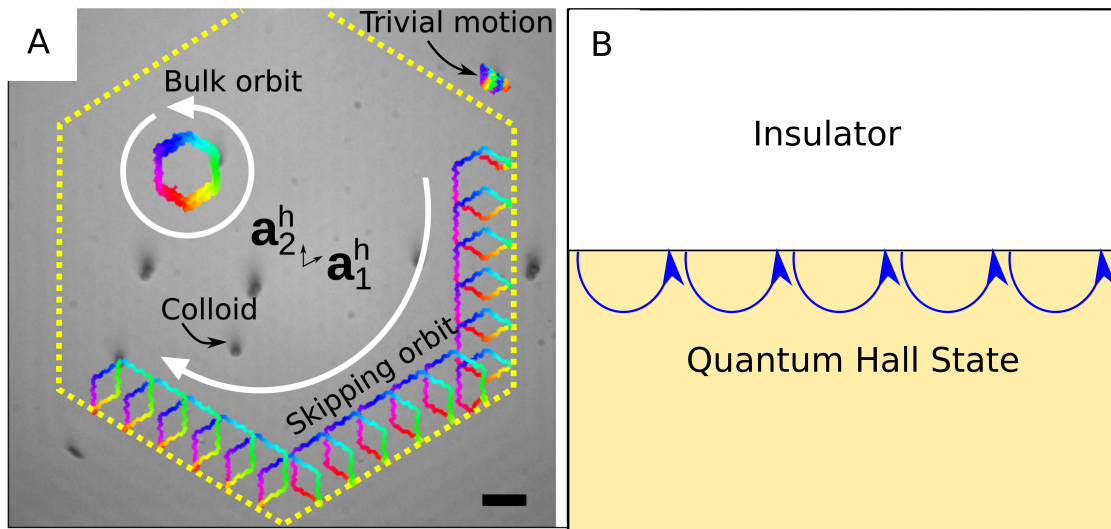


Figure 1.7: A) Microscope image of bulk, trivial, and edge (skipping orbits) trajectories of colloidal particles on a pattern consisting of a hexagonal lattice bounded by magnetic stripes B) At the edge between a trivial insulator and a quantum Hall state have to be topological protected edge states

for which due to its anisotropy the orientation of the particle becomes a new important variable. How the amount of anisotropy changes the transport behavior might be an interesting question. To study bipeds instead of single colloids leads us past what is known from the electronic system. Maybe we can find new insights that in return might be useful for the electronic analogue. The fractional quantum Hall effect and a plethora of new electronic effects are often explained using composite fermions that are electrons dressed with flux quanta. If those composite particles were anisotropic they might exhibit some of the effects shown for colloidal bipeds discussed in this thesis. If such analogies are not sufficient to catch your interest I hope the effects discussed in part II of this thesis will.

1.4 Gauge theory

The word gauge itself has a meaning of measurement. Modern theories describe physical forces in terms of fields, such as the electromagnetic field and a general feature of this kind of field theory is that the fundamental field cannot be directly measured. But as we can see, different configurations of the unobservable fields can result in identical observable quantities so they come to help us. A transformation from one such field configuration to another is called a gauge transformation and the lack of change in the measurable quantities, despite the field being transformed, is a property called gauge invariance.

For example no matter which velocity you have on the autobahn you can only drive from A to B, so the property of "velocity" would show gauge invariance. Generally, any theory that has the property of gauge invariance is considered a gauge theory. In general, this transformation will make a problem easier to solve as long as the transformation produces a result that is physically meaningful.

In general, a gauge transformation will make a problem easier to solve by exploiting symmetries in a physical system. For example, gravitational potential energy became simpler to solve mathematically. We have made transformations by adding a constant to the potential. This has allowed us to preserve the forces on a system,

$$F = \nabla(\phi) \tag{1.5}$$

We can transform ϕ by adding a constant C :

$$\phi' = \phi + C \tag{1.6}$$

$$F = -\nabla(\phi') = -\nabla(\phi + C) = \nabla(\phi) \tag{1.7}$$

And the force is conserved. However, this may not be the case in more advanced physics.

In this thesis we also use the meaning of gauge invariance. We will see that some problems have degrees of freedom that will allow us to manipulate the problem as long as we apply transformations.

1.5 Geometry of self-propulsion at low Reynolds number

A highly influential paper of Shapere and Wilczek[20] reports how the self propulsion of a periodically shape changing object within a viscous liquid in terms of a gauge theory occurs. The characteristic feature of a gauge theory is its gauge freedom. So there can be many possible choices of gauges that equally well describe the final result of the periodic change of shape. From the mathematics point of view the gauge freedom in the shape changing swimmer arises from what is called an equivalence relation, also the equivalence relation itself emerges from the idea of having the same shape. There are two different objects, if one applies rotation and translation operation on each of two different objects an they coincide with each other, they have the same shape. The task for a periodic shape changing swimmer is: given the sequence of shapes of the self propelling objects, find the

translation rotation operation that describes the shape of the object including the proper position and orientation. Due to the fact of not knowing the prior object's position and orientation we might choose for each time a reference position and orientation from the set of objects having the known shape at the time. This choice correlate with our choice of the gauge. Because of the periodicity of the shape change we will eventually return to the same initial shape. At this point we encounter the problem that for the reference shape it makes sense to also let our reference position and orientation return to its initial values. The absolute position and orientation, however, do not return to their initial values if our shape changer is a true self propelling swimmer. Indeed the difference of the final and initial position of the swimmer is exactly what we wish to compute. In the gauge theory the integral over all the changes in positions along the path of different shapes is the translation of our swimmer over one period. There is only one translation of our swimmer over a period and thus this integral cannot depend on the choice of gauge. It is a topological invariant of the loop taken in shape space independent of how we choose the connection of reference positions and orientations. One should make a choice of gauge freedom wisely in a physical manner, to be specific, the best way is to observe the symmetries if exist and select the reference positions and orientations that benefits us in solving the physical problem.

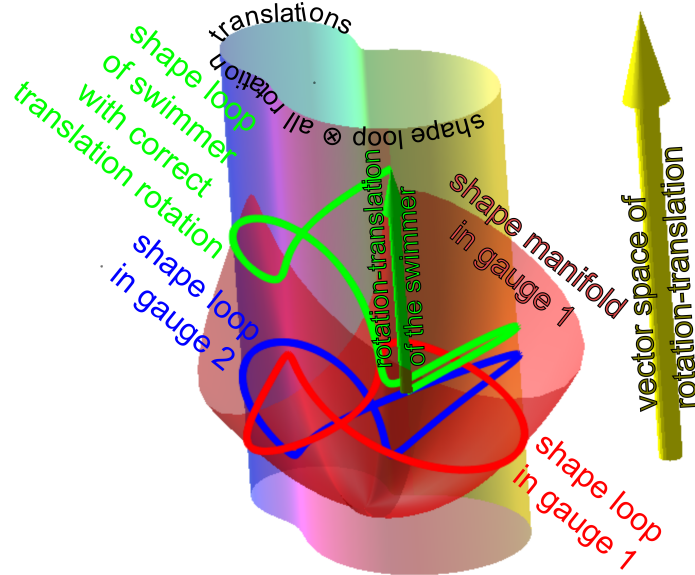


Figure 1.8: Scheme explaining the swimming of a shape changing swimmer within the gauge theory of Shapere and Wilczec[20] .

We explain the gauge theory of swimming of Shapere and Wilczec in Fig. 1.8. The set of shapes in any gauge forms a differentiable manifold. In Fig. 1.8 this manifold is depicted schematically with the red surface. The red loop is the description of the shapes the object cycles through within this choice of gauge. If we take the outer product of this loop with all translation-rotations we obtain the manifold of all possible shapes

including their position and orientation our swimmer has to loop around. The true translation-orientations of the swimmer form the non closed green curve that however starts and ends at the same shape. Both shapes with their translation-rotations are connected by the green arrow, which is a pure translation-rotation without shape change that describes the progression of the swimmer over a period. The blue loop is a different reference loop with a different gauge and different shape manifold (not shown) that would have worked equally well to describe the swimming.

The concept introduced by Shapere and Wilczek of course can be generalized to objects transported in a viscous liquid above a pattern, which changes the liquid into a space with periodic properties as a function of position and orientation. What was true for the shape changing swimmers remains true for colloidal bipeds above a pattern. The choice of gauge freedom should be used by respecting symmetries and choosing the reference position points and orientations that rule the physics of our colloidal walkers. We will describe in section 1.7 which choices of gauge best reveal the behavior of walking bipeds.

1.6 Parallel computing

What if it was possible to say one word and each person can interpret a different meaning from that. Imagine someone named Thomas comes and he would say "Do Magic" phrase to people working in a laboratory. There are three persons who listens to him. As a result of that phrase, one immediately goes and observes colloids on the pattern, the other one at the same time goes and simulates a program and the third person goes immediately in the lab to fix the magnetic coils. Therefore, all the three simultaneously doing something seems to be unrelated but the same intention in their minds. After one hour the result would be a nice video of one specific experiment, the Magic that Thomas asked for. So saying one phrase would be assigning students to different missions and they will directly go to their positions and do their jobs but they all will reach the same goal at the end. It would be great if we could have such a control over different objects and send them one message and they behave differently, however they are not human to memorize which command means which work to do. What should we do now in this case. Nature is composed of a large number of objects and events. Objects can construct or exist in parallel and events can occur or go on in parallel. Animals, humans, plants live in parallel; physical and chemical reactions occur and go on in parallel; persons work in parallel to complete projects. Things in nature are independent and connected, so they can run independently at the most of time but need to interact with each other at some time. The same thing we can have in computer. A computer is a machine that can perform tasks according to the instructions provided by humans. Earlier computer systems had one processor. The problem that has to be solved was divided into a series of instructions. Those instructions were given to the processor one after the other. In

every moment, only one instruction is executed. Then the processor, processed those instructions and gave output. This was not an efficient mechanism. Speed can be improved by increasing the frequency, but it also increases the temperature. That causes more heat dissipation. Therefore, it is not easy to increase the speed of the processor. As a result of this parallel computing was introduced. Parallel computing is a type of computation where many calculations or the execution of processes are carried out simultaneously. Parallel computing uses many processors. Therefore, multiple processors are executing instructions simultaneously. In parallel computing, a computational task is typically broken down into several, often many, very similar sub-tasks that can be processed independently and whose results are combined afterwards, upon completion. It can also save time.

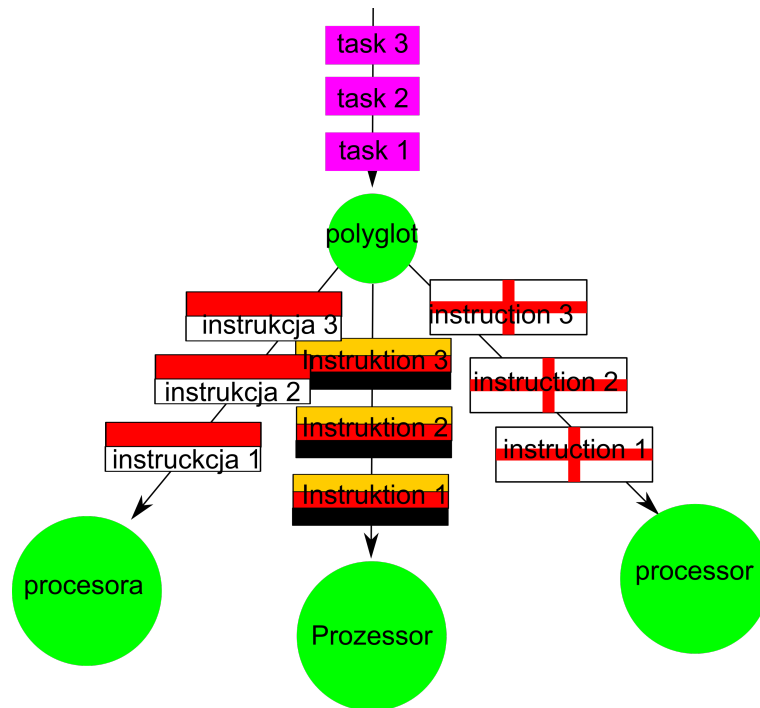


Figure 1.9: Parallel computing and splitting a polyglot series of tasks in to a series of different instructions to different processors .

The use of parallel processing is today essential for solving practical problems in science and engineering. Parallelism is a way of speeding up computations which make high time and memory demands. Communication and synchronization between the different subtasks are typically some of the greatest obstacles to getting optimal parallel program performance. Fast and robust algorithms, programmed with the necessary skill, are essential for efficiently solving urgent scientific problems in physics, medicine, biology, pharmacy and other areas, where parallelism could be helpful[48, 49, 50, 51, 52, 53, 54, 55, 56, 57, 58, 59, 60, 61, 62, 63].

1.6.1 Polyglots

Thomas' students are smart so they can translate his cryptic sentence in a way that leads to success. In the example they are interpreting "Do Magic" in three different ways. How to command stupid colloidal particles in a way Thomas commands his students. A parallel command given by a computer program must be interpreted in the correct and different way by all different colloidal particles. Thomas command is essentially quite stupid. Thank god, his students are smart to make sense of what he says. In case of the colloids the command must be smart since the colloids are stupid. In computer science a software that can be interpreted by different computer languages is called a polyglot[64]. We will need the analogue of a polyglot to control several colloidal assemblies in parallel.

1.7 Hydrodynamic friction, hydrodynamic interactions and dissipation

This thesis transfers the topological aspect of transport from the field of electron transport in topological semiconductors to the field of colloids. In semiconductors, we describe electrons mainly by Hamilton operators and for semi-classical electrons determine by Hamiltonians. The energy of the electrons is conserved in most of the theoretical descriptions. It is only recently been realized that there are topological electronic systems where viscous damping is significant and these electrons must be treated as over-damped systems. Colloids on the other hand are known to follow an over-damped dynamics such that in most circumstances inertia does not play a role. The topological dynamics of over-damped colloids discussed in this thesis therefore might give some insight into similar effects in electron fluids.

Viscous effect controls the dissipation in colloids and the proper way to explain their behaviour is with the help of the Stokes equation, Langevin type of equations, Fokker Planck equations or with the power functional theory [65]. In our case, in this thesis the colloids live in a potential energy landscape with transition states between the potential minima that exceed the thermal energy by orders of magnitude. Thermal fluctuations for this purpose are not-essential and the Stokes equation would be sufficient for a description of the colloidal phenomena. Because of the velocity or angular velocity of the colloids, they feel a friction. In the adiabatic limit that is relevant for the first two papers of the thesis, we can neglect the friction as well because the velocities and angular velocities are small. It is in the adiabatic limit that the over-damped motion becomes similar to the adiabatic motion in a Hamiltonian system where inertia becomes negligible.

We will briefly escape the adiabatic limit in the second paper. There the hydrodynamic forces \mathbf{F} and torques $\boldsymbol{\tau}$ on to a particular colloidal assembly are proportional to the

velocity \mathbf{v} and angular velocity $\boldsymbol{\omega}$ [66]:

$$\begin{pmatrix} \mathbf{F} \\ \boldsymbol{\tau} \end{pmatrix} = - \begin{pmatrix} \boldsymbol{\gamma}_T & \boldsymbol{\gamma}_C^t \\ \boldsymbol{\gamma}_C & \boldsymbol{\gamma}_R \end{pmatrix} \cdot \begin{pmatrix} \mathbf{v} \\ \boldsymbol{\omega} \end{pmatrix}, \quad (1.8)$$

where $\boldsymbol{\gamma}_T$ is the translational friction tensor, $\boldsymbol{\gamma}_R$ is the rotational friction tensor, and $\boldsymbol{\gamma}_C$ is the translation rotation coupling tensor. All tensors depend on the shape and on the orientation of the colloidal assembly. Additionally the rotational and the coupling tensor also depend on the choice of the reference point within the object. A special point of the object is the instantaneous center of rotation for which the coupling tensor becomes symmetric $\boldsymbol{\gamma}_C^t = \boldsymbol{\gamma}_C$. Since for hydrodynamic effects the instantaneous center of rotation is a physical relevant point, a gauge that describes all effects from the point of view of the instantaneous center of rotation might be a useful choice of gauge.

For several assemblies hydrodynamic interactions become relevant when higher than adiabatic speeds are used. Hydrodynamic interactions are complicated since they depend on the shapes and orientations of all interacting assemblies as well as on their relative positions. In dynamic situations shapes, orientations and separations change, which render the interactions highly nonlinear. We will describe experiments in paper 3 where hydrodynamic interactions between topologically transported colloidal assemblies with their cargo become relevant.

1.7.1 Condensation in active systems

An ideal gas is a thermodynamic system of particles with velocities distributed according to a Maxwell-Boltzmann distribution that, no matter what is the pressure and temperature, exhibits a density that is the same everywhere when averaged over time or over space. A coexistence of a condensed phase with a diluted gas develops in a van der Waals gas because of attractive interactions between the particles of this thermodynamic system. Such coexistence never occurs in a thermodynamic particle ensemble with purely repulsive interactions. It is therefore a puzzling emergent phenomenon that purely repulsive active particle ensembles exhibit a coexistence of dense with less dense dynamic phases. Depending on which active particles one speaks about the denser phase is named a swarm, a flock, a school, the jammed phase, etc..

In a high Reynolds number fluid, vorticity is generated as a consequence of the propulsion of one animal. The vorticity causes considerable loss of energy for swimming animals. Animals can swim more effectively if they are able to harvest part of that lost energy from vortices of animals in front of them. As energy is a limited resource that can affect the survival and reproductive efforts of an animal, there are adaptive benefits to having hydrodynamic mechanisms that recapture energy dissipated to the fluid. Aquatic animals often travel in highly organized formations such as schools. By aligning themselves in a

defined pattern, individuals in the group can take advantage of flow patterns generated by others to reduce drag and may save energy compared to free-stream locomotion. Vortices generated by leading individuals pass backward and impact trailing individuals. If a trailing animal is swimming in the same direction as the leading animal, its relative velocity to the surrounding fluid is less than the swimming speed of the school, so the individual body will experience a reduction in drag. Metabolic measurements showed that as the number of ducklings in the line increased, the energetic cost per duckling decreased[26]. Furthermore, it was determined that last duckling in the line swam with the least effort.

Low Reynolds number bacteria also arrange in the form of swarms. Whether the arrangement in form of a swarm is due to the animals or bacteria learning how to save energy or just due to dynamic self organization is not entirely clear. The study of active swimmers without brain therefore is an interesting field of research. Albeit all the equations on the single particle level are clear, whether the equations are those of high or low Reynolds number active particles, the collective continuum description of the phenomenon, and how it theoretically is connected to the single particle description so far is under heavy theoretical dispute.

Counterintuitive claims such as negative interfacial tension stabilizing the dense phase [67] have been made. One theory describing the swarm formation of active systems is the power functional theory[65]. Within this theory superadiabatic forces arise that are absent in a thermodynamic system that has no currents. These superadiabatic forces push the active particles toward the condensed phase and balance the entropic counter forces which in a thermodynamic system would push the system toward a constant density situation. The powerfunctional theory gives a framework to derive these superadiabatic forces as functional derivatives from a power functional.

In my third paper I will talk about the dynamic self assembly of colloidal trains that is a one dimensional active few particle model system of the formation of a condensed phase - a colloidal train - consisting of a mixture of more and less active particles. The system remains adiabatic up to a certain speed of the external magnetic field modulation, and superadiabatic forces only set in, if a certain threshold frequency is surmounted such that there emerges a relative velocity between single particles that if isolated remain inactive and active colloidal doublets that are active when isolated. As in the complexer active systems discussed in the framework of the power functional theory my colloids experience superadiabatic forces enforcing the condensation of colloids to colloidal trains.

May be due to their low dimensionality and because only few interacting particles are involved they might be a system where the connection between the single particle description and the collective description is easier to understand.

1.8 Magnetism and the dipolar interaction

The majority of interactions playing a role in my thesis are magnetic in nature. My setup is a combination of magnetic materials, incorporating ferromagnets and antiferromagnets that are the basic materials of my magnetic patterns. The pattern results from exchange bias magnetic films that are bombarded lithographically with Helium ions. The colloidal particles are paramagnetic polystyrene spheres that are filled with superparamagnetic nano-particles of magnetite. The colloidal particles move in the potential of the pattern and they interact with each other via dipolar interaction. Let me therefore first talk about exchange bias films and then about the dipolar interaction.

1.8.1 Exchange bias films

A ferromagnetic material is a material that has a remanent macroscopic magnetization, i.e. a permanent magnetization that persists after magnetization of the sample with an external magnetic field. The typical magnetization curve is symmetric with respect to a flip of the external field and exhibits a hysteresis as shown in Fig. 1.10. In order to change the remanent magnetization from one of the two zero-field values to the other one must overcome the coercive field. The ferromagnetic state forms because of negative exchange interactions between neighboring atoms within the ferromagnet. When the exchange interaction is positive the low temperature ground state is that of an antiferromagnet. When we couple a ferromagnetic material to an antiferromagnetic material, e.g. by forming thin films on top of each other. There is also exchange interaction between the neighboring atoms of either material. The macroscopic result of this is a hysteresis curve that no longer is symmetric around zero external magnetic field but around the exchange-bias field. An exchange-bias field that is larger than the coercive field will result in only one remanent magnetization. Ion bombardment of the exchange bias film can reverse the exchange bias field such that in a lithographical bombardment the bombarded regions result in a remanent magnetization that is opposite to the non-bombarded regions.[68, 69] In my thesis I use exchange bias films that were created in Poznan by the group of Maciej Urbaniak and lithographically bombarded in the group of Arno Ehresmann in Kassel.

1.8.2 Dipolar interaction

The magnetic moment μ is a vector quantity used to measure the tendency of an object to interact with an external magnetic field. The object's intrinsic magnetic properties are often visualized as emanating from a tiny bar magnet with north and south poles and is therefore also called the magnetic dipole moment. The concept of the magnetic dipole is not restricted to the modeling of atomic-sized particles and can be applied to

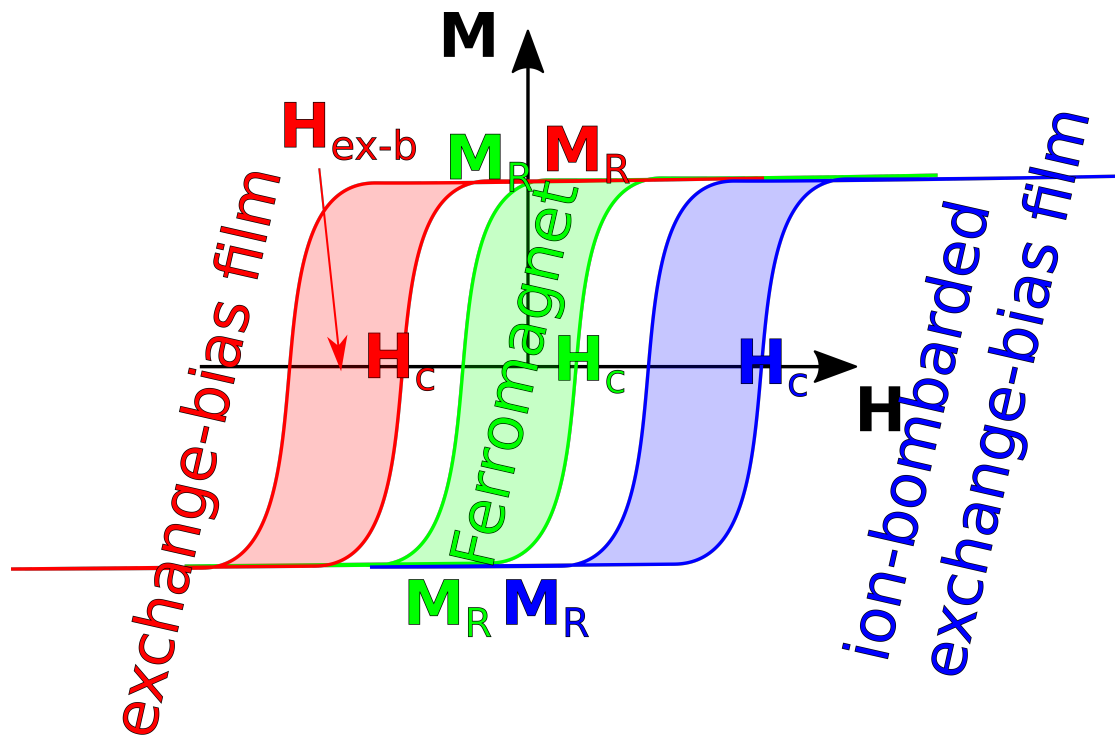


Figure 1.10: Magnetization curves of a ferromagnet (green), an exchange-bias film (red), and an ion-bombarded exchange-bias film (blue)

much larger objects and collections of objects. A compass needle and even the earth itself might be considered giant dipoles and also in our experiment, a rod which consists of several particles can be called dipole. When the field lines of two magnetic moments cross, a dipole-dipole interaction occurs. An alternative and more quantitatively useful definition of the magnetic moment is to model it as arising from a tiny current I traveling around the edge of a loop of cross sectional area A . The magnetic dipole moment μ is a vector defined as $\mu = IA$ whose direction is along A .

The magnetic moment μ will seek to align with an externally applied magnetic field B_0 . It will experience a torque τ given by the vector cross product $\tau = \mu \times B_0$. When perfectly aligned parallel to $\mu \uparrow B_0$, μ will be in its lowest energy state and experience no torque. When pointing opposite to $\mu \updownarrow B_0$, μ will be in its highest energy state because extra energy would be required to move and maintain it in this position. For any other direction the energy E of the magnetic moment μ would be given by the vector dot product: $E = -\mu \cdot B_0$. In a viscous fluid subject to an external rotating field the magnetic torque is balanced by a viscous torque and gives rise to synchronous or asynchronous dynamics of the magnetic moment [70].

When two identically paramagnetic spherical particles immersed in a viscous fluid are

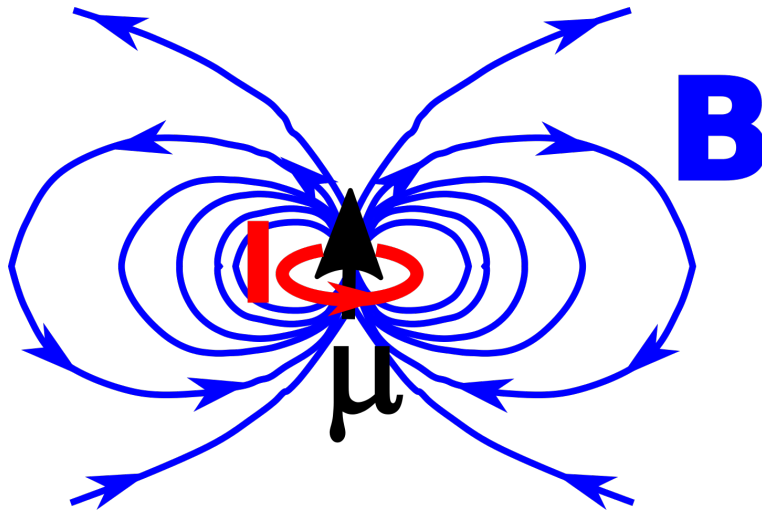


Figure 1.11: Magnetic dipole modelled as a current loop

placed in an external magnetic field, the colloidal particles will experience the interaction between two magnetic dipoles induced by the magnetic field. In Fig. 1.13a), the dipoles are aligned parallel to the field and arranged in an end to end configuration. One pole on one colloid is attracted to the opposite pole on the neighboring colloid. In contrast, when the particles are aligned perpendicular to the magnetic field, as shown in Fig. 1.13b), the particle charges on the neighboring sides of the colloids lead to repulsion. These interactions tend to align the colloidal particles to increase their attraction and reduce their potential energy, thus forming hierarchical arrays of colloidal particles.

Magnetic-field-guided colloidal assembly routes have several common characteristics. First, the assembly process is driven by magnetic dipole-dipole interactions which are directional in nature and can be either attractive or repulsive, depending on the relative configuration of the particles with respect to the applied field. Second strong magnetic interactions can be effectively and reversibly initiated by application of an external field, providing enough driving force for the rapid assembly of colloidal particles. There are generally two types of magnetic interactions experienced by colloidal particles in external magnetic fields, orienting from their permanent or induced dipole moments. The inter-particle dipole-dipole force describes the interaction of a dipole with the magnetic field induced by another dipole the packing force results from the gradient of the external magnetic field. When the inter particle dipole-dipole force is strong enough to overcome thermal fluctuations, the alignment of the dipolar particles along the direction of their magnetic moments is the direct result of the directional dipole-dipole force.

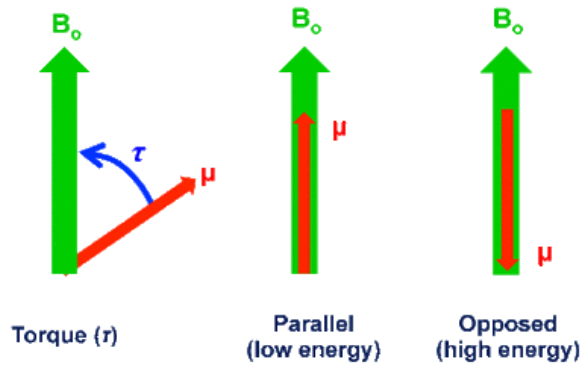


Figure 1.12: (A) For any random direction, the energy (E) of the magnetic moment (μ) would be $E = -\mu \cdot B_0$ (B) B_0 aligned opposite to $\mu \uparrow \downarrow B_0$ and it has the highest energy state. (C) B_0 aligned parallel to $\mu \uparrow \uparrow B_0$ and it has the lowest energy state.

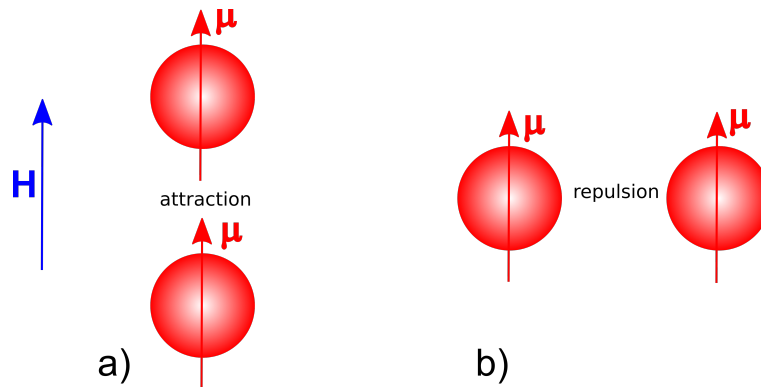


Figure 1.13: (The magnetic moment of a paramagnetic particle with a dipole moment in the same direction as the external magnetic field causes a) attraction for particles separated along the direction of the field and b) repulsion for particles separated in a direction perpendicular to the magnetic field.

Chapter 2

Materials and Methods

A good experiment must be simple. It should be as straightforward as possible. However, the experiment is not theory and nature is not as kind as I would wish. It puts certain difficulties in the way of the experiment that one must eliminate prior to having success. I have organized this chapter by first introducing the setup used for the experiment and then talking about the obstacles nature put in the way of my experiments and how I succeeded in eliminating those problems. Finally, I talk about obstacles that did not get out of my way but developed into the major topic of this thesis.

2.1 Setup

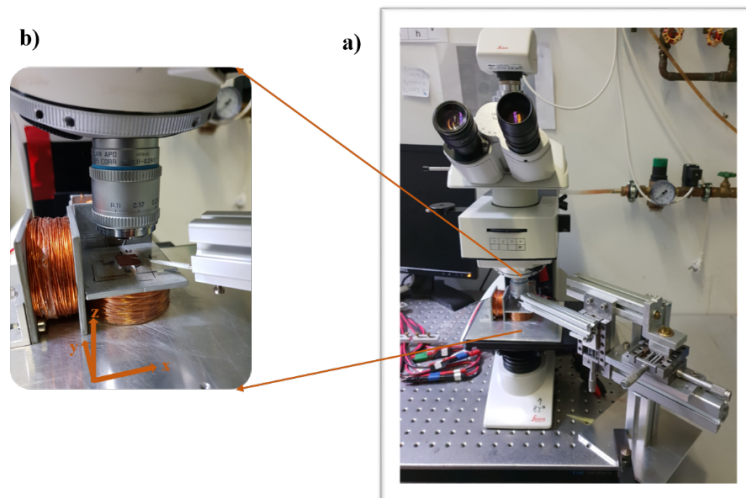


Figure 2.1: a) Picture of the experimental setup. The polarization microscope is equipped with a CCD camera on top and a set of coils on the slide table. b) Close up on the arrangement of coils. There is one coil for each main direction x -, y -, and z -direction. The magnetic pattern is placed on top of the z coil

The experimental setup is shown in Fig. 2.1. The most important part is the polarization microscope DM2500P from Leica. We use this microscope to visualize our colloidal particles and the magnetic structures. We put three coils on top of the slide table to generate the external magnetic fields (2.1). We have a special arrangement of the coils

which I have shown in Fig. 2.1b to superpose time-dependent, homogeneous external magnetic fields to the heterogeneous field of the magnetic structures. One of three coils each generates the x -, the y -, and the z -component of $\mathbf{H}_{\text{ext}}(t)$. Due to the macroscopic dimension of the coils, we can in good approximation assume that the magnetic fields are homogeneous on the observed mesoscopic length scale, however, we need to place the pattern exactly in centre of the three middle axes of the x -, y -, and z -coils. To generate the time-dependent fields the coils are connected to three bi-polar amplifiers (Kepco BOP 20-50GL) (Fig. 2.2.b) that are fed by three channels of a wave generator (Aim-TTi TGA 1244) 2.2.a) with four channels.

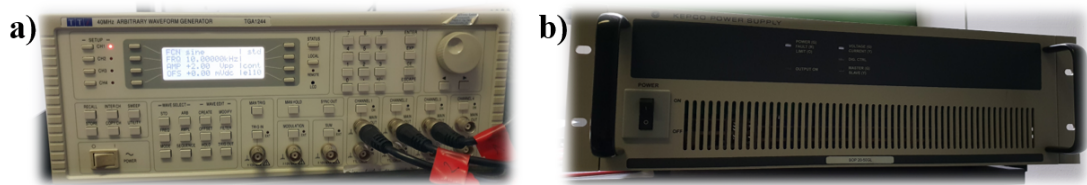


Figure 2.2: a) The four channel wave generator (Aim-TTi TGA 1244) b) the bipolar amplifier (Kepco BOP 20-50GL)

The wave generator is capable of playing arbitrary waveforms that were beforehand created with a Matlab program. To convert the applied voltage into a defined field strength the coils are calibrated with a Gauss meter (LakeShore 410). Like this, it is possible to apply any desired, time-dependent modulation of the external magnetic field.

The magnetic patterns were placed directly on top of the coil. Then we put the colloids on top of our magnetic pattern with a pipette.

A CCD-camera (Leica DFC360 FX) was attached on top of the microscope (Fig. 2.1). Together with the commercial software StreamPix, the dynamics could be recorded with a resolution of 1392×1040 at 20 frames per second. The particle trajectories were extracted from the videos using manually tracking options in ImageJ.

2.2 Elimination of perturbing effects

2.2.1 Elimination of non-universal Fourier components of the magnetic field of the pattern

All experiments were done on a lithographic pattern that is actually an exchange bias film that consists of two kinds of magnetic domains, half of them are magnetized into

the positive and rest half magnetized into negative z -direction normal to the film. All magnetic patterns were periodic patterns so their magnetic field can be described as

$$\mathbf{H}_p = \nabla\psi_p \quad (2.1)$$

could be described by a magnetostatic potential ψ_p that above the pattern fulfills the Laplace equation

$$\nabla^2\psi_p = 0 \quad (2.2)$$

and thus can be written as a Fourier series

$$\psi_p = \sum_{\mathbf{Q}_j \in \text{reciprocalLattice}} \psi_{\mathbf{Q}_j} \exp(-Q_j z) \exp(i\mathbf{Q}_j \cdot \mathbf{r}_A) \quad (2.3)$$

that generically has all kinds of Fourier coefficients $\psi_{\mathbf{Q}_j}$ that depend on the details of the pattern. At higher elevations z above the pattern higher order Fourier coefficients are reduced exponentially according to the modulus Q_j of the reciprocal lattice vector such that there only the lowest order Fourier coefficients are relevant. Thus if we elevate the particles sufficiently high above the pattern the pattern field depends only on the symmetry of the pattern. The pattern field becomes universal and we get rid of higher order Fourier coefficients that otherwise would provide a description we don't need. We coated our pattern with a photo resistance layer (AZ-1512HS, Microchem, Newton, MA) of defined thickness $1.6\mu m$ to have universal pattern fields. Cleanness of the pattern again is really important. I cleaned the pattern well with methanol and I kept it in the methanol till I wanted to start with the spin coating. Spin coating is a method used to deposit uniform thin films on flat substrates. The process of rotation is continuous until the fluid spins off the edges of the substrate until the thickness of the film is completed. I was using spin coating at a speed of 3000 rpm for 50 s, with an acceleration of 300 rpm/s. I should have been very careful while spin coating to not break the pattern while it may happen when you don't put the pattern exactly on top of the vacuum valve provided in the spin coater device. After the spin coating, the resist was baked for 1 min at $115^\circ C$ on a heat-plate. For more persistence of the photo resistant layer I put it in the oven for about 2 hours under 170 centigrade, it can be called a soft baking process. A drop of the colloidal suspension is then placed on top of the photoresist layer. Now with this extra photo resistance layer, the high density colloidal particles sediment on the photoresist spacer. Particles are then moving at a fixed, sufficiently universal, elevation.

2.2.2 Elimination of adhesion

Our colloidal particles are electrostatically stabilized colloids that interact with each other and with the photo resist surface with a Derjaguin, Landau, Verwey, Overbeek (DLVO)-potential, i.e. by the competition of an attractive van-der-Waals interaction that supports the precipitation of colloids as well as the adhesion of colloids at the photoresist, and a screened electrostatic repulsion that stabilizes the colloidal suspension

and prevents the adhesion to the photoresist. The Debye length is the screening length of the stabilizing repulsion and it depends on the ionic strength of the counter ions in the dispersed fluid. The ionic strength must be kept low to prevent the adhesion of colloids to the photoresist. I used deionized water which to clean the pattern after each use and I dried the pattern only with precision wipes. If I observed adhesion the colloidal particles can no longer be moved by the external field and I had to repeat the cleaning procedure until there would be no adhesion.

2.2.3 Elimination of structural entropy of the initial state

When I added the colloidal suspension with a pipette the colloidal particles would sediment on top of the photoresist in a random conformation. For the experiments on the parallel programmed paths of different bipeds we needed a defined initial state of the bipeds, on the pattern. Without an external field, the colloids are dispersed mainly as single particles above the pattern. The application of the external field leads to the assembly of random length and random position rods above the pattern. A glass capillary with a tip diameter of a few microns attached to a micro manipulator is used to change the length and position of the bipeds to the desired relative initial arrangement while the external field remains in the equatorial plane. In this way, the structural entropy of the initial state was eliminated and the initial states could be prepared as required.

2.3 Elimination of errors due to sign conventions

The theoretical description contains many sign conventions, and it is quite easy to get one of them mixed up. There are up and down magnetizations one can mix up. On some patterns up magnetized domains appear brighter than down magnetized domains, on other patterns, it is the other way around. One can accidentally connect the external field coils in the wrong way which alters the field direction. We usually use right handed coordinate systems, however, the computer graphics uses a left handed coordinate system. It is important to keep track of the signs. My P.h.D work started with applying cyclotron loops to my colloidal bipeds. Our expectation was quite clear from what we knew about single colloids. Imagine the simplest cyclotron loop that consists of four loops around each of the single colloidal fences of a four fold symmetric pattern in the control space. Each of those loops starts and ends in the north pole of control space and they wind around one of the fences, the next loop cycling the next fence. The loops around the fences are thus concatenated at the north pole. Such a loop can be deformed continuously to a loop that always stays at the south pole without having to cross any of the fences. The same must thus be true for the trajectory of a single colloid on the pattern. The trajectory of a single colloid subjected to a simple cyclotron loop that is concatenated in

the north must continuously be deformable into a single colloid that stays in the middle of a down (south) magnetized domain. Hence the trajectory of a cyclotron loop that is concatenated in the north must cycle around a central down magnetized domain. If we theoretically consider a biped of length b that continuously develops from a single colloid, we would expect its trajectory to continuously develop from the single colloid. Thus a trajectory of a biped of arbitrary length b subject to the same cyclotron orbit should as well cycle a down magnetized domain, not an up magnetized domain. So when I observed in the experiment a biped cycling an up magnetized domain, the first thing Thomas told me to do was to eliminate the obvious error in the sign convention. I redid the experiment over and over again but the putative error did not disappear. It was from these initial unsuccessful elimination attempts that the entire thesis developed.

What is true for a simple cyclotron loop applied to a single colloid on a square pattern remains true also for more complex cyclotron loops that wind around the fence points twice instead of once. If we concatenate the simple loop in the north, the trajectory of a single colloid will wind around a down (south) magnetized domain Fig. 2.3. However, a biped consisting of 11 single colloidal particles behaved differently and started cycling around an up magnetized domain when the cyclotron orbit latitudes were close to the equator and around the expected down magnetized domain when using more polar latitudes. I will not explain the effect in detail. It can be understood by incorporating hydrodynamic effects like in publication 2 with the proper topological adiabatic treatment of the biped of this length. What I want to say, sometimes the errors that cannot be eliminated, however how hard I tried can develop to some beautiful understanding of what is really going on. What is really going on will be described in the second part of the thesis.

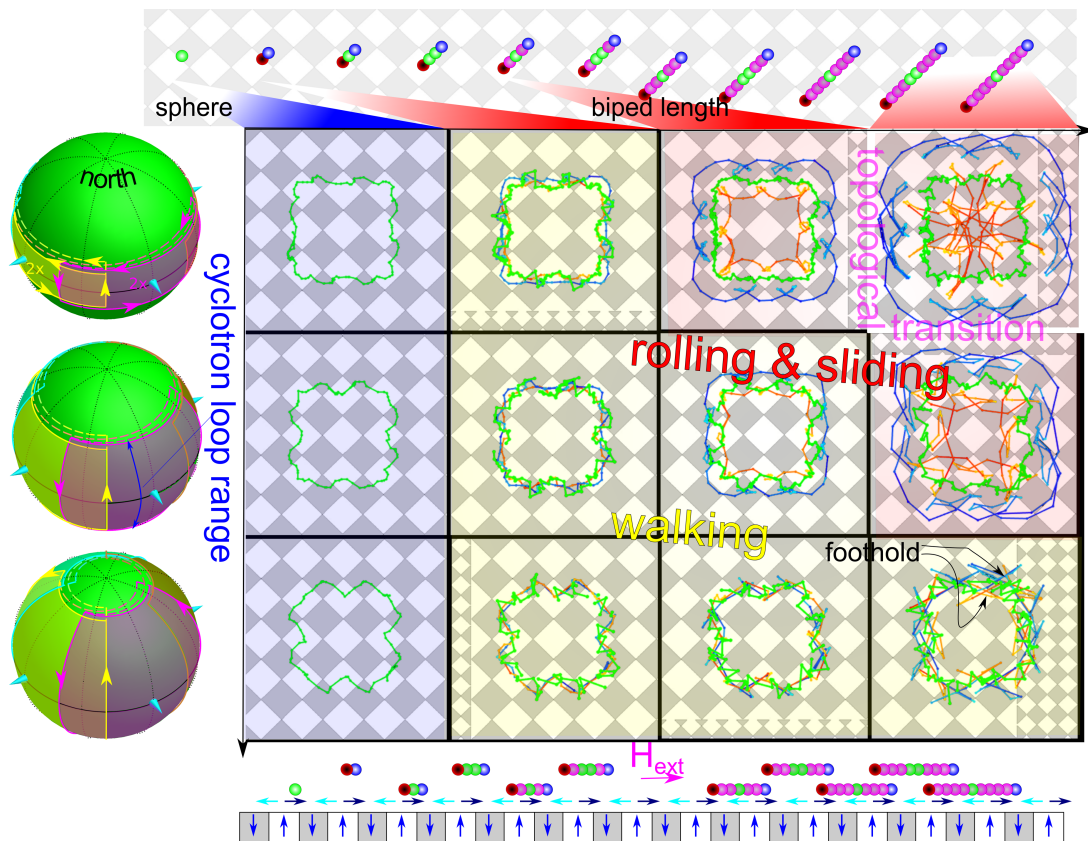


Figure 2.3: cyclotron loops applied to bipeds of different length together with trajectories of the instantaneous center of rotation (green) and the trajectories of the two feet (red and blue)

Part II

Publications

Publication 1

Simultaneous polydirectional transport of colloidal bipeds

Nature Communications, **11**, 4670 (2020)

Mahla Mirzaee-Kakhki^{a1}, Adrian Ernst^{a1}, Daniel de las Heras^{a2},
Maciej Urbaniak^b, Feliks Stobiecki^b, Jendrik Gördes^c, Meike
Reginka^c, Arno Ehresmann^c, Thomas M. Fischer^{a1}

^{a1} Experimental Physics and ^{a2} Theoretical Physics, Faculty of Physics, Mathematics and Computer Science, University of Bayreuth, 95447 Bayreuth, Germany.

^b Institute of Molecular Physics, Polish Academy of Sciences, 60-179 Poznań, Poland.

^c Institute of Physics and Center for Interdisciplinary Nanostructure Science and Technology (CINSaT), Universität Kassel, D-34132 Kassel, Germany.

In section 1.3 I have shown what was known about the topological transport of colloids in comparison to the topological transport of electrons in semiconductors. In section 1.8.2 I discussed the anisotropic nature of dipolar interactions. Using the attractive nature of the dipolar interactions along the direction of the magnetic field allows us to assemble individual colloids into more complex assemblies. This adds further internal degrees of freedom to the transported objects and we might envision that different values of these degrees of freedom might fall into topologically distinct classes of transport. If this were

the case one should be able to transport different assemblies into different directions. The same loop of the external field would result in other forms of transport for each assembly. I will take this question one step further and ask whether the problem can be inverted: Given a desired direction of transport for each of the assemblies, can we find modulation loops of the external field that might serve as parallel command to transport each of the assemblies into the desired directions? Such possibility would lay the ground for a polyglot language as described in section 1.6.1 made up of a set of modulation loops that can transport the assemblies at will. I am ready to pose the first question that arose from what we knew before starting this PhD work:









Question

Is it possible to have a colloidal assembly characterized by a continuous parameter, which falls into different topological classes of this parameter that is then transported differently and can we parallel program the transport at will?

My Contribution

That colloidal bipeds fall into topologically distinct classes of transport was not known before I discovered this fact with first experiments on bipeds. The exploitation of this fact was then a joint effort between Adrian Ernst, who worked out the mathematical part and the computer control and simulations of the experiments and me who performed all the presented experiments and prepared all the initial states. Exchange-bias films have been produced by Maciej Urbaniak and Feliks Sobiecki in Poznan, the lithographic patterns were planned in Bayreuth as a team effort, and the ion-bombardment was done by Jendrik Gördes, Meike Reginka and Arno Ehresmann in Kassel. The preparation and writing of the paper was done by all coauthors.

Simultaneous polydirectional transport of colloidal bipeds

Mahla Mirzaee-Kakhki¹, Adrian Ernst ¹, Daniel de las Heras ², Maciej Urbaniak ³, Feliks Stobiecki ³, Jendrik Gördes ⁴, Meike Reginka ⁴, Arno Ehresmann ⁴ & Thomas M. Fischer ¹✉

Detailed control over the motion of colloidal particles is relevant in many applications in colloidal science such as lab-on-a-chip devices. Here, we use an external magnetic field to assemble paramagnetic colloidal spheres into colloidal rods of several lengths. The rods reside above a square magnetic pattern and are transported via modulation of the direction of the external magnetic field. The rods behave like bipeds walking above the pattern. Depending on their length, the bipeds perform topologically distinct classes of protected walks. We design parallel polydirectional modulation loops of the external field that command up to six classes of bipeds to walk on distinct predesigned paths. Using such loops, we induce the collision of reactant bipeds, their polymerization addition reaction to larger bipeds, the separation of product bipeds from the educts, the sorting of different product bipeds, and also the parallel writing of a word consisting of several letters. Our ideas and methodology might be transferred to other systems for which topological protection is at work.

¹Experimentalphysik X, Physikalisches Institut, Universität Bayreuth, D-95440 Bayreuth, Germany. ²Theoretische Physik II, Physikalisches Institut, Universität Bayreuth, D-95440 Bayreuth, Germany. ³Institute of Molecular Physics, Polish Academy of Sciences, 60-179 Poznań, Poland. ⁴Institute of Physics and Center for Interdisciplinary Nanostructure Science and Technology (CINSaT), Universität Kassel, D-34132 Kassel, Germany. ✉email: Thomas.Fischer@uni-bayreuth.de

A time-dependent energy landscape can transport objects with different properties into different directions. This is the basic idea behind any sorting process, including sieving. On a microscopic level, an optical lattice can be used to sort particles based on the strength of the interaction between the particles and the lattice sites¹. Ratchets² can also be used for the directed transport of distinct microscopic objects³. Simultaneous sorting of heterogeneous materials can be achieved with particles driven through periodically modulated energy landscapes⁴. In general, these mechanisms do not allow to precisely control the direction of the transported objects.

The simultaneous transport of colloidal assemblies that can be adapted to requirements such as the presence or absence of colloidal cargo would allow to switch between multiple tasks on lab-on-the-chip devices. To this end, depending on their intrinsic properties, colloidal assemblies need to respond differently to an externally given command. The analog in computer science is known as a polyglot, a program that can be simultaneously compiled and executed in different languages. Typically, the polyglot performs the same task in all valid languages. However, much more powerful polyglots can be coded to perform different and independent tasks for each language⁵. A current of electrons is the only computational element in computer science. The ability to execute commands in parallel gains relevance if several computational elements are used. For example, in biochemistry the nodes of a metabolic network trigger different reactions in parallel. Other areas that would benefit from using parallel commands include the parallel computing with entangled quantum states^{6–8}, with DNA oligonucleotides^{9–14}, and with soft matter devices¹⁵ such as membranes¹⁶, reaction-diffusion computers¹⁷, microfluidic computers^{18,19} and colloidal computers^{20,21}.

Here we develop a parallel polydirectional command for the robust transport of colloidal rods above magnetic patterns. The parallel polydirectional command addresses simultaneously and independently the transport of rods of different lengths, and it is hence more efficient than multiplexing, which addresses one command at a time. We provide a fully explained parallel polydirectional command ultimately based on topological protection.

Results

Experimental setup. Paramagnetic colloidal particles (diameter 2.8 μm) immersed in water are placed on top of a two-dimensional magnetic pattern. The pattern is a square lattice of alternating regions with positive and negative magnetization relative to the direction normal to the pattern, see Fig. 1a. A uniform time-dependent external field of constant magnitude is superimposed to the nonuniform time-independent magnetic field generated by the pattern. The external field induces strong dipolar interactions between the colloidal particles which respond by self-assembling into rods of 2–19 particles.

The orientation of the external field changes adiabatically along a closed loop (Fig. 1b). Despite the field returning to its initial direction, single colloidal particles can be topologically transported by one-unit cell after completion of one loop^{22,23}. The transport occurs provided that the loop winds around specific orientations of the external field. In particular, around those orientations given by the unit vectors of the square magnetization pattern²³. Colloidal rods formed by several particles can also be transported. The rod aligns with the external field since dipolar interactions are stronger than the buoyancy. Hence, if the external field is not parallel to the pattern, one end of the rod remains on the ground while the other one is lifted. As a result, the rods walk through the pattern, see Brownian dynamics

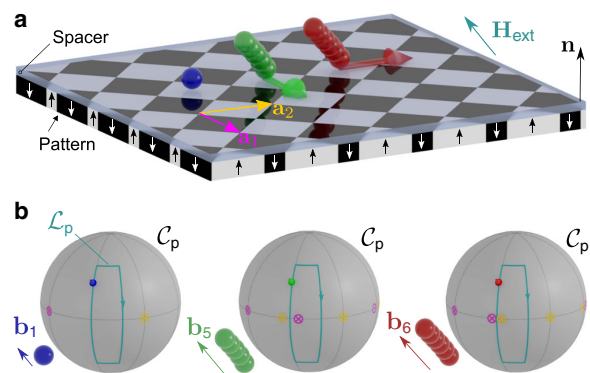


Fig. 1 Schematic of the colloidal transport. **a** A square magnetic pattern with lattice vectors \mathbf{a}_1 and \mathbf{a}_2 is magnetized with regions of positive (white) and negative (black) magnetization parallel to the vector normal to the pattern \mathbf{n} . Spherical colloidal particles (blue) are placed on top of the pattern immersed in water. Due to the presence of a strong homogeneous external field, some colloids self-assemble into rods of different length (green and red). **b** Our control space C_p is a sphere that represents all possible directions of the external field \mathbf{H}_{ext} . The direction of the external field varies in time performing a closed loop \mathcal{L}_p . The colored arrow tip on the loop corresponds to the orientation of the external field depicted in **a**. The orientation of the bipeds (\mathbf{b}_1 , \mathbf{b}_5 , and \mathbf{b}_6) is parallel to \mathbf{H}_{ext} . If the loop winds around special directions (yellow and pink equatorial circles), colloidal rods move as bipeds one-unit cell after completion of one loop (**a**). The topological properties of control space depend on the length of the rod, allowing the design of parallel polydirectional loops that move rods of different lengths simultaneously along different directions. Here, the loop transports b_5 -bipeds with five colloidal particles by $\Delta\mathbf{r}(\mathcal{L}_5) = \mathbf{a}_1$ (green arrow in **a**), b_6 -bipeds with six colloidal particles by $\Delta\mathbf{r}(\mathcal{L}_6) = \mathbf{a}_2$ (red arrow in **a**), and does not transport single colloids b_1 .

simulations in Supplementary Movie 1. For this reason, we refer to the rods as bipeds^{24–28}.

Parallel polydirectional loops. To transport the bipeds, the loop also needs to wind around special orientations of the external field. Surprisingly, these special orientations depend on the length of the bipeds, see Fig. 1b. Bipeds of different length fall into different topological classes such that their displacement upon completion of one parallel polydirectional loop can be different in both magnitude and direction. A sketch of the process is shown in Fig. 1. As it is the case for single colloids, the biped motion is topologically protected and hence robust against perturbations. As we show next, it is possible to design parallel polydirectional loops that simultaneously and independently transport bipeds of different lengths.

For example, parallel didirectional loops can be used to simultaneously transport bidisperse bipeds into two different directions. Fig. 2a shows the experimental trajectories of a set of bipeds of lengths b_5 and b_6 , with $b_n = nD$ and D the diameter of the colloidal particles.

Parallel tridirectional loops can be used to initiate the polymerization addition reaction of two bipeds of different lengths by setting them on a collision course and letting the product of the polymerization be transported into a third direction. In Fig. 2b we show experimental trajectories of biped educts of lengths b_3 and b_7 polymerizing to a product biped of length b_{10} .

In Fig. 2c, bipeds of lengths b_3 , b_7 , b_2 , b_5 , and b_{10} are driven by a complex parallel tetradirectional loop that simultaneously programs the bipeds to write the letters T, E, T, R, and A,

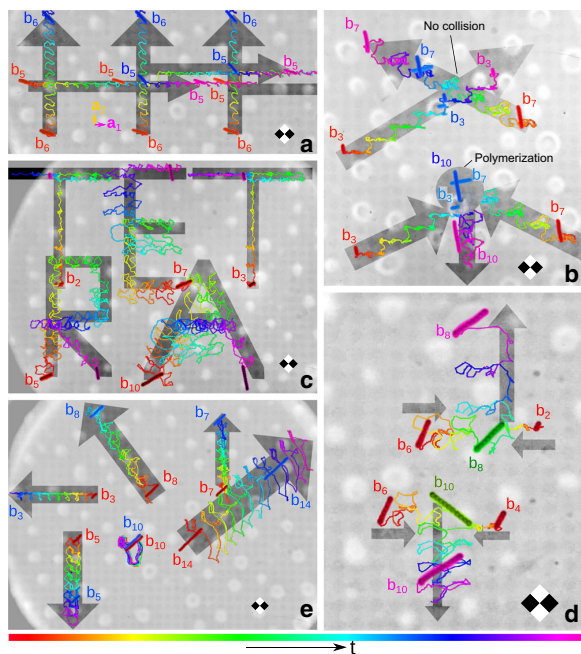


Fig. 2 Experimental trajectories of bipeds driven by parallel polydirectional loops. **a** parallel didirectional loop of robustness $\rho = 0.16$ and compaction $c = 1/2$ transporting several bipeds b_5 into the \mathbf{a}_1 -direction and bipeds b_6 into the \mathbf{a}_2 -direction. **b** parallel tridirectional loop of robustness $\rho = 0.3$ and compaction $c = 7/8$ setting two bipeds b_3 and two bipeds b_7 on a collision course. One pair of bipeds collides and polymerizes to a longer biped b_{10} that is then transported into a third direction. The non-colliding bipeds continue their motion. **c** Parallel tetradirectional loop of robustness $\rho = 0.2$ and compaction $c = 30/54$ commanding bipeds of five different lengths $\{b_3, b_7, b_2, b_5, b_{10}\}$ to simultaneously write four different letters. The biped b_2 is topologically equivalent to the biped b_3 and hence writes the same letter (T). **d** Parallel pentadirectional loop of robustness $\rho = 0.11$ and compaction $c = 5/6$ commanding a biped b_2 and a biped b_4 to polymerize with two colliding bipeds b_6 and then separate as they form a biped b_8 and a biped b_{10} . **e** Parallel hexadirectional loop of robustness $\rho = 0.06$ and compaction $c = 4/8$ transporting six bipeds of different lengths into six different directions. The color of both bipeds and trajectories indicates the time progress of one control loop (see bottom colorbar). A square region of the pattern of diagonal $2a \approx 22 \mu\text{m}$ is sketched in each panel to indicate the scale and the relative orientation.

respectively. Note that bipeds of lengths b_2 and b_3 perform the same trajectory (letter T). As we show below the reason is that $b_2 < b_3 < a$ with $a \approx 11 \mu\text{m}$ the lattice constant of the pattern. Both b_2 and b_3 bipeds respond in the same way to the parallel polydirectional loop despite being at different locations. The parallel polydirectional loop does not address the location of the bipeds but only their shape.

We use a parallel pentadirectional loop for the quality control of a competing polymerization addition reaction, Fig. 2d. The loop initiates the addition of a b_2 and a b_6 biped as well as the addition of a b_4 and a b_6 biped. Both, the b_2 and the b_4 bipeds are set on a topologically nonequivalent collision course with b_6 bipeds. The products of the addition polymerization reactions are a b_8 and a b_{10} biped that are topologically distinct and can be separated from each other as well as from the transport direction of the educts.

In Fig. 2e we plot the trajectories of six bipeds of different lengths after completion of several parallel hexadirectional loops

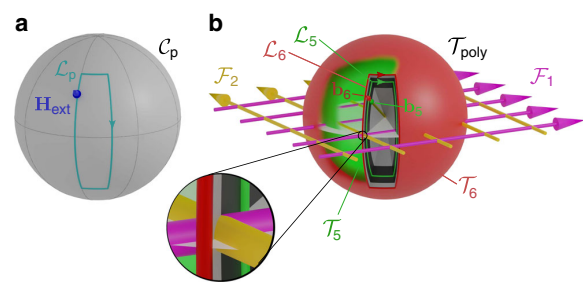


Fig. 3 Control and transcription spaces. **a** Polydirectional control space C_p . Each point on the sphere represents the orientation of the external field. Commands are given as closed loops \mathcal{L}_p . **b** Polydirectional transcription space T_{poly} contains all unidirectional transcription spaces T_n that are concentric spheres of radius b_n . Each point in T_n represents the orientation of a biped of length b_n . One point in C_p is transcribed into a ray in T_{poly} . The unidirectional loops \mathcal{L}_5 (green) and \mathcal{L}_6 (red) wind around different fence lines and they pass on different sides of the (pink) \mathcal{F}_1 - and (yellow) \mathcal{F}_2 -line as can be seen in the magnified inset.

that transport all six different bipeds consistently into six different directions.

Supplementary Movies 2–6 show walking bipeds with tracked experimental trajectories as well as the driving parallel polydirectional loops. The details of the parallel polydirectional loops are provided in Supplementary Note 1 and Supplementary Figs. 1–3. Supplementary Movie 7 shows the trajectories of the tetradirectional command, panel Fig. 2c, according to Brownian dynamics simulations. The agreement between simulations (Supplementary Movie 7) and experiment (Supplementary Movie 4) is excellent.

Theory. As we show next, the reason we can independently and simultaneously transport up to six different particles is topological protection. Let $\mathbf{H}_{\text{ext}}(t)$ be the uniform time, t , dependent external field, and $\mathbf{H}_p = \nabla\psi$ the spatially nonuniform and time-independent magnetic field generated by the pattern, with $\psi(\mathbf{r})$ the magnetostatic potential of the pattern, and $\mathbf{r} = (\mathbf{r}_A, z)$ the position vector with components \mathbf{r}_A in the plane parallel to the pattern and z normal to it.

Control space. The polydirectional control space C_p is the surface of a sphere, Fig. 3a, which represent all possible orientations of \mathbf{H}_{ext} . Parallel commands are given in the form of closed loops \mathcal{L}_p in C_p .

Transcription space. The orientation of the (dipolar) biped is locked to that of the external field with the northern foot being a magnetic north pole and the southern foot being a south pole. Let \mathbf{b}_n denote the vector from the northern foot to the southern foot of a biped of length b_n , Fig. 1a. The southern (northern) foot is on the ground if \mathbf{H}_{ext} points into the south (north) of C_p . When \mathbf{H}_{ext} crosses the equator of C_p , the biped is parallel to the pattern and the transfer between the feet occurs. Given the one-to-one correspondence between the biped orientation \mathbf{b}_n and that of the external field, we use \mathbf{b}_n to define unidirectional transcription spaces T_n given by the surface of a sphere of radius b_n . Each point on T_n corresponds to an orientation of a biped of length b_n and there exists a one-to-one mapping between C_p and T_n . All unidirectional transcription spaces T_n can be jointly represented in a polydirectional transcription space T_{poly} as concentric spheres of radius b_n , Fig. 3b. One point in polydirectional control space C_p is simultaneously translated into a ray in polydirectional transcription space T_{poly} . The intersection between the ray and each

unidirectional transcription space is a point that indicates the orientation of the rod. The entire modulation loop \mathcal{L}_p in \mathcal{C}_p is transcribed into a cone with arbitrary cross-section in $\mathcal{T}_{\text{poly}}$. The intersection between \mathcal{T}_n and the cone is \mathcal{L}_n , the modulation loop for bipeds of length b_n .

Topological classes. A biped is subject to a total potential dominated by $-\mathbf{H}_{\text{ext}} \cdot \mathbf{H}_p$, the coupling between the external and the pattern fields^{22,23}. This coupling leads to an effective biped potential V_n proportional to the difference in magnetostatic potential at the two feet. That is,

$$V_n(\mathbf{r}, \mathbf{b}_n) \propto \psi(\mathbf{r} + \mathbf{b}_n/2) - \psi(\mathbf{r} - \mathbf{b}_n/2), \quad (1)$$

with the biped centered at \mathbf{r} . Note V_n depends explicitly on \mathbf{H}_{ext} via the one-to-one correspondence between \mathbf{b}_n and \mathbf{H}_{ext} . Transport of a biped b_n after completion of one modulation loop \mathcal{L}_n occurs provided that \mathcal{L}_n winds around fences, which are those orientations \mathbf{b}_n for which the potential is marginally stable²³, i.e., the set of biped orientations for which $\nabla V_n = 0$ and $\det(\nabla \nabla V_n) = 0$. For the present square pattern, both conditions are fulfilled along two perpendicular lines in $\mathcal{T}_{\text{poly}}$ running through the origin ($b_n = 0$) and parallel to the lattice vector directions. The biped potential is periodic and invariant under the simultaneous transformation $\mathbf{b}_n \rightarrow \mathbf{b}_n + \mathbf{a}_i$ and $\mathbf{r} \rightarrow \mathbf{r} + \mathbf{a}_i/2$ with \mathbf{a}_i , $i = \{1, 2\}$, a lattice vector, cf. Eq. (1). The same periodicity in $\mathcal{T}_{\text{poly}}$ applies therefore to the fences, which form a square grid of two mutually perpendicular sets of parallel lines separated by one lattice vector, \mathcal{F}_1 and \mathcal{F}_2 , see Fig. 3b. The fences lie in the equatorial plane of $\mathcal{T}_{\text{poly}}$ (the plane of biped orientations parallel to the pattern). In each unidirectional transcription space \mathcal{T}_n the fences are points on the equator. Winding around a single fence line of \mathcal{F}_i transports the biped by one lattice vector $\pm \mathbf{a}_i$, depending on whether the loop winds in the same (+) or opposite (−) sense than the axial fence vector. Note that fence lines and lattice vectors are rotated by ninety degrees, cf. Figs. 1 and 2. After completion of a loop \mathcal{L}_n , a biped b_n is displaced by

$$\Delta \mathbf{r}(\mathcal{L}_n) = w_n^1(\mathcal{L}_n) \mathbf{a}_1 + w_n^2(\mathcal{L}_n) \mathbf{a}_2, \quad (2)$$

where $\mathbf{w}_n = (w_n^1, w_n^2)$ is the set of winding numbers of \mathcal{L}_n around the fences \mathcal{F}_1 and \mathcal{F}_2 . Two bipeds b_n and b_m of lengths smaller than the lattice constant a fall in the same topological class since for both of them there exist only two fence lines. Hence, any parallel polydirectional loop \mathcal{L}_p in \mathcal{C}_p is transcribed into modulation loops \mathcal{L}_n and \mathcal{L}_m that have the same set of winding numbers, i.e., $\mathbf{w}_n = \mathbf{w}_m$. However, two bipeds where at least one length is larger than the lattice constant, can be transported independently since it is always possible to find a parallel polydirectional loop in \mathcal{C}_p that is transcribed into two loops \mathcal{L}_n and \mathcal{L}_m with different winding numbers. That is, there exists a parallel polydirectional loop for which b_n and b_m fall into different topological classes. Examples of such loops are shown in Fig. 3.

Polydirectional degree. Theoretically and provided that no more than one biped is shorter than the lattice constant, it is always possible to find a parallel polydirectional loop \mathcal{L}_p that transports a collection of bipeds of different lengths independently. We call the number of simultaneously controlled lengths the degree of the parallel polydirectional loop. In Fig. 2 we have shown parallel polydirectional loops of degrees 2–6.

Robustness. The limitations in practice arise due to several factors such as the precision of the orientation of the field or deviations due to colloidal polydispersity. Let $\Delta(\mathcal{L}_n)$ be the minimum Euclidian distance from the unidirectional loop \mathcal{L}_n and

all the fences in $\mathcal{T}_{\text{poly}}$. Then $\Delta(\mathcal{L}_n)$ provides a direct measurement of the robustness of the transport of a biped b_n ; the larger value of Δ , the more robust the transport is. We define the robustness of a parallel polydirectional loop of degree l transporting a set of bipeds of lengths $\{b_{n_1}, \dots, b_{n_l}\}$ as the minimum value of all individual distances to the fences, i.e.,

$$\rho(\mathcal{L}_p) = \frac{2}{a} \min\{\Delta(\mathcal{L}_{b_{n_1}}), \dots, \Delta(\mathcal{L}_{b_{n_l}})\}, \quad (3)$$

where the prefactor $2/a$ normalizes the robustness such that $0 < \rho < 1$. The robustness decreases with the polydirectional degree, see values in Fig. 2. Experimentally the transport with parallel hexadirectional loops \mathcal{L}_p of robustness as low as $\rho = 0.06$ is still reliable.

Compaction. The parallel polydirectional loop is more efficient than multiplexing. That is, addressing sequentially each command, understood as the transport of one biped by one-unit vector. Using parallel polydirectional commands, a single command corresponds to a fundamental loop crossing the equator of \mathcal{C}_p twice. We define the compaction c of a target transport as the ratio of the number of parallel polydirectional commands required and the number of commands in multiplexing. We have implemented a program that optimizes the driving loop by reducing the number of commands, while fulfilling the desired robustness requirements for a given set of target bipeds and displacements. The more robustness we require the less compact the parallel polydirectional loop is. One needs to find a compromise between compaction and robustness. Both the compaction and the robustness are indicated in Fig. 2.

Even though we have not designed tasks that are prompted to be compacted, we achieve a compaction of up to 1/2 and much better values can be obtained for suitable tasks. An example with compaction $c = 1/72$ and robustness $\rho = 0.02$ is shown in Fig. 4 and Supplementary Movie 8, where thirteen bipeds of different lengths between b_2 and b_{19} are transported into roughly the same direction but with different magnitudes of the total displacement, which are in all cases commensurate with the lattice constant a .

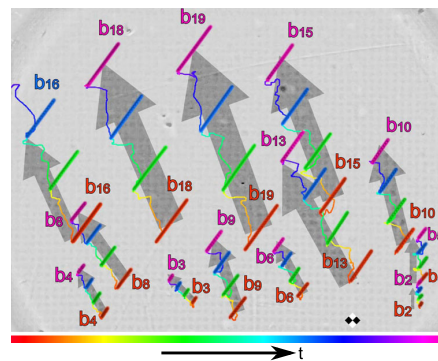


Fig. 4 Experimental trajectories of bipeds with lengths between b_2 and b_{19} . The bipeds are driven by a fundamental loop on a pattern with lattice constant $a \approx 7 \mu\text{m}$. The color of each of the thirteen bipeds and their trajectories indicates the time progress of the repeating control loop (see colorbar). The biped b_4 shares the same winding number with the biped b_6 . The biped b_{16} shares the same winding number with the biped b_{18} . The low robustness, $\rho = 0.02$, causes discrepancies between the theoretically computed and the experimentally observed winding numbers for the bipeds b_{13} and b_{15} . The compaction of the loop is $c = 1/72$. A square region of the pattern of diagonal $2a$ is sketched for scale and to indicate the relative orientation.

The modulation loop is shown in Supplementary Fig. 4. Although the robustness is low, the experimental and theoretical winding numbers agree with each other. Only for b_{13} and b_{15} the experimental values slightly deviate from the expected winding numbers (error $\Delta w = \pm 1$). Despite this deviation, the modulation can still be used to separate the bipeds but it can no longer be used to steer the bipeds independently into any direction since that requires an exact matching of experimental and theoretical winding numbers.

Discussion

The complete and simultaneous control over a collection of different objects that we have shown here would be much more difficult to achieve using the ratchet effect. To highlight the differences, consider the transport of stochastic on-off ratchets², in which a periodic biased potential consisting of two nonequivalent minima is repeatedly switched on and off. The potential nonequivalently confines a particle to a local minimum during the on-phase. When the potential is switched off, the particles can freely diffuse. Effective ratchet-like transport occurs by adjusting the duration of the off-period, since the diffusive time to escape from each potential minimum depends on the escape direction. A ratchet always needs a finite characteristic frequency, determined by the intrinsic dynamics of the system. It is very difficult to adjust several frequencies for different species such that the ratchet effect can work simultaneously for particles of e.g., different shapes. In our approach, which is conceptually closer to a Thouless pump²⁹ than to the ratchet effect, we also have a potential that is biased by the external magnetic field. However, we avoid ratchet effects and we do not have an off-period. The bipeds always stay in their local minimum to which they are nonergodically confined. Transport occurs solely due to the parametric dependence of the potential on the external field and the enslaved biped direction. Particles follow adiabatically the local minimum at any time during the modulation. Hence, the transport is not the result of a smart choice of dynamic parameters but due to the complexity of the parametric dependence of the topology of the potential on the external field. The transport occurs in the adiabatic limit of vanishing driving frequency. Since the topology is robust, the transport is also robust and feasible in a finite range of frequencies.

Nevertheless, high modulation frequencies must be avoided due to a broadening of the fences. This broadening has almost no effect when manipulating one or two biped lengths, but it makes it very difficult to prescribe the motion of a collection of bipeds due to the occurrence of ratchets. These two-dimensional ratchets lead not only to flux reversal but also to a directional locking into new directions⁴. Another reason to avoid high modulation frequencies is the shape of the rods. The straight shape of the bipeds is due to the dipolar interactions, but the bipeds are quite flexible. High modulation frequencies alter the shape of the rods, changing therefore the topological properties of the transport. This limitation can be alleviated using rigid anisotropic colloidal particles instead of an assembly of colloidal beads.

We have restricted here to rod-like colloidal particles. Elongated enough particles will behave in a similar fashion independently of the precise shape. We expect particles with significant different shapes, e.g., L- or triangular-like colloidal particles, to have completely different topological properties such that it might be possible to control their transport independently.

In summary, using topological protection we have developed a colloidal parallel polydirectional command which delivers an unprecedented control over the simultaneous motion of a collection of colloidal particles. The parallel polydirectional command addresses individually but simultaneously the motion of up

to six colloidal bipeds of different lengths. Brownian diffusion does not play any role in our system since the external energy is very large compared to the thermal energy. Hence, it would be possible to construct a macroscopic analog of the system using e.g., an arrangement of NbB-magnets³⁰. Downscaling the system from the meso- to the nanoscale is challenging since thermal fluctuations might play a role, broadening the fences and facilitating therefore ratchets.

The parallel polydirectional command paves the way to exciting new applications in colloidal science such as e.g., the automatic quality control of chemical reactions and the parallel computing with colloids. Using directional interparticle interactions, such as in the case of patchy colloids³¹, it might be possible to program the assembly of colloids into clusters of complex and predefined shapes that are then transported to the desired direction. Moreover, our methodology and ideas for the simultaneous control of objects that belong to different topological classes can be transferred to other systems for which topological protection is at work.

Methods

Pattern. The pattern is a thin Co/Au layered system with perpendicular magnetic anisotropy lithographically patterned via ion bombardment^{32,33}. The pattern consists of a square lattice of magnetized domains with a mesoscopic pattern lattice constant of either $a = 11 \mu\text{m}$ or $a = 7 \mu\text{m}$, see a sketch in Fig. 1a. The magnetic pattern is spin coated with a $1.6 \mu\text{m}$ polymer film that serves as a spacer.

External field. The uniform external magnetic field has a magnitude of $H_{\text{ext}} = 4 \text{ kA m}^{-1}$ (smaller than the coercive field of the magnetic pattern) and it is generated by three computer-controlled coils arranged around the sample at 90° .

Preparation of the initial states. Paramagnetic colloids are dispersed in water and placed above the magnetic pattern. Without external field the colloids are dispersed mainly as single particles above the pattern. Application of the external field leads to the assembly of random length and random position rods above the pattern. A glass capillary with tip diameter of a few micron attached to a micro manipulator is used to change the length and position of the bipeds to the desired relative initial arrangement while the external field remains in the equatorial plane.

Visualization. The colloids and the pattern are visualized using reflection microscopy. The pattern is visible because the ion bombardment changes the reflectivity of illuminated regions as compared to that of the masked regions. A camera records video clips of the bipeds.

Compacted parallel polydirectional loop. To find the loop \mathcal{L}_p for given target displacements w_{n1}, \dots, w_{nl} for a set of target lengths b_{n1}, \dots, b_{nl} we start by calculating all fence points for each target length. Then, we transcribe the fence points back to control space C_p by rescaling. All fence points in C_p lie on the equator (see Fig. 1b yellow and pink circles) and hence they differ only by the azimuthal angle of the external field. For every neighboring fence azimuthal angles we choose one intermediate azimuthal angle between them. These intermediate points are then transcribed to each of the unidirectional transcription spaces of the target set of bipeds and we calculate their minimum distance Δ to the fences. The intermediate points having transcriptions with Δ smaller than a fixed threshold are discarded. Every pair formed by two of the non-discarded points defines a fundamental parallel polydirectional loop. Every fundamental parallel polydirectional loop causes a unidirectional displacement for every target length and hence can be represented as a displacement in a $2l$ -dimensional vector space of the l target lengths. As the target displacements can be represented in this vector space, the parallel polydirectional loop \mathcal{L}_p can be found as an integer linear combination of fundamental parallel polydirectional loops, i.e., by solving the resulting system of linear equations. Note that only an integer number of every fundamental loop is valid as a solution since only integer winding numbers are possible. If the selected threshold for the robustness is too large, it may be impossible to find an integer solution, but there is always a solution if we sufficiently reduce the minimum robustness. There exist an infinite number of parallel polydirectional loops decoding the same displacements and the one found by solving the linear system of equations is just one of them, not necessarily the most compact. Therefore, we obtain a compaction of this parallel polydirectional loop by searching for pairs (and triplets) of fundamental loops in the parallel polydirectional loop that can be replaced by a single fundamental loop having the same net displacement. This is repeated in an iterative scheme until no further compaction of the loop is found. See Supplementary Movie 9 for a detailed visual explanation of the algorithm.

Computer simulations. All parallel polydirectional loops considered here have been also implemented in computer simulations and the colloidal transport matches that found experimentally. Compare, for example, the experimental and simulated trajectories shown in Supplementary Movies 4 and 7, respectively. We simulate the system using overdamped Brownian dynamics. The equation of motion is integrated in time using the standard Euler algorithm. Colloidal particles are modeled as point particles interacting via a Weeks–Chandler–Anderson and a dipolar interparticle potential. Each point particle is subject to the colloidal single particle potential proportional to $-\mathbf{H}_{\text{ext}} \cdot \mathbf{H}_p(\mathbf{r})$.

Fences. We express the magnetostatic potential as a Fourier series, see refs. ^{22,23}. The Fourier modes decay exponentially such that at sufficiently high elevations only the first mode contributes (the spacer forces the colloids to be at high elevations). The fences are found by simultaneously solving the equations $\nabla V_n = 0$ and $\det(\nabla \nabla V_n) = 0$, which for the case of a square pattern is straight forward. See the example for point particles (b_0) in ref. ²³.

Data availability

All the data supporting the findings are available from the corresponding author upon reasonable request.

Received: 9 April 2020; Accepted: 25 August 2020;

Published online: 16 September 2020

References

- McDonald, M. P., Spalding, G. C. & Dholakia, K. Microfluidic sorting in an optical lattice. *Nature* **426**, 421–424 (2003).
- Reimann, P. Brownian motors: noisy transport far from equilibrium. *Phys. Rep.* **361**, 57–265 (2002).
- Skaug, M. J., Schwemmer, C., Fringes, S., Rawlings, C. D. & Knoll, A. W. *Nanofluidic rocking Brownian Mot. Sci.* **359**, 1505–1508 (2018).
- Gopinathan, A. & Grier, D. G. Statistically locked-in transport through periodic potential landscapes. *Phys. Rev. Lett.* **92**, 130602 (2004).
- Add a language to a polyglot. user62131 et al. Posted Dec 6 '16 at 18:59 <https://codegolf.stackexchange.com/questions/102370/add-a-language-to-a-polyglot> (2017).
- DiVincenzo, D. P. Quantum computation. *Science* **270**, 255–261 (1995).
- Shor, P. W. Polynomial-time algorithms for prime factorization and discrete logarithms on a quantum computer. *SIAM J. Comput.* **26**, 1484–1509 (1997).
- Kitaev, A. Y. Fault-tolerant quantum computation by anyons. *Anna Phys.* **303**, 2–30 (2003).
- Adleman, L. Molecular computation of solutions to combinatorial problems. *Science* **266**, 1021–1024 (1994).
- Lipton, R. J. DNA solution of hard computational problems. *Science* **268**, 542–545 (1995).
- Qian, L. & Winfree, E. Scaling up digital circuit computation with DNA strand displacement cascades. *Science* **332**, 1196–1201 (2011).
- Amir, Y. et al. Universal computing by DNA origami robots in a living animal. *Nat. Nanotechnol.* **9**, 353–357 (2014).
- Church, G. M., Gao, Y. & Kosuri, S. Next-generation digital information storage in DNA. *Science* **337**, 1628 (2012).
- Rothemund, P. W. K. & Folding, D. N. A. to create nanoscale shapes and patterns. *Nature* **440**, 297–302 (2006).
- Ilievski, F., Mazzeo, A. D., Shepherd, R. F., Chen, X. & Whitesides, G. M. Soft robotics for chemists. *Angew. Chem. Int. Ed.* **50**, 1890–1895 (2011).
- Päun, G. Computing with membranes. *J. Comput. Syst. Sci.* **61**, 108–143 (2000).
- Adamatzky, A., Costello, B. D. L. & Asai, T. Reaction-diffusion computer. Elsevier (2005).
- Prakash, M. & Gershenfeld, N. Microfluidic bubble logic. *Science* **315**, 832–835 (2007).
- Kou, S. et al. Fluorescent molecular logic gates using microfluidic devices. *Angew. Chem. Int. Ed.* **47**, 872–876 (2008).
- Phillips, C. L. et al. Digital colloids: reconfigurable clusters as high information density elements. *Soft Matter* **10**, 7468–7479 (2014).
- Cui, J. et al. Nanomagnetic encoding of shape-morphing micromachines. *Nature* **575**, 164–168 (2019).
- Loehr, J. et al. Lattice symmetries and the topologically protected transport of colloidal particles. *Soft Matter* **13**, 5044–5075 (2017).
- de las Heras, D., Loehr, J., Lönne, M. & Fischer, T. M. Topologically protected colloidal transport above a square magnetic lattice. *N. J. Phys.* **18**, 105009 (2016).
- Asbury, C. L. Kinesin: world's tiniest biped. *Curr. Opin. Cell Biol.* **17**, 89–97 (2005).
- Shik, M. L. & Orlovsky, G. N. Neurophysiology of locomotor automatism. *Physiol. Rev.* **56**, 465–501 (1976).
- Hamacher, D., Herold, F., Wiegel, P., Hamacher, D. & Schega, L. Brain activity during walking: a systematic review. *Neurosci. Biobehav. Rev.* **57**, 310–327 (2015).
- Holmes, P., Full, R. J., Koditschek, D. & Guckenheimer, J. The dynamics of legged locomotion: models, analyses, and challenges. *SIAM Rev.* **48**, 207–304 (2006).
- Sherman, W. B. & Seeman, N. C. A precisely controlled DNA biped walking device. *Nano Lett.* **4**, 1203–1207 (2004).
- Thouless, D. J. Quantization of particle transport. *Phys. Rev. B* **27**, 6083–6087 (1983).
- Rossi, A. M. E. B. et al. Hard topological versus soft geometrical magnetic particle transport. *Soft Matter* **15**, 8543–8551 (2019).
- Wang, Y. et al. Colloids with valence and specific directional bonding. *Nature* **491**, 51–55 (2012).
- Chappert, C. et al. Planar patterned magnetic media obtained by ion irradiation. *Science* **280**, 1919–1922 (1998).
- Kuświk, P. et al. Colloidal domain lithography for regularly arranged artificial magnetic out-of-plane monodomains in Au/Co/Au layers. *Nanotechnology* **22**, 095302 (2011).

Acknowledgements

This work is funded by the Deutsche Forschungsgemeinschaft (DFG, German Research Foundation) under project number 440764520.

Author contributions

M.M.K., A.d.E., D.d.I.H., and T.M.F. designed and performed the experiment, and wrote the paper with input from all the other authors. M.U. and F.S. produced the magnetic film. J.G., A.r.E., and M.R. performed the fabrication of the micromagnetic domain patterns within the magnetic thin film.

Funding

Open Access funding provided by Projekt DEAL.

Competing Interests

The authors declare no competing interests.

Additional information

Supplementary information is available for this paper at <https://doi.org/10.1038/s41467-020-18467-9>.

Correspondence and requests for materials should be addressed to T.M.F.

Peer review information *Nature Communications* thanks David Grier, Giovanni Volpe and the other, anonymous, reviewer(s) for their contribution to the peer review of this work. Peer reviewer reports are available.

Reprints and permission information is available at <http://www.nature.com/reprints>

Publisher's note Springer Nature remains neutral with regard to jurisdictional claims in published maps and institutional affiliations.



Open Access This article is licensed under a Creative Commons Attribution 4.0 International License, which permits use, sharing, adaptation, distribution and reproduction in any medium or format, as long as you give appropriate credit to the original author(s) and the source, provide a link to the Creative Commons license, and indicate if changes were made. The images or other third party material in this article are included in the article's Creative Commons license, unless indicated otherwise in a credit line to the material. If material is not included in the article's Creative Commons license and your intended use is not permitted by statutory regulation or exceeds the permitted use, you will need to obtain permission directly from the copyright holder. To view a copy of this license, visit <http://creativecommons.org/licenses/by/4.0/>.

© The Author(s) 2020

Publication 1



Supporting Information

SUPPLEMENTARY NOTE 1

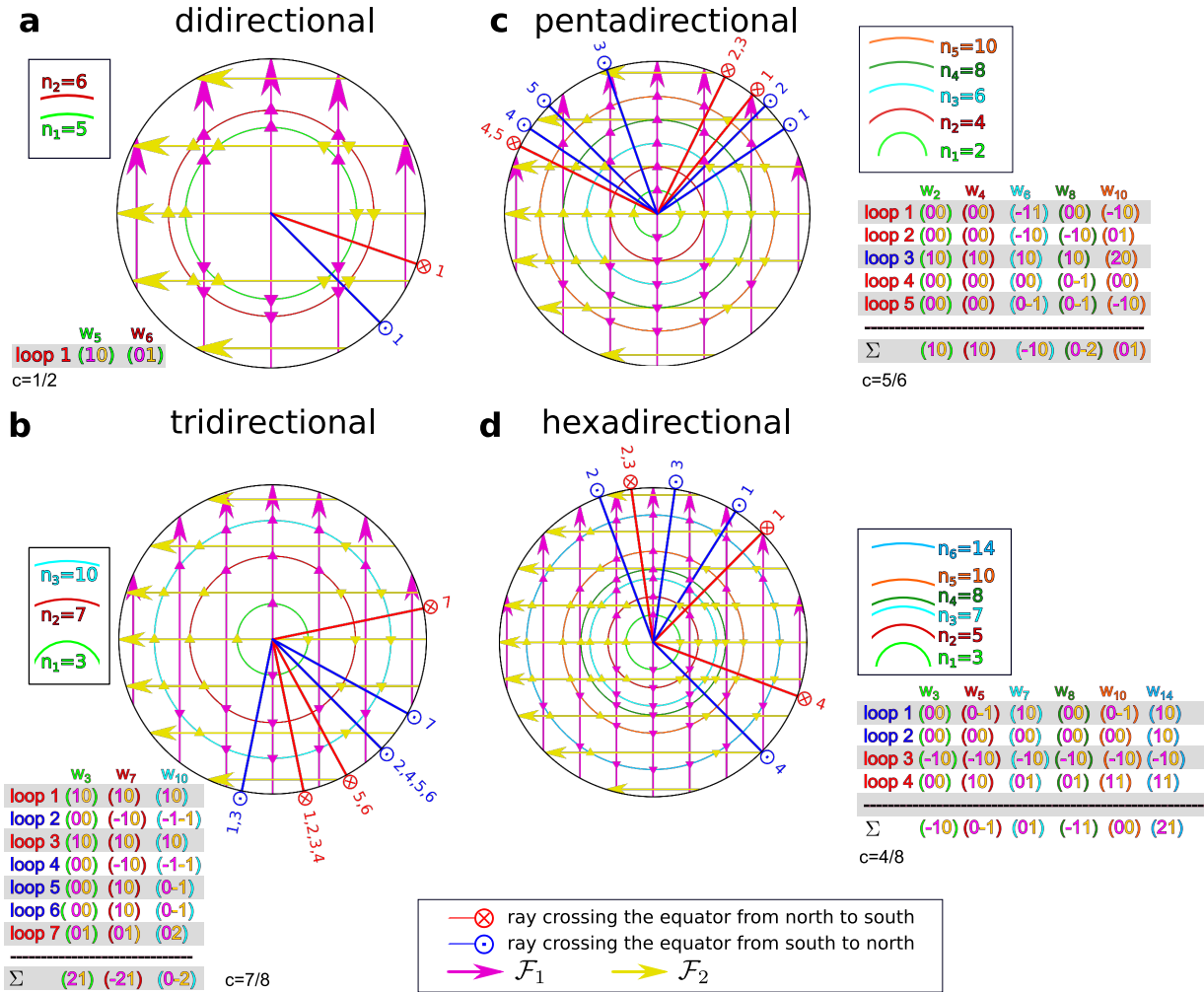
We describe here the parallel polydirectional loops used to control the simultaneous motion of bipeds shown in both Fig. 2 of the main text and the Supplementary Movies. In all cases, the loops are shown in polydirectional transcription space $\mathcal{T}_{\text{poly}}$. The loops transport a set of l bipeds of lengths b_{n1}, \dots, b_{nl} . Supplementary Fig. 1 shows the loops that control the motion of the parallel didirectional command $l = 2$ (a), the parallel tridirectional command $l = 3$ (b), the parallel pentadirectional command $l = 5$ (c), and the parallel hexadirectional command $l = 6$ (d). The parallel tetradirectional loop $l = 4$ is depicted in Supplementary Fig. 2.

In both figures we plot a top view of the equatorial plane in $\mathcal{T}_{\text{poly}}$, the cuts of the target unidirectional spheres $\mathcal{T}_{n1}, \dots, \mathcal{T}_{nl}$ with the equatorial plane (colored concentric circles), the fences \mathcal{F}_i with $i = 1, 2$, and the rays in $\mathcal{T}_{\text{poly}}$ that are transcribed into $\mathcal{T}_{\text{poly}}$ from the equatorial crossings of the parallel polydirectional loop \mathcal{L}_p in control space \mathcal{C}_p . A fundamental parallel polydirectional loop \mathcal{L}_p in \mathcal{C}_p can wind in the clockwise (-) or counterclockwise (+) direction around the fence points within the smaller enclosed area. In Supplementary Fig. 1 and Supplementary Fig. 2 we show tables next to each equatorial plane indicating whether the loop winds clockwise (red) or counterclockwise (blue).

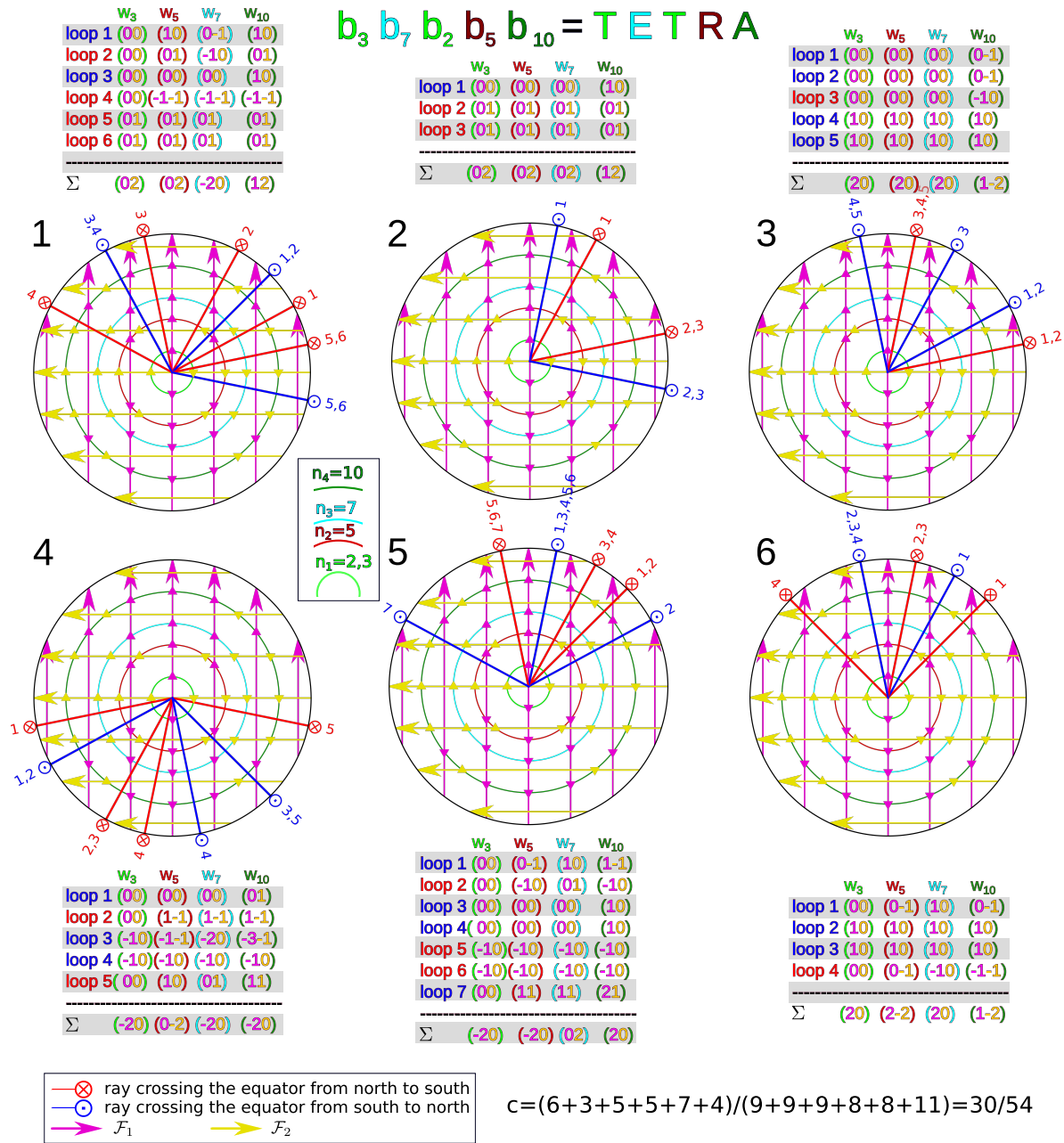
Up and down triangles are drawn at the intersections of the fences with the unidirectional transcription spheres. Triangles are up (down) if the scalar product of the tangent vector of the ray toward the triangle with the tangent vector of the fence is positive (negative). Taking the difference of up triangles and down triangles on a unidirectional arc inside a fundamental cone and multiplying with the winding sense of the fundamental loop gives the winding number of the particular unidirectional fundamental loop \mathcal{L}_{ni} for the chosen target length b_{ni} . Hence, the winding numbers can be read directly from the equatorial plots. In addition, all winding numbers are listed in the tables.

In Supplementary Fig. 3 we show a complex heptadirectional loop. We aim the reader to decipher the associated winding numbers and trajectories.

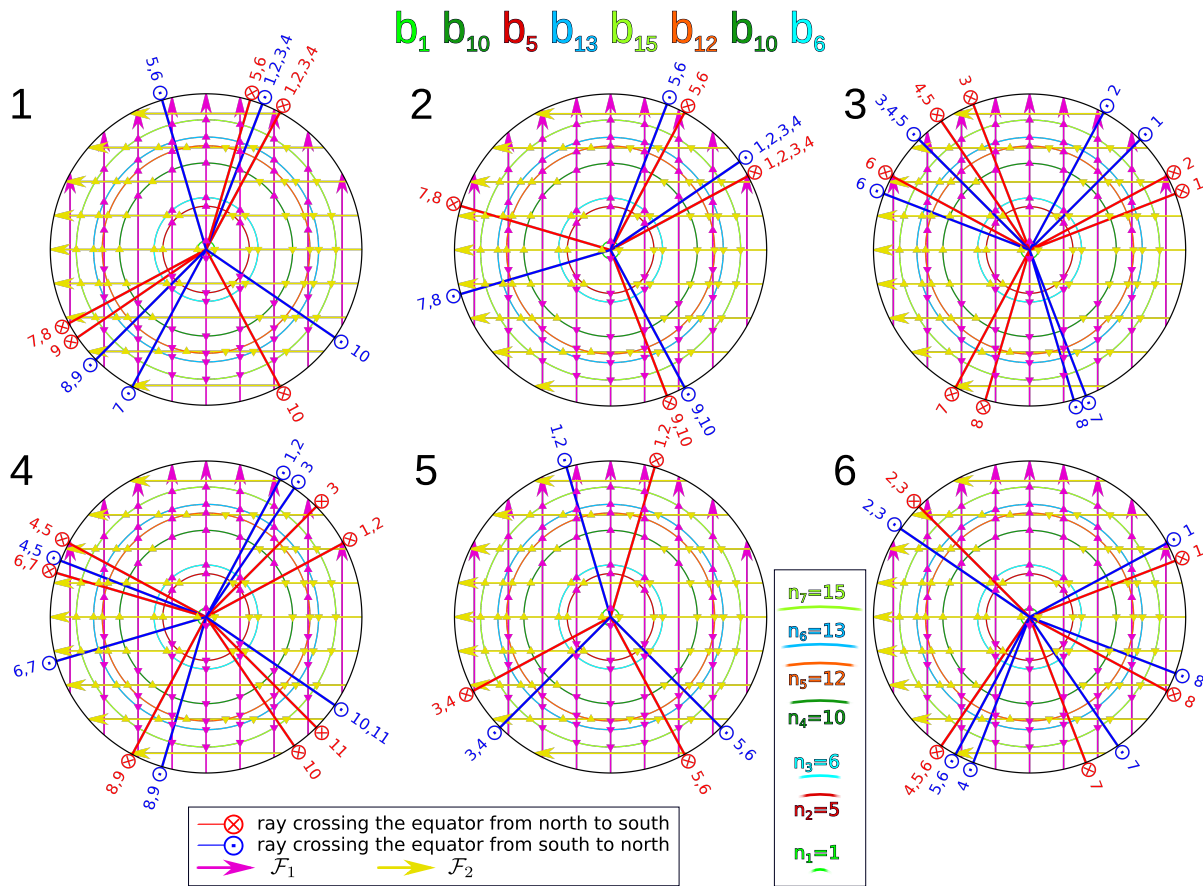
Finally, in Supplementary Fig. 4 we show a complex undecasorting loop with a table comparing the experimental and theoretical winding numbers.



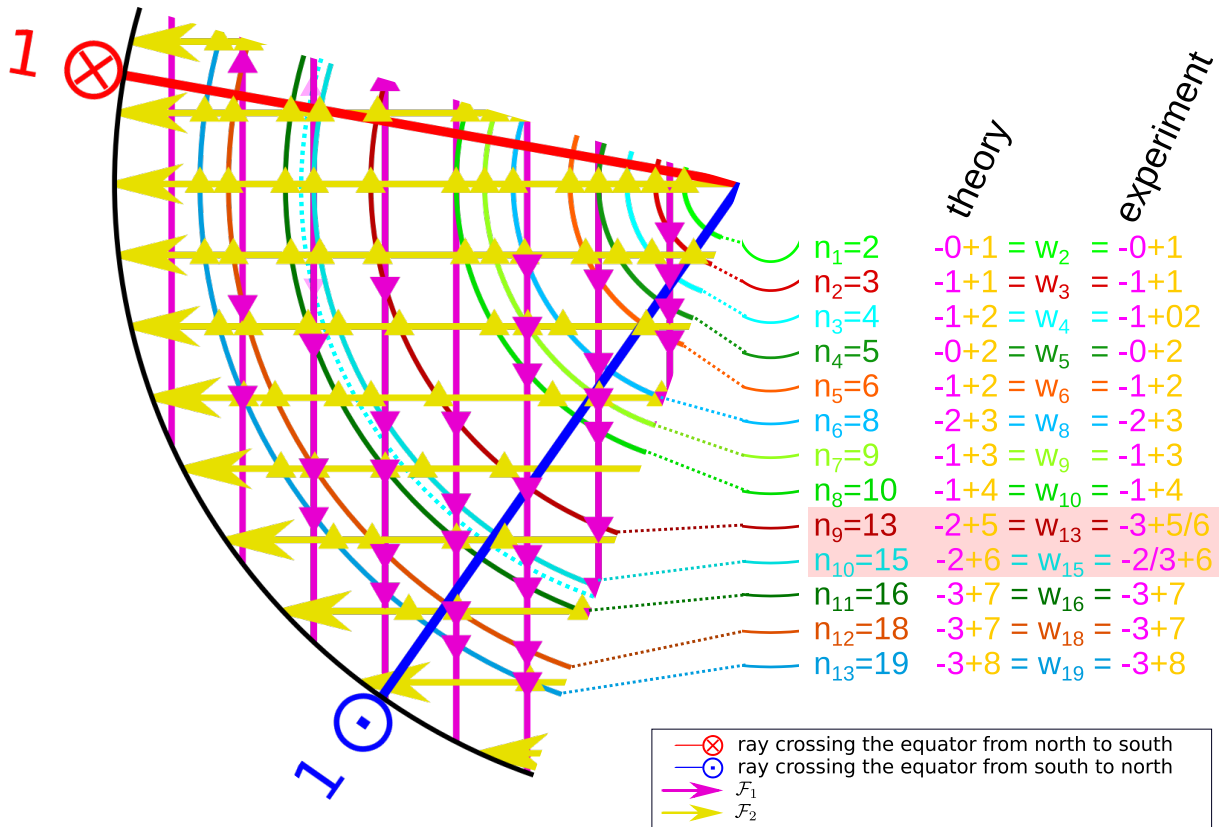
Supplementary Fig. 1. **Modulation loops in transcription space $\mathcal{T}_{\text{poly}}$.** Top view of the equatorial plane of $\mathcal{T}_{\text{poly}}$ showing the fences \mathcal{F}_1 and \mathcal{F}_2 , the unidirectional transcription spaces (concentric circles) \mathcal{T}_{n_i} with $i = 1, \dots, l$ the number of different bipeds transported by the loop, and the modulation loops of **a** the parallel didirectional command, **b** the parallel tridirectional command, **c** the parallel pentadirectional command and **d** the parallel hexadirectional command. A table indicating the winding numbers around each fence and the compaction of the loop are also depicted for each case. The procedure to read the loops is as follows. Pick the first fundamental loop 1 and determine its orientation (± 1 for mathematical positive respectively negative sense). For example, loop 1 of the parallel didirectional command (parallel hexadirectional command) has negative (positive) orientation. Next, subtract the number of pink-down triangles from that of pink-up triangles on the b_{n_1} arcs of the fundamental loop 1 and multiply it with the orientation of the loop to obtain the \mathbf{a}_1 -displacement of the n_1 -biped during the loop 1. Repeat same procedure with the yellow triangles to obtain the \mathbf{a}_2 -displacement. Repeat this for the other lengths $b_{n_2} - b_{n_l}$ to obtain all unidirectional displacements. Count the total number of fundamental loops of the polydirectional command and compare it with the number of nearest neighbor displacements needed if multiplexing. To each polydirectional command we provide a table with the winding numbers of the fundamental loops as well as the sum of the concatenated complex polydirectional command for comparison. Fundamental loops with positive (negative) orientations are marked as blue (red) in the table.



Supplementary Fig. 2. **Modulation loop in transcription space $\mathcal{T}_{\text{poly}}$ for the parallel tetradirectional command.** The loop induces a set of $l = 5$ bipeds to write the word TETRA as shown in Fig. 2c of the main text and the Supplementary Videos. Each letter is written in six different steps. Each equatorial plane shown in the figure represents one of these steps, as indicated. See caption of Fig. 1 for a complete explanation on how to read the fundamental loops. The word TETRA appears when the bipeds are ordered as $b_3, b_7, b_2, b_5, b_{10}$.



Supplementary Fig. 3. **Parallel heptadirectional command.** The loop encrypts seven letters, each one with six steps. Each equatorial plane contains the fundamental loops of one step. All fundamental loops have positive orientation here. The procedure to read the loops is the same as that explained in the caption of Fig. 1. The encrypted word appears when the bipeds are ordered as $b_1, b_{10}, b_5, b_{13}, b_{15}, b_{12}, b_{10}, b_6$. The compaction of the loop is $c = 30/54$ (see caption of Fig. 1 for an explanation on how to calculate the compaction). If you find a robust parallel heptadirectional command with less fundamental loops encoding the same word, please let us know!



Supplementary Fig. 4. **Modulation loops in transcription space $\mathcal{T}_{\text{poly}}$.** Top view of the equatorial plane of $\mathcal{T}_{\text{poly}}$ showing the fences \mathcal{F}_1 and \mathcal{F}_2 , the unidirectional transcription spaces (concentric circles) \mathcal{T}_{ni} with $i = 1, \dots, 13$ of the thirteen different bippeds transported by the loop, and the modulation loops of parallel undecasorting command. A table indicating the theoretical winding numbers around each fence and the experimentally observed winding numbers of the motion illustrated in Fig 4 of the main text are listed for a comparison. Discrepancies in winding numbers occur for the bippeds b_{13} and b_{15} , which are marked in red in the table. An incomplete locking between \mathbf{H}_{ext} and \mathbf{b}_{13} due to nonadiabatic effects could be the reason for observed differences for the b_{13} -biped, for which \mathcal{T}_{13} , \mathcal{F}_2 and \mathcal{L}_{13} almost fall on top of each other. The dotted transcription space is a transcription space for biped size $b_{15.3} > b_{15}$, that would contain an extra crossing of the fence \mathcal{F}_1 , shown as transparent pink triangle demonstrating that a 2 % increase in length of the biped could explain the discrepancies between experiment and theory for the b_{15} -biped.

Description of Additional Supplementary Files

Supplementary movie 1.mp4 Brownian dynamics simulation of a b_5 biped subject to the loop presented in figure 1 and figure 3. The foot of the biped must slide into the position that commensurate with the lattice when the control loop of the external field passes close to a fence point.

Supplementary movie 2.mp4 Reflection microscopy recording of the experiment of the didirectional command in figure 2a. To the right we show the motion of the external field in control space and the equatorial plane of the polydirectional transcription space.

Supplementary movie 3.mp4 Reflection microscopy recording of the experiment of the tridirectional command in figure 2b. To the right we show the motion of the external field in control space and the equatorial plane of the polydirectional transcription space.

Supplementary movie 4.mp4 Reflection microscopy recording of the experiment of the tetradirectional command in figure 2c. To the right we show the equatorial plane of the polydirectional transcription space. The tetradirectional command consists of six complex loops that are repeated three times and they have different rays in the equatorial planes.

Supplementary movie 5.mp4 Reflection microscopy recording of the experiment of the pentadirectional command in figure 2d. To the right we show the equatorial plane of the polydirectional transcription space.

Supplementary movie 6.mp4 Reflection microscopy recording of the experiment of the hexadirectional command in figure 2e. To the right we show the equatorial plane of the polydirectional transcription space.

Supplementary movie 7.mp4 Brownian dynamics simulation of the tetradirectional command shown in figure 2c. Corresponding experiments are shown in Supplementary Movie 4.

Supplementary movie 8.mp4 Reflection microscopy recording of the experiment of the undecasorting command in figure 4. To the right we show the equatorial plane of the polydirectional transcription space. At the end of the movie we show that the bipeds are indeed self assembled bipeds that depolymerize to monomers and dimers if we switch off the external field.

Supplementary movie 9.mp4 Visual explanation of the algorithm to find a compacted loop with the desired transport directions.

Publication 2

Gauge invariant and gauge dependent aspects of topological walking colloidal bipeds

Soft Matter (submitted 16. 9. 2020)

Mahla Mirzaee-Kakhki^{a1}, Adrian Ernst^{a1}, Daniel de las Heras^{a2},
Maciej Urbaniak^b, Feliks Stobiecki^b, Andreea Tomita^c, Rico
Huhnstock^c, Iris Koch^c, Arno Ehresmann^c, Dennis Holzinger^c,
Thomas M. Fischer^{a1}

^{a1} Experimental Physics and ^{a2} Theoretical Physics, Faculty of Physics, Mathematics and Computer Science, University of Bayreuth, 95447 Bayreuth, Germany.

^b Institute of Molecular Physics, Polish Academy of Sciences, 60-179 Poznań, Poland.

^c Institute of Physics and Center for Interdisciplinary Nanostructure Science and Technology (CINSaT), Universität Kassel, D-34132 Kassel, Germany.

In section publication 1 we showed a magnetic polyglot language to let colloidal bipeds walk on a square patterns. The physics of the walking was not analyzed in too much detail. In section 1.5 we have shown that gauge theories are intimately connected to topological theories and we argued that a choice of the redundant gauge might be useful

to emphasize the underlying physics. In section 1.7 we have seen that describing the motion of objects in a low Reynolds number fluid takes on a specific symmetry for the instantaneous center of rotation. On the other hand biped variables separate into enslaved conformational variables and the center of mass location of the bipeds. Two gauges might be natural for the description of their motion. The question that naturally follows from publication 1 therefore is:

Question

Is a modified version of Wilceks shape space gauge freedom applicable to the transport of colloidal bipeds and can we learn something about the active and passive character of the walks from using different gauges when characterizing the transport?

My Contribution

The physics of walkers on four and three fold lattices was a joint effort between Adrian Ernst, who worked out the mathematical part and the computer control and simulations of the experiments and me who performed all the presented experiments and prepared all the initial states. Exchange-bias films have been produced by Maciej Urbaniak and Feliks Sobiecki in Poznan, the lithographic patterns were planned in Bayreuth as a team effort, and the ion-bombardment was done by Andreea Tomita, Rico Huhnstock, Iris Koch, Arno Ehresmann, and Dennis Holzinger in Kassel. The preparation and writing of the paper was done by all coauthors.

Gauge invariant and gauge dependent aspects of topological walking colloidal bipeds

Mahla Mirzaee-Kakhki^a, Adrian Ernst^a, Daniel de las Heras^a, Maciej Urbaniak^b, Feliks Stobiecki^b, Andreea Tomita^c, Rico Huhnstock^c, Iris Koch^c, Arno Ehresmann^c, Dennis Holzinger^c, and Thomas M. Fischer^{a1}

Received Date
Accepted Date

DOI: 10.1039/xxxxxxxxxx

www.rsc.org/journalname

Paramagnetic colloidal spheres assemble to colloidal bipeds of various length in an external magnetic field. When the bipeds reside above a magnetic pattern and we modulate the direction of the external magnetic field, the rods perform topologically distinct classes of protected motion above the pattern. The topological protection allows each class to be robust against small continuous deformations of the driving loop of the external field. We observe motion of the rod from a passive central sliding and rolling motion for short bipeds toward a walking motion with both ends of the rod alternately touching down on the pattern for long bipeds. The change of character of the motion occurs in form of discrete topological transitions. The topological protection makes walking a form of motion robust against the breaking of the non symmorphic symmetry. In patterns with non symmorphic symmetry walking is reversible. In symmorphic patterns lacking a glide plane the walking can be irreversible or reversible involving or not involving ratchet jumps. Using different gauges allows us to unravel the active and passive aspects of the topological walks.

1 Rolling, walking, and limping

Rolling is a process where a wheel winds around its axis and thereby translates on a support. If the propulsion distance of the wheel matches the wheel circumference the rolling is with a non-slip condition. Otherwise the rolling is with slip. Walking is generically a symmetric process differing from rolling, where both feet of a walking person perform alternating steps. The spatial period of walking is two steps, - not one step -, since the conformation of a person is restored after two steps and the conformation after an odd number of steps is related to the conformation after an even number of steps by a non-symmorphic group operation (a half period translation followed by a reflection known as a glide plane). The non-symmorphic symmetry can be broken in a trivial manner for example by breaking one of our legs in which case we start limping and the broken leg functions differently than its non-broken mirror image partner.

We may view symmetric walking as a symmetry reduced form of rolling and limping as a symmetry reduced form of walking.

For a rolling wheel all orientations of the wheel are of equivalent importance. A full rotation of the wheel passes through all equivalent orientations of the wheel in a continuous way. For a symmetric walker the symmetry of the motion is reduced to a two fold discrete symmetry as compared to the continuous symmetry of the wheel. The symmetry is further reduced when the walker limps.

A subtle, albeit psychologically undesirable¹ way of breaking the non-symmorphic symmetry of a symmetric walker is by letting him walk on a periodic structure with a period of the pattern commensurable with his step width. If the pattern has the period of one step but lacks the mirror symmetry of the non-symmorphic group operation of our two-step-periodic walker, we expect one foot to perform in a symmetry broken way compared to the other foot. One example of such walking is the motor protein Kinesin. It accomplishes transport by walking with its two heads (not its two feet) along a microtubule. The microtubule is a chiral periodic structure that lacks mirror symmetries such that we expect differences between the two heads even when the two heads walk in a "hand-over-hand" mechanism, where the kinesin heads step past one another, alternating the lead position^{2,3}.

A subtle way to allow for symmetric walking on a periodic pattern is to use a pattern with primitive unit vectors of two steps. If the space group of the pattern is non-symmorphic, containing the non-symmorphic group operation of our walker, the walker can

^{a1}University of Bayreuth, Physics, Universitätsstr. 30, 95447 Bayreuth (Germany) E-mail: Thomas.Fischer@uni-bayreuth.de

^bInstitute of Molecular Physics, Polish Academy of Sciences, ul. M. Smoluchowskiego 17, 60-179 Poznań (Poland).

^cInstitute of Physics and Center for Interdisciplinary Nanostructure Science and Technology (CINSA-T), University of Kassel, Heinrich-Plett-Strasse 40, D-34132 Kassel (Germany)

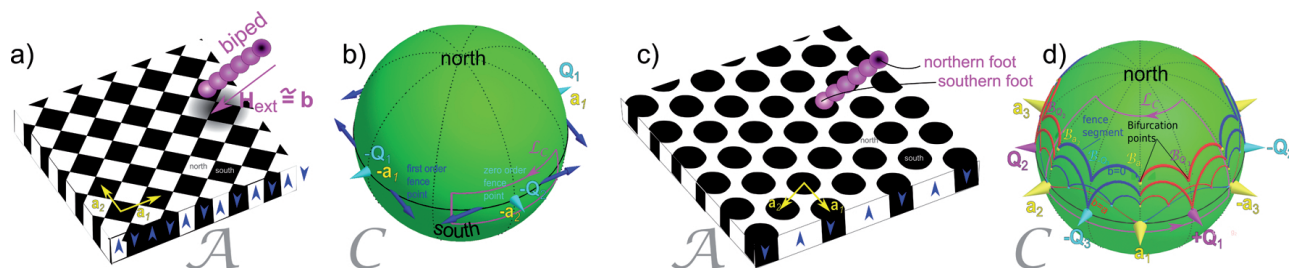


Fig. 1 a) Square (c) hexagonal) magnetic pattern with up (white) and down (black) magnetized regions, characterized by the primitive unit vectors \mathbf{a}_i (yellow) and primitive reciprocal unit vectors \mathbf{Q}_i (magenta). Colloids (magenta) assemble into a rod that functions as a biped with feet at both ends. The biped walks across the pattern as we apply modulation loops of the external magnetic field. The external field and thus the orientation \mathbf{b} varies on the surface of a sphere b) and d). The walk depends on how the modulation loops in control space wind around the fence points (segments) in control space b), d) that in general vary with the length b of the biped. We show a typical fundamental loop \mathcal{L}_C (purple) that causes different topologically protected transport for small and larger bipeds. Fence points for the square lattice in b) are the points pierced by the cyan and blue arrows. For the hexagonal lattice in d) segments of fence lines are depicted in red and blue and they meet in bifurcation points where the curvature of the fence diverges.

still walk in a symmetric way.

If instead we use a symmorphic pattern containing only symmorphic group elements the walker is expected to walk in a symmetry-broken way. Its left foot has to step onto a position that is not related by a symmetry operation to the position the right foot steps upon.

A further way of breaking the symmetry of a walker exists for driven systems, where the walker responds to external commands. If those commands lack a non-symmorphic symmetry in time our walker will perform a walk lacking the non-symmorphic glide symmetry.

2 Robust walking

Rolling and walking are both usually generated by a cyclic change of certain parameters that control and drive the motion. These parameters can be as diverse as certain signals of the spinal chord for walking humans^{4,5} or walking animals⁶, the concentration of complementary DNA-strands as well as temperature in DNA-bipeds⁷, or the geometric shape for geometric swimmers at low Reynolds numbers^{8,9}. We can thus define a control space \mathcal{C} that is the space of possible parameters that might occur while we drive the motion. For robust walking the result of a slightly perturbed loop in control space \mathcal{C} must result in a successful sequence of walking steps albeit the disturbance of the loop. For robotic walkers mathematical algorithms such as Lyapunov function based control algorithms or control barrier functions are employed to guarantee safe walking¹⁰. Another powerful way of ensuring such robust behavior is the use of topological invariants^{11–23}. If the control space \mathcal{C} is a not simply connected space the winding number $w(\mathcal{L}_C)$ of a loop \mathcal{L}_C around the holes in control space constitutes a topological invariant. A walk on a pattern is a topological walk if the number of steps $n_{step} = mw(\mathcal{L}_C)$ on the pattern is a non zero but low integer multiple ($m = \pm 1, \pm 2, \dots$) of the winding number irrespective of the details of how precisely and with which speed the loop in control space winds around a hole.

This robustness includes perturbations that break the non-symmorphic symmetry. When the walking is topologically robust, then the stronger foot of the walker must consistently make up for

its weaker partner in order to secure the commensurability with the period of the pattern. The robustness, however, also holds when we extend the two fold symmetry of a walker to the continuous symmetry of a rolling wheel. The space of orientations of a wheel is a not simply connected space and thus topological invariants can be used to control their motion on a pattern. In this work we morph the topological sliding rolling of a colloidal wheel into the topological equivalent motion of self assembled colloidal rods that either slide and roll or walk on symmorphic and non-symmorphic magnetic lattices. We show the topological robustness of the transport by successively deforming the wheel into a biped and by continuously changing the character of the motion from rolling toward walking. Topological transitions toward larger bipeds with discretely increasing step widths occur as the self assembled biped grows longer.

3 Experimental setup

We illustrate the richness of biped motion using a square magnetic lattice (Fig. 1a)^{24,25} with a glide plane and a magnetic hexagonal lattice (Fig. 1c) containing no glide plane. We study experimentally and with computer simulations the character of the biped motion. In the experiments, paramagnetic colloidal particles assembled to a rod of $n = 2 - 11$ particles move above a thin Co/Au layered system with perpendicular magnetic anisotropy lithographically patterned via ion bombardment^{25–27}. The pattern consists of a square (hexagonal) lattice of magnetized domains with a mesoscopic pattern lattice constant $a \approx 7 \mu\text{m}$ see a sketch in Figs. 1(a) and (c). The whole pattern is magnetized in the $\pm z$ -direction normal to the film. The magnetic pattern is spin coated with a $1.6 \mu\text{m}$ polymer film that serves as a spacer. The paramagnetic colloidal particles (diameter $2R = 2.8 \mu\text{m}$) are immersed in water. A uniform time-dependent external magnetic field $\mathbf{H}_{\text{ext}}(t)$ of constant magnitude ($H_{\text{ext}} = 4 \text{kAm}^{-1}$) is superimposed to the non-uniform and time-independent magnetic field generated by the pattern \mathbf{H}_p . The external field $\mathbf{H}_{\text{ext}}(t)$ is varied on the surface of a sphere and hence the topology of our control space \mathcal{C} is that of a punctured sphere (certain bifurcation or fence points are removed from the sphere which renders the sphere not

simply connected, see Figs. 1 (b) and (d)). We perform periodic modulation loops \mathcal{L}_C of the external field in control space \mathcal{C} to drive the system. The external field is strong enough to cause the paramagnetic particles to assemble into a rod because of induced dipolar interactions between them. The two ends of the rod are the two feet of our self assembled biped. The dipolar interactions are stronger than the buoyancy of the biped causing the biped to align with the external field, which generically lifts one foot of the biped from the ground while the other foot remains on the ground. Note that the locking of the orientation of the biped to the external field with the continuous variation of the external field causes each foot to always keep its magnetic character, i.e. the northern foot located at \mathbf{r}_N being a magnetic north pole and the southern foot at \mathbf{r}_S being a south pole. The vector $\mathbf{b} = \mathbf{r}_S - \mathbf{r}_N$ denotes the northern foot to southern foot vector of the biped. The locking of the biped orientation \mathbf{b} to the external field \mathbf{H}_{ext} allows to interchangeably use the sphere of biped orientations or the sphere of external field orientations as the control space. The southern foot will be on the ground when the external field points into the south of \mathcal{C} . The northern foot will be on the ground when the external field points into the north of \mathcal{C} . The transfer of support between the two feet occurs when the external field is within the tropics of \mathcal{C} .

The external magnetic field has negligible lateral gradients and the position of the biped is governed by the field gradients of the magnetic pattern. These gradients decay exponentially with the distance from the pattern. Therefore the location of the walker is with the grounded foot sitting within a local minimum of the colloidal potential (a foothold). The transfer of support is accompanied by a release of the lifting foot from the minimum of the colloidal potential and a sliding of the touching down foot into a new minimum (foothold). Generically the transfer of support will be associated with frustration as the length $b = 2(n-1)R$ of the biped will not match with the distance between consecutive minima.

4 Topological rolling transport of single spheres

Let us refer to the two-dimensional space the walker steps upon as action space \mathcal{A} . Special closed modulation loops in control space \mathcal{C} induce open walks in action space \mathcal{A} . In Refs.^{24,25,28} we demonstrated how the bulk rolling of single colloidal spheres (point particles) above magnetic lattices with different symmetries is topologically protected. We summarize here the main aspects of the sphere transport and refer the reader to Refs.^{24,25,28} for a complete description. For each lattice symmetry there exist special fundamental modulation loops of \mathbf{H}_{ext} in \mathcal{C} that induce transport of colloids in \mathcal{A} by a primitive lattice vector \mathbf{a}_i . These fundamental loops share a common feature, they wind around special objects that lie in \mathcal{C} ^{24,25,28} roughly in the direction of a primitive reciprocal unit vector perpendicular to the primitive lattice vector \mathbf{a}_i of the transport. A sphere does not walk because it is isotropic and has no foot. It adiabatically slides or rolls²⁹ on an externally controlled time scale and for very particular non trivial loops on a square lattice and in half of the non trivial loops on hexagonal

lattice it irreversibly slides on a faster intrinsic time scale. The character of the transport thus is that of a wheel rolling with slip between the wheel and the ground.

In the simplest case, a square lattice, the control space is characterized by just four zero order "fence" points on the equator lying along the directions of the primitive reciprocal lattice vectors²⁴, see Fig 1b). For a hexagonal lattice the objects are fence segments connecting bifurcation points in \mathcal{C} , see Fig 1d). We call a modulation loop encircling one of these objects a fundamental loop \mathcal{L}_{Q_i} . Each of these fundamental loops induces adiabatic transport in the sense that a single colloidal particle follows a minimum of the colloidal potential at any time. Hence, the position of the particle in \mathcal{A} parametrically depends on the position of the external magnetic field in \mathcal{C} . All modulation loops discussed in what follows can be viewed as concatenations of fundamental loops. The motion of a sphere is an adiabatic motion if the loop is encircling the object without cutting through it.

5 Theory of adiabatic topological walks

Because the transport of a colloidal sphere is topological it is robust to perturbations. Mathematically the surface of a colloidal sphere is a manifold of genus $g=0$ and it is topologically equivalent to a biped. In theory we may continuously distort the shape of a sphere into that of a biped. In experiments this distortion is achieved by an assembly of a discrete number of spheres into a biped rod rather than by continuously distorting a colloidal particle. If the perturbation introduced by this change of shape is not too strong the result of a control loop must be the same no matter whether the object is a sphere or a biped. Longer bipeds fall into topological equivalence classes that are different from that of a point particle.

We may write the pattern magnetic field as²⁴

$$\mathbf{H}_p = \nabla\psi \quad (1)$$

where

$$\psi(\mathbf{r}) \propto e^{-Qz} \sum_{n=1}^N \exp(i\mathbf{r}_A \cdot \mathbf{R}_N^n \cdot \mathbf{Q}_1) \quad (2)$$

is the magnetic potential and depends on the position $\mathbf{r} = (\mathbf{r}_A, z)$ that we have split into a lateral vector \mathbf{r}_A in action space \mathcal{A} and the normal component z . Making use of the periodicity of the pattern, topologically action space is equivalent to a torus. A path leading from one unit cell to a neighboring unit cell becomes a path that winds around the torus once. The vector \mathbf{Q}_1 denotes one of the N lowest non vanishing reciprocal lattice vectors of the 2D-lattice and $Q = 2\pi/a$ its modulus. The lattice is invariant under a 2D rotation \mathbf{R}_N by the angle $2\pi/N$ and the other $N-1$ equivalent reciprocal lattice vectors are obtained by successive rotations $\mathbf{Q}_{n+1} = \mathbf{R}_N \cdot \mathbf{Q}_n$. The projection of the pattern magnetic field onto the external field and averaged over the biped is the biped potential

$$V_{\text{biped}} \propto \psi(\mathbf{r}_S) - \psi(\mathbf{r}_N) \quad (3)$$

where \mathbf{r}_S and \mathbf{r}_N are the positions of the southern and the northern foot of the biped. The vector $\mathbf{b} = \mathbf{r}_S - \mathbf{r}_N$ denotes

the northern foot to southern foot vector of the biped. When the external magnetic field is strong compared to the pattern field the orientation \mathbf{b} is locked to the direction of the external field $\mathbf{b} \parallel \mathbf{H}_{ext}$. We may thus choose the vector space of \mathbf{b} as control space. In the limit $b \ll a$ the biped potential reduces to a point particle potential

$$V_{point} \propto \mathbf{b} \cdot \mathbf{H}_p \propto \mathbf{H}_{ext} \cdot \mathbf{H}_p \quad (4)$$

5.1 Gauges

We have discussed the topological properties of V_{point} in references^{24,25,28}.

We would like to write the position of both feet as a sum of an absolute position and a conformational position

$$\mathbf{r}_{S/N} = \mathbf{r}_{abs} + \mathbf{r}_{con,S/N} \quad (5)$$

such that the conformation position after the period T of a closed fundamental control loop \mathcal{L}_C is restored

$$\mathbf{r}_{con,S/N}(T) = \mathbf{r}_{con,S/N}(0) \quad (6)$$

and the translation $\Delta \mathbf{r}_{abs} = \mathbf{a}_i$ by lattice vector over a period is blamed onto the absolute position \mathbf{r}_{abs} . The decomposition equ. 5 carries a gauge freedom. We will make use of two choices of gauge. The *center gauge* simply choses the absolute position to be the center of the biped $\mathbf{r} = \mathbf{r}_{Abs} = (\mathbf{r}_S + \mathbf{r}_N)/2$ and the conformational coordinates as $\mathbf{r}_{con,S/N} = \pm \mathbf{b}/2$. This choice of gauge is useful since it splits the position into a vector $\mathbf{r} = (\mathbf{r}_A, z)$ in action space and a vector \mathbf{b} in control space. An alternative choice of the absolute position is the instantaneous center of rotation:

$$\mathbf{r}_{Abs} = \mathbf{r}_{ICR} \quad (7)$$

such that

$$d\mathbf{r}_{ICR} = d\mathbf{b} \cdot \nabla_{\mathbf{b}} \mathbf{r}_{ICR} = \mathbf{0} \quad (8)$$

exactly if

$$d\mathbf{b} \cdot \nabla_{\mathbf{b}} |\mathbf{r}_{ICR} - \mathbf{r}_S| = d\mathbf{b} \cdot \nabla_{\mathbf{b}} |\mathbf{r}_{ICR} - \mathbf{r}_N| = 0 \quad (9)$$

We call this gauge the *walker gauge* because equation 9 will hold whenever the biped foot remains within a non moving foothold such that either $\mathbf{r}_{ICR} = \mathbf{r}_S$ or $\mathbf{r}_{ICR} = \mathbf{r}_N$. Equations 8 and 9 state that the edge \mathbf{r}_{ICR} of the triangle defined by $\mathbf{r}_S, \mathbf{r}_N$ and \mathbf{r}_{ICR} can only translate if the triangle changes its shape. In particular the walker does not translate when one foot is grounded. The only translational motion of an ideal walker $d\mathbf{r}_{ICR,ideal} = \mathbf{b}_{transfer} \delta(t - t_{transfer}) dt$ occurs when the instantaneous center of rotation longitudinally moves from one foot to the other by the momentary vector $\mathbf{b}_{transfer}$ during the transfer of support. The *walker gauge* shows how essential is the lift of one foot from the non moving foothold and the grounding of the next foot for effective walking. The center of an ideal walker in contrast moves on a circle around the grounded foot while one of the feet is grounded. It does not move when the grounding is transferred between the feet. The motion of the biped center and the instantaneous center of rotation for a general ideal or non ideal walker are quite

different. Nevertheless the motion of both points over a period is the same and thus gauge independent because of equation 6. We decompose the motion of the instantaneous center of rotation into a longitudinal and transversal component

We anticipate the longitudinal component of the motion as the autonomous walking component of the motion. The transversal component arises if a foothold is moving. This motion is a passive transport of the walker with the foothold. The *walker gauge* is useful to decompose the motion into walking and passive advection. Note, however, that the decomposition into walking and advection in contrast to the full motion is gauge dependent.

6 Adiabatic walks on square patterns

6.1 Walkers gauge

In Fig. 2a we show the driving loop $\mathcal{L}_{-Q_2}^{-1}(\Delta\phi)$ in the control space \mathcal{C} of a square pattern. The loop clockwise circulates the fence point of $-Q_2$ direction with an azimuthal width of $\Delta\phi$. In Fig. 2b) we plot simulated trajectories on square patterns of the southern (blue) and northern (red) foot together with the instantaneous center of rotation \mathbf{r}_{ICR} that we color in green when the motion is longitudinal (along \mathbf{b}), orange when it is transversal, and white when it is a mixture of longitudinal and transversal motion. Two trajectories are shown. One for a small biped of length $b = 0.6a$ and one of a large biped of length $b = 2.8a$. The long biped longitudinally autonomously walks, while the smaller biped also shows some passive mixed sliding of the foothold (white part of the instantaneous center of rotation trajectory).

In Fig. 2c) we plot experimental trajectories of the southern (blue) and the northern (red) foot of various bipeds assembled from colloidal spheres of radius $R = 2.8 \mu m$ on a square pattern of lattice constant $a = 7 \mu m$. We also plot the trajectory instantaneous center of rotation (green). All bipeds are subject to the loop $\mathcal{L}_{-Q_2}^{-1}(\Delta\phi)$ of width $\Delta\phi = 65^\circ$. A video clip of bipeds of different lengths subject to this loop are shown in the video clip [adfigure2.mp4](#). In Fig. 2c) bipeds consisting of 3 – 11 colloidal particles are shown. Two consecutive footholds the southern foot steps upon are marked in orange to emphasize the step width of our walkers. We also overlay a microscope image of the final biped position for the 11-particle biped. The instantaneous center of rotation alternates between the southern and the northern foot. In Fig. 2d) we plot the simulated and experimentally determined total, longitudinal and transversal displacement of the instantaneous center of rotation as a function of the length b of the biped. The displacement is shown for a loop of width $\Delta\phi = 70^\circ$ for the simulations and $\Delta\phi = 65^\circ$ and $\Delta\phi = 200^\circ$ for the experiments. The total simulated displacement induced by the control loop is a primitive unit vector for small bipeds and increases by two lattice constants when the biped length times the sine of half the azimuthal loop width $b_t \sin(\Delta\phi/2) = na$ is an integer multiple of the length of the unit vector. The experimental displacement shows similar behavior, however also even displacements are observed when $b_t \sin(\Delta\phi/2)/a$ is close to an integer. Presumably this occurs because the control loop is not entirely symmetric around Q_2 such that the two higher order fences pass through the loop at slightly different biped sizes. Comparing the

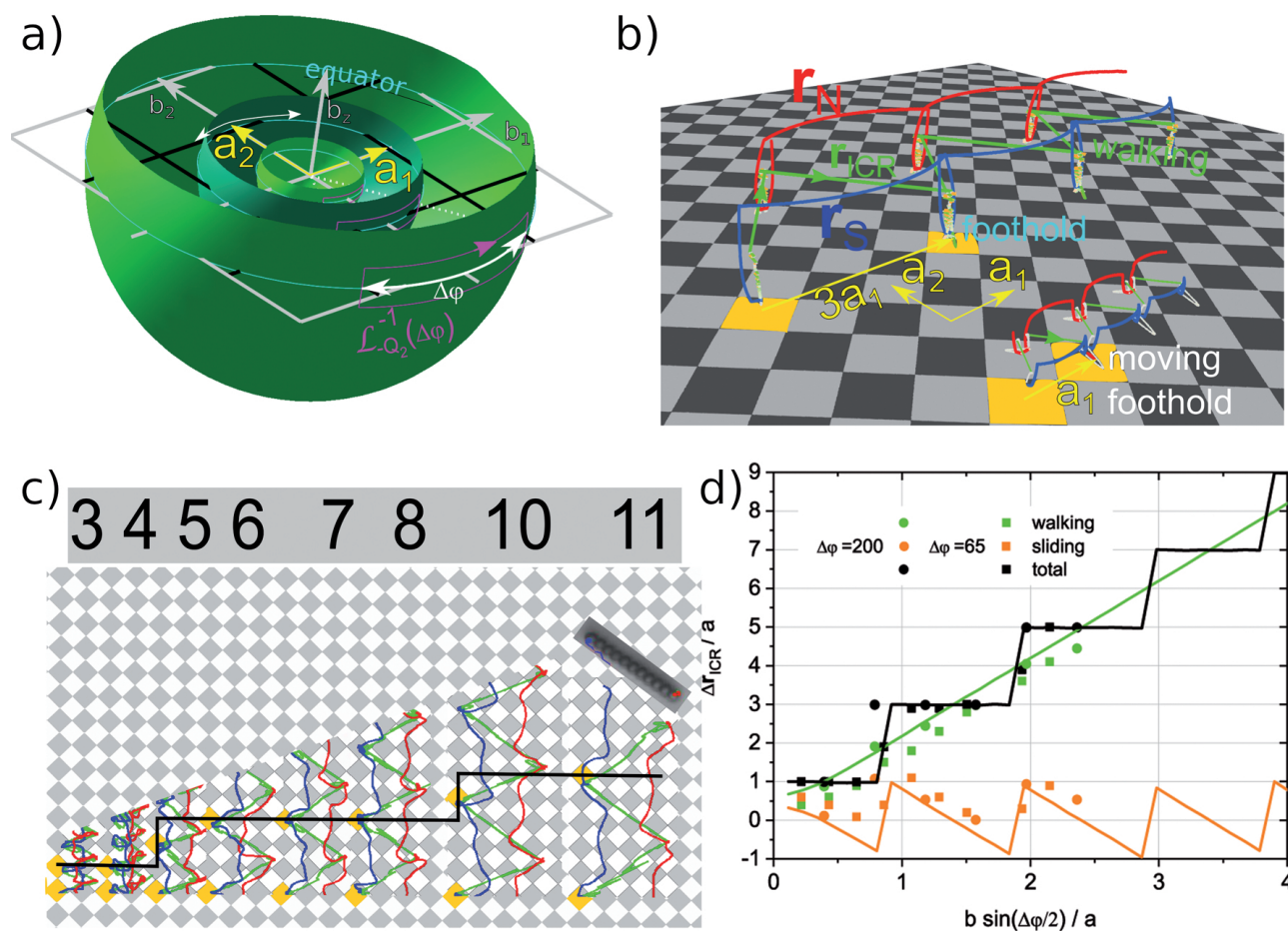


Fig. 2 a) control spaces of bipeds of lengths $b = 0.5a, 1.05a, 2.1a$ with a fundamental loop $\mathcal{L}_{-Q_2}^{-1}(\Delta\phi)$ of width $\Delta\phi = 70^\circ$. Fence lines are drawn in gray and black. b) simulated trajectories of both feet (blue and red) and the instantaneous center of rotation r_{ICR} for a biped of length $b = 0.6a$ and $b = 2.8a$. Longitudinal moves of the instantaneous center of rotation are shown in green, transversal moves in orange and mixed moves in white. c) experimental trajectories of the feet (blue and red) of bipeds assembled from 3 – 11 colloidal spheres of radius $R = 2.8\mu m$ on a square pattern of lattice constant $a = 7\mu m$ are shown together with the path of the instantaneous center of rotation (green). We also overlay a microscope images of the final biped position of the 11-particle biped. Two consecutive footholds of the southern foot for each walker are marked in orange. d) plot of the simulated and experimentally determined total, longitudinal and transversal displacement of the instantaneous center of rotation subject to the loop of width $\Delta\phi = 70^\circ$ for the simulations and $\Delta\phi = 65^\circ$ and $\Delta\phi = 200^\circ$ for the experiments. Videoclips of bipeds subject to the same loop are shown in the videoclip [adfigure2.avi](#).

simulated and experimental total displacement we find excellent agreement.

We also depict the longitudinal and transversal displacement of the instantaneous center of rotation. The longitudinal displacement $\Delta \mathbf{r}_l = \mathbf{a}_1 2b \sin(\Delta\phi/2)/a$ is proportional to the biped length b and increases continuously with the length of the biped. The transversal displacement does not exceed the length of a primitive unit vector $\Delta \mathbf{r}_t = 2\mathbf{a}_1 (b \sin(\Delta\phi/2)/a - \text{round}[b \sin(\Delta\phi/2)/a])$. If we decompose the experimental displacement into longitudinal and transversal displacement we find the experimental longitudinal component to be systematically lower than the longitudinal component of the simulations. The experimental transversal component shows some trend to follow the discontinuous behavior of the transversal simulated component. We believe this relatively poor agreement to arise from the fact that in contrast to the total displacement the individual displacements are not topologically protected, but are susceptible to weak perturbations such as imperfections of the lithographic pattern, misalignments between the control loop and the pattern, and the deviation of the colloidal biped from an idealized paramagnetic line.

6.2 Center gauge

For a better understanding of the topology of the motion the *center gauge* is more useful and the potential in this gauge reads (see eq. 3):

$$V_{biped} \propto \psi(\mathbf{r} + \mathbf{b}/2) - \psi(\mathbf{r} - \mathbf{b}/2) \quad (10)$$

with the biped centered at the position \mathbf{r} . The biped potential is periodic and invariant under the simultaneous transformation $\mathbf{b} \rightarrow \mathbf{b} + \mathbf{a}$ and $\mathbf{r} \rightarrow \mathbf{r} + \mathbf{a}/2$ where \mathbf{a} is a primitive lattice vector. The biped potential reverses sign $V_{biped} \rightarrow -V_{biped}$ when one reverses the biped vector $\mathbf{b} \rightarrow -\mathbf{b}$. The fence is the set $\mathcal{F} = \{(\mathbf{r}_A, \mathbf{b}) | \nabla_A V_{biped} = 0 \text{ and } \det(\nabla_A \nabla_A V_{biped}) = 0\}$. Its projection into \mathcal{C} is the set $\mathcal{F}_C = \{\mathbf{b} | (\mathbf{r}_A, \mathbf{b}) \in \mathcal{F} \text{ for some } \mathbf{r}_A\}$.

In Figure 2a) we construct the projection of the fence onto the spherical control space of a biped of finite length b on a square pattern from that of a colloidal sphere (a point particle see²⁴). For convenience we show the control space of a biped of length b as a sphere of radius b . Pieces of three such spheres are shown in Fig. 2a). As for point particles zero order fences lie along the b_1 and b_2 coordinates. Because the biped potential is periodic in \mathbf{b} with period \mathbf{a} these zero order fences repeat as higher order fences every lattice vector (gray and black lines in Figure 2a)). The minima near the black fences are displaced from the minima near the gray fences by half the lattice vector. For small bipeds $b < a$ the control space is topologically equivalent to that of a point particle. Larger biped control spaces are cut also by higher order fences displaced from the origin and are therefore topologically different from small biped control spaces with more fence points on the equator. Each winding of a control loop around one of the fences adiabatically propels the biped by a unit vector perpendicular to the fence. The fundamental loop $\mathcal{L}_{-Q_2}^{-1}(\Delta\phi)$ in Fig. 2a) winds clockwise around the central fence along the $-b_2$ axes for all biped sizes but also around the black displaced fences parallel to the b_2 -axes for the $b = 2.1a$ bipeds. The $b = 2.1a$

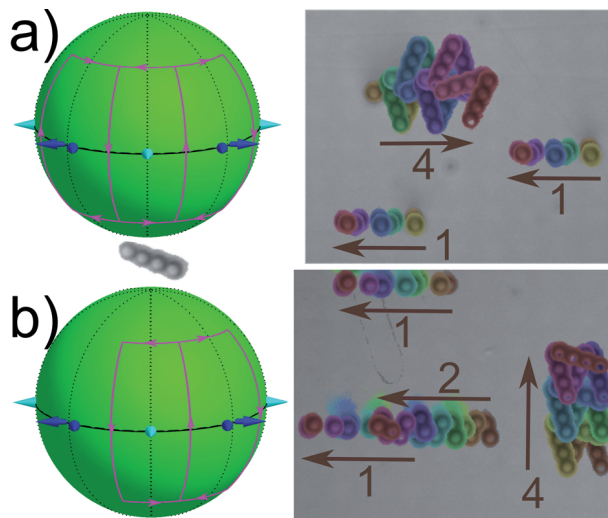


Fig. 3 a) control space for a biped consisting of four colloids ($b = (4 - 1)2R$) together with a loop encircling the zero order y -fence in the positive and the 1st order x - and y - fences in the negative sense. Bipeds consisting of four colloids are transported in the $+x$ -direction while single colloidal particles are transported in the $-x$ -direction. We show an overlay of microscope images of the same bipeds at different times with the different times color coded from yellow toward red. b) The same control space as in A) subject to a loop encircling the zero order y -fence in the positive and the 1st order x - and y - fence in the negative sense. Bipeds consisting of four colloids are transported in the $+y$ -direction while single colloidal particles and doublets are transported in the $-x$ -direction. An overlay of microscope images of various bipeds is provided using the same color coding as in A). Videoclips showing the complementary motion of different bipeds subject to the complex loops in this figure are shown in the videoclip [adfigure3.avi](#)

bipeds therefore are propelled three times as fast as the small bipeds. Much alike human beings bipeds with longer legs move faster than smaller bipeds. The increase in speed however happens in discrete steps as the speed is topologically enforced to be a multiple of a lattice vector per cycle.

The *walker gauge* may shed some light on what part of the motion is true walking and what part is sliding. In contrast to the gauge independent description in terms of winding numbers the decomposition into active and passive motion relies on a gauge and does not survive a gauge transformation.

7 Selective combinations of fundamental loops

The control space of the square lattice in Fig. 2a) contains fence points at the positions

$$\phi_{\mathcal{F},n,m} = \arcsin \frac{na}{b} + m \frac{\pi}{2}. \quad (11)$$

with $m = 0, 1, 2, 3, \dots$ and n an integer. For bipeds larger than the lattice constant ($b > a$) fundamental loops around these new $n \neq 0$ fence points will not transport small bipeds, but only bipeds of the proper length. Moreover the azimuthal position for the higher order fences depend on the biped length ($\frac{d\phi_{\mathcal{F}}}{db} \neq 0$), allowing to adiabatically transport larger bipeds that fall into the appropriate

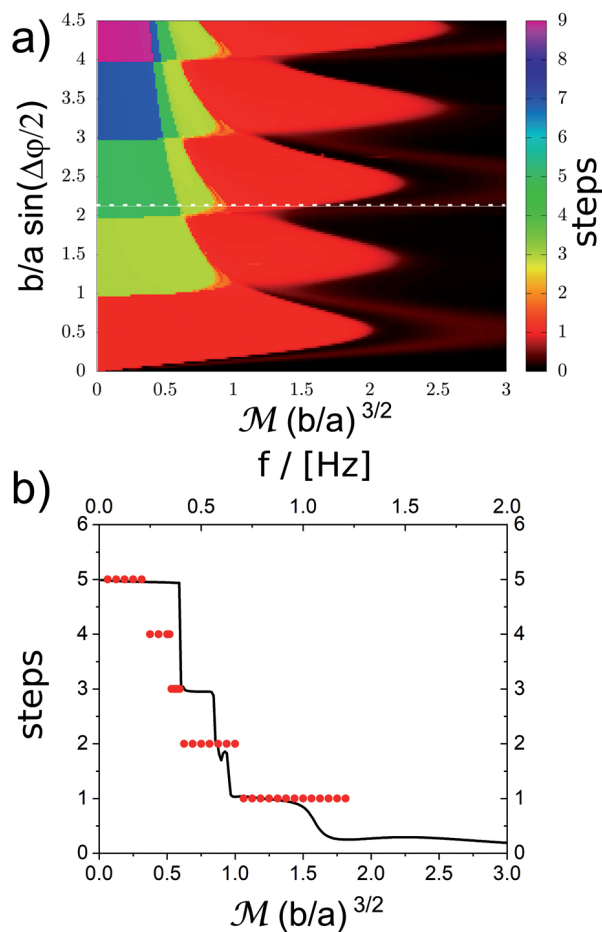


Fig. 4 a) Brownian dynamics simulations of the displacement of the biped as a function of the Mason number and the effective length of the biped. b) the experimental data of a biped of length $b/a \sin \Delta\phi/2 \approx 2.1$ versus the frequency of the driving (red circles) and the simulated data for the same effective length versus Mason number.

length range. In Fig. 3a), we show the complex loops in control space that transport small bipeds into the $-x$ -direction and bipeds consisting of four colloids of biped length $b = (4 - 1)2R$ into the $+x$ -direction. In Fig. 3b) the four colloids are transported in the $+y$ -direction perpendicular to the single colloid transport direction. A video clip showing the complementary motion of different bipeds subject to these complex loops are shown in the video clip *adfigure3.mp4*. The longer the biped the more fence points exist in control space and the more directions of motion can be invoked by the proper combination of fundamental loops. A protocol how to exploit the fence pattern in a systematic way can be found in reference³⁰.

8 Topological effects of hydrodynamic friction

The topological protection of the walker is based on the fact that the grounded foot of the walker remains within its local foothold as long as we do not approach the equator of control space where

the transition of the foothold of the left toward the right foot occurs. For this the instantaneous center of rotation must remain with the grounded foot.

In a low Reynolds number fluid hydrodynamic friction opposes the rotation of a biped with the external field. The hydrodynamic friction of a rotating stick is minimal when the instantaneous center of rotation is centered in the biped rather than in one of its feet. Increasing the speed of the control loop therefore causes competition for the instantaneous center of rotation between the biped center and the biped feet.

When the hydrodynamic forces exceed the pattern forces, which happens especially when the biped foot to foot vector endpoint is close to one of the fences one may lose an integer number of steps per loop. The Mason number $\mathcal{M} = \eta 2\pi f / \mu_0 \chi_{eff} H_{ext} H_p$ (with η the shear viscosity of the fluid and χ_{eff} the effective magnetic susceptibility of a colloidal particle) is a dimensionless measure of the driving frequency $f = T^{-1}$ of a loop. In Fig. 4a), we plot Brownian simulation data of the number of steps of a biped versus its effective length $b \sin(\Delta\phi/2)/a$ and versus the dimensionless frequency $\mathcal{M}(b/a)^{3/2}$. The topological protection of an integer number of steps of the biped also holds when the driving is not adiabatic. However, the faster the driving the lower the number of biped steps per loop.

The experimental data in Fig. 4b) shows odd and even steps and roughly follows the simulations. The lack of detailed agreement may be easily understood as we have neglected the presence of the solid support as well as hydrodynamic interactions between the colloidal beads in the simulations. However the topological locking to integer steps seems to be a robust feature of the dynamics also at higher frequencies.

9 Symmorphic hexagonal pattern

9.1 Control space

In Figure 5a) we plot the fence (red and blue) in the Wigner Seitz cell (cyan) of a hexagonal lattice as a function of b . In theory we could in principle also change the length of the biped such that our control space is augmented by one dimension. In the experiments the biped length will be fixed and the control space is the cut of a sphere of radius b with this augmented control space. In Fig. 5a) fence areas are bordered by bifurcation lines (yellow, magenta, and cyan) with the bifurcation lines meeting in topological transition points that are located in the center and at the corners of the Wigner Seitz cell. A cut of the periodically continued fence with a sphere of radius b constitutes the control space \mathcal{C} of a biped of fixed length b . In 5b) we show the normalized spherical control spaces for $b = 0.33a$, $b_t = a/\sqrt{3}$, $0.7a$) and $b_t = a$. If the fence segments of two bipeds can be continuously deformed into each other without changing the number of bifurcation points the bipeds exhibit equivalent transport behavior. The behavior of the bipeds changes at the topological transition lengths $b_t = a\sqrt{(n^2 + nm + m^2)}/3$, where n and m are integers.

If we project the bifurcation lines of Fig. 5a) to the plane $b_z = 0$ we obtain the projected fence lines in Fig. 5c). The yellow line segments between the topological transition points are along the lattice vectors and the magenta (cyan) segments are parallel to

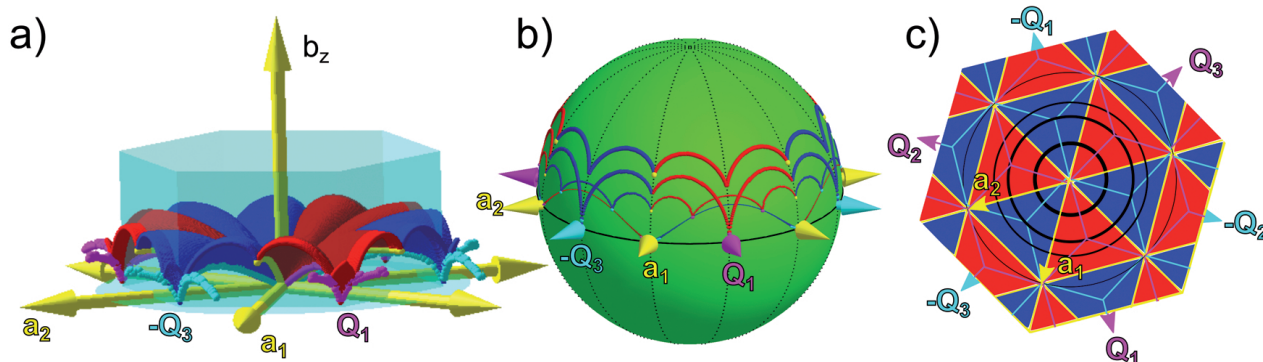


Fig. 5 a) Fences (red and blue) within the Wigner Seitz cell (cyan) of a hexagonal lattice with unit vectors \mathbf{a}_1 and \mathbf{a}_2 . Bifurcation lines (yellow, cyan and magenta) are lines where the curvature of the fences diverges. The bifurcation lines meet at topological transition points located in the center and at the corners of the Wigner Seitz cell. b) fence segments and bifurcation points on the control space \mathcal{C} of the external field obtained from Fig. a) by cutting the fence with a sphere of radius $b = 0.33a$ (upper fence), $b_t = a/\sqrt{3}$, $b = 0.7a$, and $b_t = a$ (thinnest fence) and projecting it to a unit sphere. Topologically nontrivial loops must wind around one of the bifurcation points of the biped. There are modulation loops that circle around a bifurcation point of a biped of one but not the other length. c) projection of the bifurcation lines of Fig. a) in an extended zone scheme onto the plane $b_z = 0$ together with cuts (black) of the spheres from Fig. b) with this plane. Topological transitions in the biped behavior occur when ever the radius moves across one of the topological transition points.

the positive (negative) reciprocal lattice vectors when folded into the Wigner Seitz cell. The cyan segments are anti parallel to the positive reciprocal lattice vectors. The circle of biped length b cuts through these segments and the number N_a (N_Q) of yellow (magenta or cyan) segments cut exactly once are the number of bifurcation points of type \mathcal{B}_a and \mathcal{B}_Q in the northern fence in Fig. 5b).

9.2 Stationary manifold

For a fixed length of the biped the stationary manifold $\mathcal{M} = \{(\mathbf{r}_A, \mathbf{b}) | \nabla_{\mathcal{A}} V_{\text{biped}} = 0\} \subset \mathcal{C} \otimes \mathcal{A}$ can be shown to be a manifold of genus $g = N_a + N_Q - 5$ that is cut into three pieces \mathcal{M}_+ and \mathcal{M}_- of genus $g_+ = g_- = (N_a - 2)/2$ and \mathcal{M}_0 of genus $g_0 = N_Q - 3$, where the stationary points are maxima, minima, respectively saddle points of the biped potential. The holes in $\mathcal{C} \otimes \mathcal{A}$ and in \mathcal{M} are inherited from the holes of \mathcal{A} (a torus). A loop $\mathcal{L}_C \subset \mathcal{C}$ in control space has several preimage loops $\mathcal{L}_{\mathcal{M}_i} \subset \mathcal{M}$, ($i = 1, 2, \dots, m$), ($m = 4, 5$, or 6) on \mathcal{M} . If one of these loops entirely lies in \mathcal{M}_- and winds around holes in \mathcal{M}_- the loop will be projected into action space as a minimum loop $\mathcal{L}_A \subset \mathcal{A}$ that winds around the torus and therefore adiabatically transports the biped. Fundamental loops in control space that enter and exit the region north of the fence via fence segments of the same color (red or blue) cause adiabatic transport. A preimage loop that winds around holes of \mathcal{M}_- but crosses over to \mathcal{M}_0 also transports but in form of a ratchet. Fundamental loops in control space that enter and exit the region north of the fence via fence segments of different color cause ratchet transport. At fixed biped length b one form of adiabatic transport changes to another form of adiabatic transport only via an intervening ratchet. The adiabatic speed of a longer biped can be higher once we insert more bifurcation points of type \mathcal{B}_a into a fence in control space and this happens the first time for $b > a$ beyond the lowest fence in Fig. 5b) and c).

9.3 Response to loops in action space

The hexagonal pattern lacks a glide plane and the fence is no longer located at the equator but in the northern hemisphere and the number of minima of the potential per unit cell of the lattice differs depending on whether the external field is north or south of the fence. For this reason even if we apply a loop that extends as much to the north as to the south of control space, the motion of the biped is a limping motion. We see this in Fig. 6 by the instantaneous center of rotation (green) meeting the southern (blue) foot within a southern foothold (bubble) and the northern (red) foot within one of the two (white) interstitials between three bubbles. When the motion is adiabatic the northern foothold can hold the northern foot at its location while we exit the region of control space north of the fence. In contrast for a ratchet the northern foot of the biped prior to crossing the fence is in a vanishing foothold and therefore irreversibly jumps to the remaining foothold in the other interstitial when we exit the northern region. Simultaneously the southern foot jumps above the southern foothold (bubble). During the jump the orientation of the biped is fixed and therefore the instantaneous center of rotation moves away from the northern foothold far above the magnetic pattern before it returns to the northern foot after the jump. The northern foot stays with the remaining northern foothold only for the short period of the loop from the fence to the equator. The southern foot touches down to the southern foothold when we cross the equator, and the adiabatic propulsion caused by the northern segment of the loop in control space is booked in the *walker gauge* by a transfer of the instantaneous center of rotation from the northern to the southern foot. In Fig. 6a) we show the control space of a biped of length $b = 1.4a$ with 36 red and blue fence segments north of the equator. A symmetric loop around $-\mathbf{Q}_3$ enters and exits the north of control space via a red fence segment and thus causes an adiabatic walk simulated with Brownian dynamics to the right of Fig. 6b). A different asymmet-

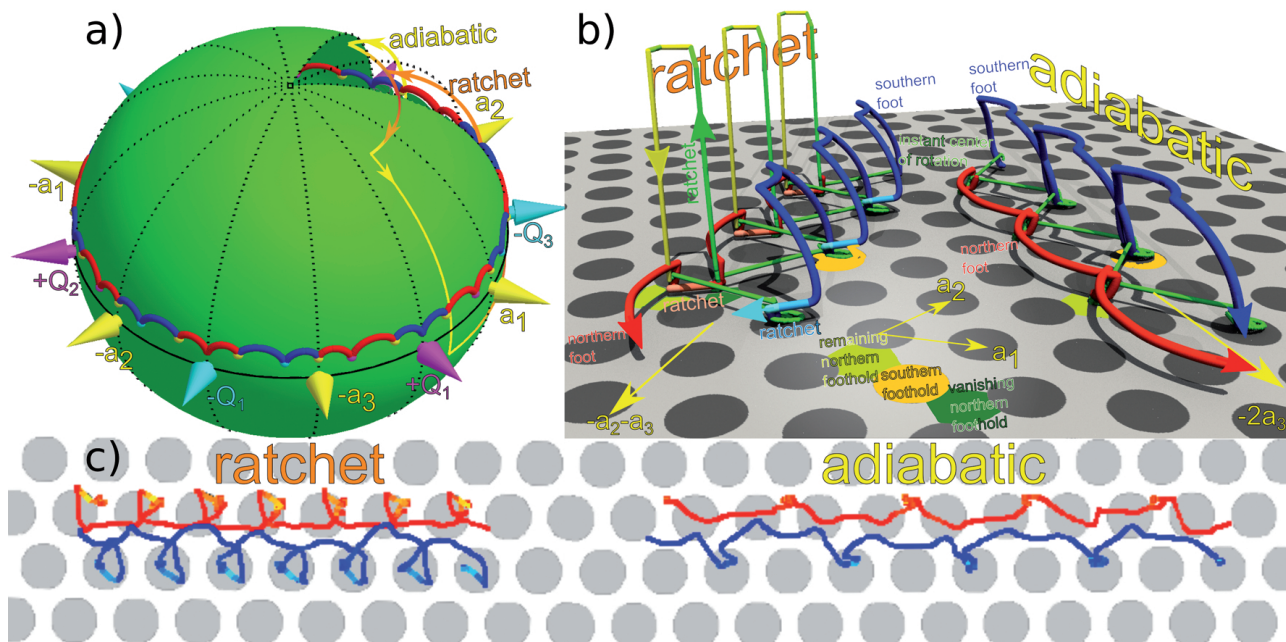


Fig. 6 a) Control space and fence of a biped of length $b = 1.4a$ with an asymmetric control loop causing a ratchet and a symmetric control loop causing adiabatic transport. b) Simulated trajectories of the northern and southern foot and the instantaneous center of rotation of the same biped for the asymmetric and for the symmetric loop. In the ratchet trajectories brighter colors of the trajectories label the regions of higher speed when the ratchet jumps occur. c) Experimentally measured ratchet and adiabatic trajectories of the feet of the bipeds of lengths $b = 1.2a$ and $b = 1.2a$ respectively. The trajectories are colored with brighter colors where the velocity is higher. Videoclips of the two experimental bipeds are shown in the videoclip *adfigure6.avi*

ric loop in Fig. 6a) enters the north of \mathcal{C} via a blue segment and exits via the same red fence segment as the symmetric loop. Upon entry the northern foot resides in a foothold that vanishes upon exit through the red fence and therefore jumps to the remaining foothold, i.e. the remaining foothold in which the southern foot of the adiabatic loop had stayed in through the entire northern part of the adiabatic loop. The net motion is $-2a_3$ for the symmetric loop and $-a_2 - a_3$ for the asymmetric loop.

In Fig. 6c) we show the experimental trajectories of two bipeds of length $b = 1.2a$ subject to an asymmetric and a symmetric loop, the first performing a ratchet motion, the second an adiabatic motion. Ratchet jumps are visible as a motion of higher speed, with both feet making parallel displacements such that the relative orientation of the feet remain the same. Note that the adiabatic trajectories are mirror symmetric such that it is not possible to tell the direction of the motion from the trajectories. The ratchet trajectories in contrast are chiral and the direction of the motion can be told from this chirality. The direction is with the southern foot jumping into the bubble not out of the bubble. Similarly the direction can be inferred from the northern foot jumping from the foothold that is the center of curvature of the arc segment of the southern foot toward the foothold that is not a center of curvature of an arc segment of the southern foot. In the video clip *adfigure6.mp4* the motion of the two experimental bipeds can be followed in full detail. The computation of the instantaneous center of rotation from the motion of the two feet is rather sensitive to noise in the measurements and led to results dominated by the

noise for these experiments. We do not show the instantaneous centers of rotation of the two experiments for this reason.

10 Discussion

The bipeds studied in this work are rigid bipeds having no joints. For these bipeds it is straight forward to compute the winding numbers of the driving loops in control space. Some of the objects one winds around are fixed and do not move with the size of the biped. Higher order objects arising from the periodicity of the problem as a function of the biped vector \mathbf{b} move in control space as the length of the biped grows. Part of the motion is therefore topologically protected independently of the size, others only beyond a certain size and only if one adapts the modulation loop to the increasing size.

Robotic bipeds have joints and other internal degrees of freedom of the conformation of a biped. Which of our findings of this work remain true when dealing with colloidal bipeds that have joints? The answer of course is that everything remains topologically protected if the conformation of a biped with joints does not deviate too strong from that of a rigid rod. In Fig. 7 and in the video clip *adfigure7.mp4* we show the motion of a colloidal biped on a square lattice that is deformed by viscous and magnetic stress³¹ by a loop enclosing the vicinity of the equator. The shape of the biped at large Mason number alternates between an S-shaped conformation (stage 6 in Fig. 7) and its chiral mirror image (stage 4 in Fig. 7). The same biped returns to a straight rod shape as the external field direction moves along the longitu-

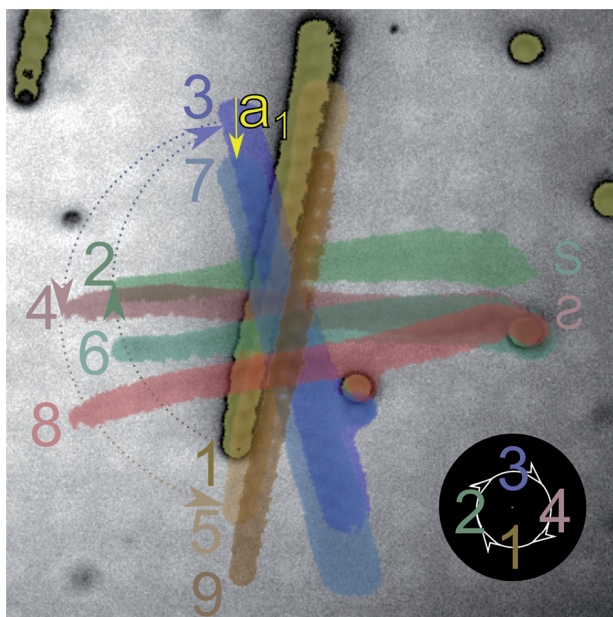


Fig. 7 Overlay of nine microscope images of a shape changing flexible colloidal rod at different times of the driving loop. The shape changing rod performs a topologically protected non-adiabatic walk on the pattern. A videoclip of the biped is shown in the videoclip [adfigure7.avi](#)

dinal sections of the loop. The non-adiabatic walking motion of these bipeds remains locked to a unit vector of the lattice, which proves that also flexible bipeds are topologically protected.

11 Conclusions

The adiabatic walking step width of self assembled paramagnetic colloidal rods on a periodic magnetic lattice is topologically locked to be commensurate with the magnetic lattice. For this reason driving loops can be classified by winding numbers around fences (bifurcation points with fence segments) in control space. The walking is robust against a variety of static, adiabatic, and dynamic perturbations of the system. While the description of the absolute motion of the biped is gauge invariant the decomposition into an active and a passive motion is gauge dependent.

12 Appendix

We use Brownian dynamics to simulate the motion of the bipeds on top of the magnetic pattern. Each biped consists of N particles where each particle sees the magnetic potential

$$V(\mathbf{x}_A, \mathbf{H}_{\text{ext}}(t), z) \propto -\mathbf{H}_{\text{ext}}(t) \cdot \mathbf{H}_p(\mathbf{x}_A) e^{-(z-z_0) \frac{2\pi}{a}}, \quad (12)$$

where $\mathbf{H}_{\text{ext}}(t)$ is the external field at time t , $\mathbf{H}_p(\mathbf{x}_A)$ is the magnetic field created by the pattern at a fixed height z_0 above the pattern at the position of the particle position \mathbf{x}_A in action space \mathcal{A} and z is the distance of the particle from the pattern. The equation of motion is then given by

$$\xi \dot{\mathbf{x}}_A(t) = -\nabla_{\mathcal{A}} V(\mathbf{x}_A, \mathbf{H}_{\text{ext}}(t), z) + \eta(t), \quad (13)$$

where ξ is the friction coefficient and η is a Gaussian random force with a variance given by the fluctuation-dissipation theorem. We use a constant value of ξ which neglects all hydrodynamic interactions between the particles. The equation is then integrated in time t with a standard Euler algorithm. To restore the rigid shape of the biped and the enslavement of the orientation \mathbf{b} to the external magnetic field $\mathbf{H}_{\text{ext}}(t)$, after every simulation step the center \mathbf{x}_c of the biped is determined by the mean position of all particles

$$\mathbf{x}_c(t) = \frac{1}{N} \sum_{i=1}^N \mathbf{x}_i(t) \quad (14)$$

and its direction \mathbf{b} by the direction of the external field \mathbf{H}_{ext} . The new position for every particle is calculated as

$$\mathbf{x}_i(t) = \mathbf{x}_c(t) + (2i - (N + 1)) \frac{R}{H_{\text{ext}}} \cdot \mathbf{H}_{\text{ext}}(t), \quad i = 1 \dots N. \quad (15)$$

The particles are then shifted the same amount along an axis perpendicular to the pattern such that the lowest particle has the distance z_0 from the pattern. We use a time step dt in the range from $\frac{T}{dt} \approx 2 \cdot 10^4$ to $2 \cdot 10^5$, where the period T is proportional to the arc length S of the modulation loop in control space \mathcal{C} .

Acknowledgements

This work is funded by the Deutsche Forschungsgemeinschaft (DFG, German Research Foundation) under project number 440764520.

Author contributions

MMK, AdE, DdlH, & TMF designed and performed the experiment, and wrote the manuscript with input from all the other authors. MU & FS produced the magnetic film. AT, RH, IK, ArE & DH performed the fabrication of the micromagnetic domain patterns within the magnetic thin film.

Conflict of interest

There are no conflicts to declare.

References

- 1 D. Jongenee, R. Withagen, R. Withagen, F. T. J. M. Zaai; Do children create standardized playgrounds? A study on the gap-crossing affordances of jumping stones *J. Env. Psychology*, **44**, 45-52, (2016)
- 2 A. Yildiz, M. Tomishige, R. D. Vale, and P. R. Selvin; Kinesin walks hand-over-hand *Science* **303** 676-678. (2004)
- 3 C. L. Asbury; Kinesin: world's tiniest biped *Current Opinion in Cell Biology* **17** 89-97 (2005)
- 4 M. L. Shik, and G. N. Orlovsky; Neurophysiology of locomotor automatism *Physiological Reviews* **56**, 465-501 (1976)
- 5 D. Hamacher, F. Herold, P. Wiegel, D. Hamacher, and L. Schega; Brain activity during walking: A systematic review *Neuroscience and Biobehavioral Reviews* **57** 310-327 (2015)
- 6 P. Holmes, R. J. Full, D. Koditschek, and J. Guckenheimer The Dynamics of Legged Locomotion: Models, Analyses, and Challenges *SIAM Rev.*, **48**, 207-304. (2006)

- 7 W. B. Sherman and N. C. Seeman; A Precisely Controlled DNA Biped Walking Device *Nano Letters* **4**, 1203-1207. (2004)
- 8 A. Shapere, and F. Wilczek; Geometry of self-propulsion at low Reynolds number. *Journal of Fluid Mechanics*, **198**, 557-585. (1989)
- 9 A. Shapere, and F. Wilczek; Efficiency of self-propulsion at low Reynolds number. *Journal of Fluid Mechanics*, **198**, 587-599. (1989)
- 10 Q. Nguyen, H. Ayonga, G. W. Jessy, A. D. Aaron and S. Koushil; 3D Dynamic Walking on Stepping Stones with Control Barrier Functions 2016 IEEE **55TH** CONFERENCE ON DECISION AND CONTROL (CDC) Book Group Author(s):IEEE Book Series: *IEEE Conference on Decision and Control*, 827-834 (2016).
- 11 M. Z. Hasan, and C. L. Kane; Colloquium: Topological insulators. *Rev. Mod. Phys.* **82**, 3045-3067 (2010).
- 12 S-Q. Shen; Topological insulators: Dirac equation in condensed matters, *Springer Science, and Business Media* (2013).
- 13 M. C. Rechtsman, J. M. Zeuner, Y. Plotnik, Y. Lumer, D. Podolsky, F. Dreisow, S. Nolte, M. Segev, and A. Szameit; Photonic Floquet topological insulators *Nature* **496**, 196-200 (2013).
- 14 M. Xiao, G. Ma, Z. Yang, P. Sheng, Z.Q. Zhang, and C.T. Chan; Geometric phase and band inversion in periodic acoustic systems *Nature Phys.* **11**, 240-244 (2015)
- 15 A. Murugan and S. Vaikuntanathan; Topologically protected modes in non-equilibrium stochastic systems *Nat. Comm.* **8**, 13881 (2017).
- 16 A. M. E. B. Rossi, J. Bugase, and Th. M. Fischer Macroscopic Floquet topological crystalline steel and superconductor pump *Eur. Phys. Lett.* **119**, 40001 (2017).
- 17 C. L. Kane, and T. C. Lubensky; Topological boundary modes in isostatic lattices. *Nat. Phys.* **10**, 39-45 (2014).
- 18 J. Paulose, B. G. Chen, and V. Vitelli; Topological modes bound to dislocations in mechanical metamaterials. *Nature Physics* **11**, 153-156 (2015).
- 19 L. M. Nash, D. Kleckner, A. Read, V. Vitelli, Ari M. Turner, and W. T. M. Irvine; Topological mechanics of gyroscopic metamaterials *Proc. Nat. Acad. Sci.* **112**, 14495-14500 (2015).
- 20 S. D. Huber; Topological mechanics *Nature Physics* **12**, 621-623 (2016).
- 21 M. J. Rice, and E. J. Mele; Elementary Excitations of a Linearly Conjugated Diatomic Polymer *Phys. Rev. Lett.* **49**, 1455-1459 (1982).
- 22 B. I. Halperin Quantized Hall conductance, current-carrying edge states, and the existence of extended states in a two-dimensional disordered potential *Phys. Rev. B* **25**, 2185-2190 (1982).
- 23 M. S. Rudner, N. H. Lindner, E. Berg, and M. Levin; Anomalous Edge States and the Bulk-Edge Correspondence for Periodically Driven Two-Dimensional Systems *Phys. Rev. X* **3**, 031005 (2013).
- 24 D. de las Heras, J. Loehr, M. Lönne, and Th. M. & Fischer; Topologically protected colloidal transport above a square magnetic lattice. *New J. Phys.* (2016), **18**, 105009.
- 25 J. Loehr, D. de las Heras, M. Lönne, J. Bugase, A. Jarosz, M. Urbaniak, F. Stobiecki, A. Tomita, R. Huhnstock, I. Koch, A. Ehresmann, D. Holzinger, and Th. M. Fischer; Lattice symmetries and the topologically protected transport of colloidal particles. *Soft Matter* (2017), **13**, 5044-5075.
- 26 C. Chappert, H. Bernas, J. Ferré, V. Kottler, J.-P. Jamet, Y. Chen, E. Cambriil, T. De-Volder, F. Rousseaux, V. Mathet, and H. Launois; Planar patterned magnetic media obtained by ion irradiation. *Science* (1998), **280**, 1919-1922.
- 27 P. Kuświk, A. Ehresmann, M. Tekielak, B. Szymański, I. Sveklo, P. Mazalski, D. Engel, J. Kisielewski, D. Lengemann, M. Urbaniak, C. Schmidt, A. Maziewski, and F. Stobiecki; Colloidal domain lithography for regularly arranged artificial magnetic out-of-plane monodomains in Au/Co/Au layers *Nanotechnology* **22**, 095302 (2011)
- 28 J. Loehr, M. Lönne, A. Ernst, D. de las Heras, and Th. M. Fischer; Topological protection of multiparticle dissipative transport. *Nat. Comm.* (2016), **7**, 11745.
- 29 D. Harland, and N. S. Manton; Rolling Skyrmions and the nuclear spin-orbit force *Nuclear Physics B* **935**, 210-241 (2018)
- 30 M. Mirzaee-Kakhki et al. Simultaneous polydirectional transport of colloidal bipeds *Nature Comm.* **11**, 4670, (2020)
- 31 S. Melle and J. E. Martin; Chain model of a magnetorheological suspension in a rotating field *J. Chem. Phys.* **118**, 9875-9881 (2003).

Publication 3

Colloidal trains

Soft Matter, **16**, 1594-1598 (2020)

Mahla Mirzaee-Kakhki^{a1}, Adrian Ernst^{a1}, Daniel de las Heras^{a2},
Maciej Urbaniak^b, Feliks Stobiecki^b, Andreea Tomita^c, Rico
Huhnstock^c, Iris Koch^c, Jendrik Gördes^c, Arno Ehresmann^c, Dennis
Holzinger^c, Meike Reginka^c, Thomas M. Fischer^{a1}

^{a1} Experimental Physics and ^{a2} Theoretical Physics, Faculty of Physics, Mathematics and Computer Science, University of Bayreuth, 95447 Bayreuth, Germany.

^b Institute of Molecular Physics, Polish Academy of Sciences, 60-179 Poznań, Poland.

^c Institute of Physics and Center for Interdisciplinary Nanostructure Science and Technology (CINSaT), Universität Kassel, D-34132 Kassel, Germany.

In publication 2 we have shown how a walker loses power when we increase the modulation frequency. Since walkers are at least partially active walkers while the motion of single colloids is entirely passive, single colloids stall at lower frequencies than bipeds consisting of two or more colloids. In sections 1.7 and 1.8.2 we have shown how colloids might interact with each other via long range interactions. Here we want to use such interactions to let walkers carry along cargo in the form of single colloids. I pose the final question of this thesis:

Question

Can the topological transport of one type of the bipeds be used to transfer this transport to single colloids when the bipeds come close to single colloids?

My Contribution

I discovered the biped assisted motion of single colloids with preliminary experiments and I performed all experiments derived from this and presented in the manuscript. Adrian Ernst worked out the computer control and simulations of the experiments. Exchange-bias films have been produced by Maciej Urbaniak and Feliks Sobiecki in Poznan, the lithographic patterns were planned in Bayreuth as a team effort, and the ion-bombardment was done by Andreea Tomita, Rico Huhnstock, Iris Koch, Jendrik Gördes, Arno Ehresmann, and Dennis Holzinger in Kassel. The preparation and writing of the paper was done by all coauthors.



Cite this: *Soft Matter*, 2020, **16**, 1594

Received 15th November 2019,
Accepted 8th January 2020

DOI: 10.1039/c9sm02261a

rsc.li/soft-matter-journal

Colloidal trains†

Mahla Mirzaee-Kakhki,^a Adrian Ernst,^a Daniel de las Heras,^{id}^b Maciej Urbaniak,^{id}^c Feliks Stobiecki,^{id}^c Andreea Tomita,^{id}^d Rico Huhnstock,^d Iris Koch,^d Jendrik Gördes,^d Arno Ehresmann,^{id}^d Dennis Holzinger,^{id}^d Meike Reginka^d and Thomas M. Fischer^{id}*^a

Single and double paramagnetic colloidal particles are placed above a magnetic square pattern and are driven with an external magnetic field processing around a high symmetry direction of the pattern. The external magnetic field and that of the pattern confine the colloids into lanes parallel to a lattice vector of the pattern. The precession of the external field causes traveling minima of the magnetic potential along the direction of the lanes. At sufficiently high frequencies of modulation, only the doublets respond to the external field and move in direction of the traveling minima along the lanes, while the single colloids cannot follow and remain static. We show how the doublets can induce a coordinated motion of the single colloids building colloidal trains made of a chain of several single colloids transported by doublets.

1 Introduction

Biomimetics is used to implement biological functions to artificial devices, fulfilling tasks in a non biological environment. Well known examples are artificial swimmers^{1–3} and active systems⁴ that can be used to *e.g.* transport a load. Microscopic dynamics can also be inspired by large scale transport systems such as trains. A railroad train is powered either by a separate locomotive or by multiple units of self propelled equally powered carriages. In nature the motility of family members of animals trailing behind each other is neither concentrated in the animal heading the trail nor is it distributed equally amongst family members. Young goslings trailing behind one of their parents need less but not zero power to follow their more powerful mother goose.⁵ When elephants travel they walk in a line placing their youngest in between the grownups with a grownup at the head and at the tail. In the spirit of other bioinspired magnetic colloidal dynamics^{1–3,6,7} we generate a biomimetic train of a collective ensemble of paramagnetic colloids. Single colloids are too weak to move on their own along the line and must be assisted to move by

pushing of the train with a larger paramagnetic colloidal doublet. The train is confined to an effectively one dimensional lane created *via* a colloidal potential which is generated by the combination of a magnetic square pattern and an external magnetic field. The power of each unit in the train is generated by modulating the external field on a control loop. Colloidal trains can only move above a square lattice if a sufficiently flat potential valley is created by orienting the external field roughly in direction of a primitive unit vector of the square magnetic pattern.

In contrast to other magnetically actuated motions that are either coupled *via* elastic bonds¹ or consist of particles in intimate contact^{2–4,6,7} our particles are well separated individuals that can couple and decouple from the colloidal train and thus switch between individual and collective behavior.

2 Setup

We illustrate the doublet assisted motion of a train of single colloids using a square magnetic lattice,^{8,9} Fig. 1(a). In the experiments, single paramagnetic colloidal particles or doublets of particles move on a plane above a thin Co/Au layered system with perpendicular magnetic anisotropy lithographically patterned *via* ion bombardment.^{9–11} The pattern is a square lattice of magnetized domains with a mesoscopic pattern lattice constant $a \approx 7 \mu\text{m}$, see a sketch in Fig. 1(a). The pattern is magnetized in the $\pm z$ -direction, normal to the film. The pattern is spin coated with a $1.6 \mu\text{m}$ polymer film that serves as a spacer between the pattern and the colloids. The paramagnetic colloidal

^a *Experimentalphysik X, Physikalisches Institut, Universität Bayreuth, D-95440 Bayreuth, Germany. E-mail: Thomas.Fischer@uni-bayreuth.de*

^b *Theoretische Physik II, Physikalisches Institut, Universität Bayreuth, D-95440 Bayreuth, Germany*

^c *Institute of Molecular Physics, Polish Academy of Sciences, 60-179 Poznań, Poland*

^d *Institute of Physics and Center for Interdisciplinary Nanostructure Science and Technology (CINSA-T), University of Kassel, D-34132 Kassel, Germany*

† Electronic supplementary information (ESI) available. See DOI: 10.1039/c9sm02261a

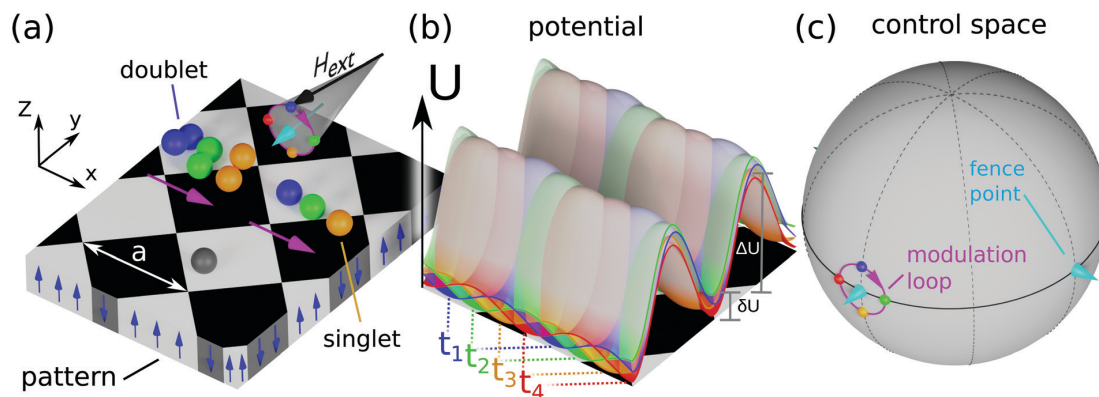


Fig. 1 Schematic of the setup. (a) Single and double spherical colloidal particles are placed on top of a lithographic magnetic square pattern (lattice constant $a \approx 7 \mu\text{m}$) of up (white) and down (black) magnetized domains along the z -axis. An isolated single colloid (gray) does not move at the modulation frequency applied in the experiments. Doublets are able to respond to the external field and can also induce motion of single colloids. The color (blue, green, and orange) of the doublet and of the singlet represents the position at three different times (t_1, t_2 , and t_3) during the modulation loop. (b) Magnetic potential U created by the pattern and the external potential for four different times ($t_i, i = 1, 2, 3, 4$) during one modulation loop (red, blue, green, and orange) of the external field. The ratio between the large and the small barriers of the potential is $\Delta U/\delta U \approx 10$. (c) Each point in control space \mathcal{C} (gray sphere) corresponds to a different orientation of the external field. The experimental modulation loop is highlighted in purple. The loop winds around a fence point (cyan) of control space. The colors of the four potentials in (b) and the coloring of the moving colloidal positions (a) correspond to the four colored points on the loop in control space.

particles (diameter $2.8 \mu\text{m}$) are immersed in water. A uniform time-dependent external magnetic field \mathbf{H}_{ext} of constant magnitude ($H_{\text{ext}} = 4 \text{ kA m}^{-1}$) is superimposed to the non-uniform and time-independent magnetic field generated by the pattern \mathbf{H}_p ($H_p \approx 1 \text{ kA m}^{-1}$). The external field is strong enough such that some of the paramagnetic particles self-assemble into doublets due to induced dipolar interactions between the single colloidal particles. The doublets then align with the direction of the external field. Our control space \mathcal{C} is the surface of a sphere that represents all possible orientations of the external field. We vary the external field $\mathbf{H}_{\text{ext}}(t)$ with time t performing periodic closed modulation loops in \mathcal{C} .

Both \mathbf{H}_p and \mathbf{H}_{ext} create a potential $U \propto -\mathbf{H}_{\text{ext}} \cdot \mathbf{H}_p$. The potential is a periodic function of the position of the colloids in the magnetic lattice and it depends parametrically on the orientation of the external field in control space \mathcal{C} . At every time during the modulation loop, the colloids are attracted toward the minima of the potential. Full details about the computation of U and the motion of single colloids are given in ref. 8 and 9. Here, we briefly explain the points relevant to the present study. For a square lattice, there exist four special points (fence points) in \mathcal{C} . The four points represent four directions of \mathbf{H}_{ext} which are parallel and antiparallel to the lattice vectors of the square pattern. If the modulation loop of \mathbf{H}_{ext} in \mathcal{C} winds around one of the fence points, then the minima of the potential move one unit cell above the square pattern.^{8,9} The motion is topologically protected, with the set of winding numbers around the fence points defining the topological invariants.

If \mathbf{H}_{ext} points in the direction of a fence point, the magnetic potential U is effectively one-dimensional with valleys along the direction perpendicular to \mathbf{H}_{ext} . For example, let the lattice vectors of the magnetic pattern point along x and y , Fig. 1(a).

The magnetic potential U exhibits deep valleys along x , Fig. 1(b), when \mathbf{H}_{ext} points along $-y$, Fig. 1(c). If \mathbf{H}_{ext} slightly deviates from the direction of a fence point, see modulation loop in Fig. 1(c), then secondary minima of U appear along the direction of the valleys, Fig. 1(b). The variation of the potential along the valley δU is much smaller than in the transversal direction ΔU . In our experimental setup, we find $\Delta U/\delta U \approx 10$. Modulating the external field directions along a loop that encloses a fence point, Fig. 1(c), causes the minima of U to travel by one unit vector of the lattice upon completion of the loop. The frequency of the loop ω can be chosen such that single colloids cannot follow the potential minimum on their own but doublets move in direction of the traveling minima. If a doublet is on a collision course with a single colloid, then the doublet can render the single colloid mobile and drive it through the potential valley, Fig. 1(a).

3 Results

In Fig. 2 we plot the speed of an isolated single colloid and that of an isolated doublet *versus* the driving angular frequency ω of the modulation loop in \mathcal{C} . At low frequencies, lower than the topological critical frequency ω_t , the motion is adiabatic and topologically protected. Singlets and doublets follow the potential minimum at all times. Hence, the displacement caused by a loop is topologically locked to the primitive lattice vector and particles move at the topological speed given by the lattice constant a times the frequency, *i.e.*, $v_t = \omega a/2\pi$. However, at higher frequencies $\omega > \omega_t$ the speed drops below v_t , mostly due to viscous and adhesive forces impeding the motion. For singlets, the speed decreases with increasing frequency until the critical frequency ω_c is reached. At ω_c the isolated single

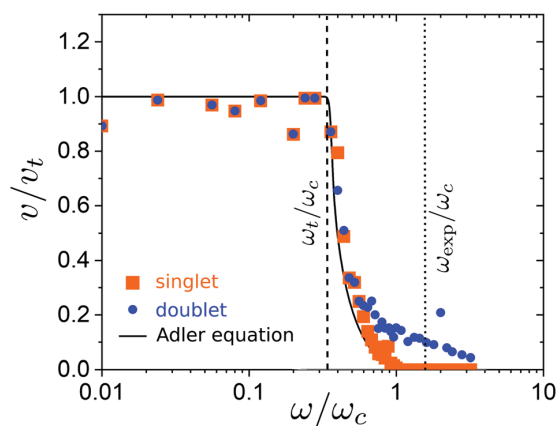


Fig. 2 Scaled magnitude of the velocity of singlets (orange squares) and doublets (blue circles) as a function of the scaled driving frequency. The black solid line is a fit of the singlet velocity using the generalized Adler eqn (1). The vertical lines indicate the scaled experimental frequency ω_{exp} and the topological frequency ω_t below which the motion is topologically protected.

colloids stop moving. The speed of the singlets is well described by a generalized Adler equation¹²

$$v/v_t = \begin{cases} 1 & \text{if } \omega \leq \omega_t \\ 1 - \sqrt{\frac{(\omega - \omega_t)((\omega_c - \omega)\omega_t + \omega\omega_c)}{(\omega_c - \omega_t)\omega^2}} & \text{if } \omega_t < \omega < \omega_c \\ 0 & \text{if } \omega \geq \omega_c \end{cases} \quad (1)$$

The force due to the potential acting on a doublet is roughly twice the force acting on a single colloidal particle. The viscous friction on the doublet, however, is less than twice the friction of a single colloid because of hydrodynamic interactions.¹³ Hence, the doublet can still move at frequencies higher than the critical frequency of the singlets, and we have a regime

where the doublet moves while the singlet is at rest. The experiments are performed at an angular frequency of $\omega \approx 52 \text{ s}^{-1} > \omega_c$, such that singlets do not move, and doublets move with a speed of roughly one eighth of the topological speed ($v_d/v_t \approx 0.125$), see Fig. 2.

In Fig. 3 we show a time sequence of microscope images showing the dynamics of the colloids. We distinguish single colloids (red) that are immobile from colloidal trains (green, cyan and yellow) consisting of one, two, and three doublets at the tail, and of one up to five single colloids at the front of the trains. The singlets and doublets in a train are well separated from each other by a primitive unit vector of the lattice. All trains move into the positive x -direction with the doublets pushing the singlets. Nothing particular happens to the cyan train with one doublet and one singlet moving through the field of view at the doublet speed v_d . The green train with one doublet and three singlets moves with half the doublet speed, Fig. 3(a) and (b), collects two further singlets, Fig. 3(c), and stalls, Fig. 3(d), until the two singlets close to the pushing doublets form a second doublet, Fig. 3(e). This increases the power of the train such that it resumes to move, Fig. 3(e) and (f) at the doublet speed. In Fig. 3(g) a third doublet is formed leaving only one singlet in the green train before it exits the field of view. Interestingly, when the green train passes the red singlets (sitting on the next track to the right) the front immobile red single colloid is mobilized and performs a single translation by one unit vector in the positive x -direction, compare the position of the red colloids next to the green train in Fig. 3(e) and (f). The yellow train originally consists of one doublet and two singlets, Fig. 3(a). It collects two further singlets, Fig. 3(b) and (c), and then moves as one doublet and four singlets train at a relatively slow speed $v \approx 0.15v_d$ through the image. No further doublets are formed from the singlets of the yellow train as it moves. In Fig. 4 we plot the speed of a train as a function of both the number of singlets in front of the train and the number of doublets at its tail. A train with no doublet is immobile and a train with more than one doublet can push up

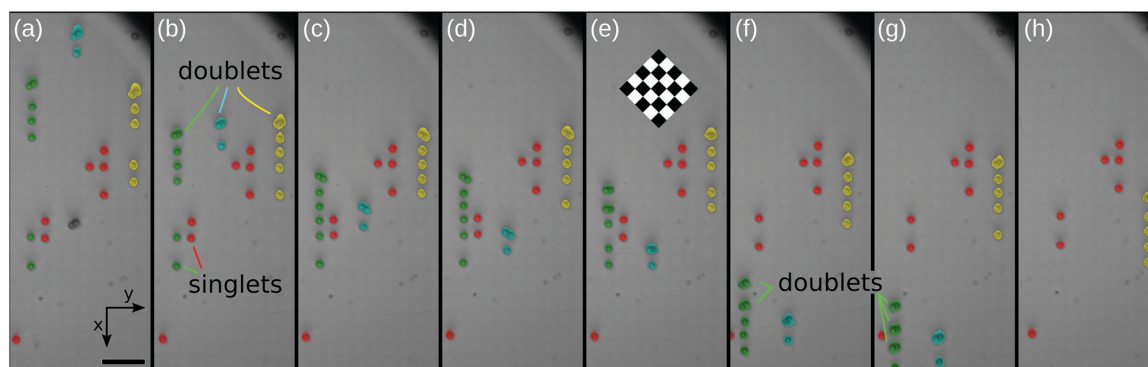


Fig. 3 Time sequence of microscope images of the pattern illustrating the motion of colloidal trains. Each train has been artificially colored differently. The images correspond to the times (a) $t = 0 \text{ s}$, (b) $t = 8 \text{ s}$, (c) $t = 13 \text{ s}$ (d) $t = 15 \text{ s}$ (e) $t = 17 \text{ s}$ (f) $t = 23 \text{ s}$ (g) $t = 25 \text{ s}$ and (h) $t = 30 \text{ s}$. The period of one modulation loop is $2\pi/\omega_{\text{exp}} \approx 0.12 \text{ s}$. Scale bar is $20 \mu\text{m}$. A sketch of the pattern has been superimposed in (e). A video clip recorded at twenty frames per second showing the motion of trains and the non motion of singlets is provided in the ESI† (adfig3a.mp4). A second video clip (adfig3b.mp4) recorded at sixty frames per second shows a time-resolved slow motion of the doublet during the course of a few modulation loops.

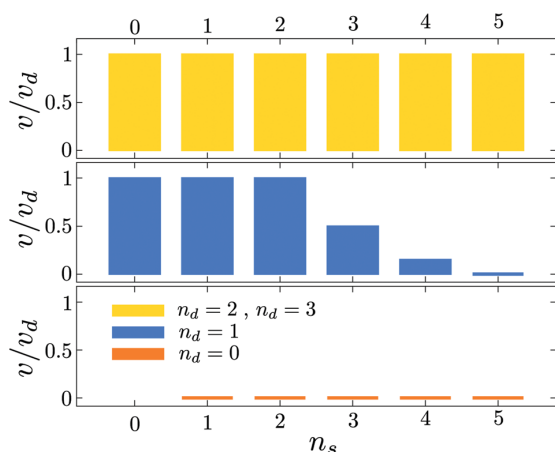


Fig. 4 Speed of the train (scaled with the speed of a doublet v_d) versus the load, i.e. the number of singlets in the train n_s . Data for different numbers of doublets in front of the train: $n_d = 0$ (orange), $n_d = 1$ (blue), $n_d = 2$ and 3 (yellow).

to five single colloids at the unloaded doublet speed. For one doublet we see a gradual transition from motion at the doublet speed v_d for trains with up to two singlets toward no motion for trains with five singlets.

Remarkably, none of the trains ever derails. This is due to the special properties of the confining colloidal potential which are inherited from the square pattern. In Fig. 5 we show the colloidal motion on a glass slide with no magnetic confining pattern. Doublets also move when performing a modulation loop without the magnetic pattern (albeit not by a unit vector) and singlets are generically at rest. However due to the absence of the confining potential, when one doublet moves onto a singlet, the singlet does not stay on track but is pushed to the side to let the doublet pass.

So far we have shown the coordinated motion of colloids in one direction. However, by changing the global orientation of the driving loop (winding around other fence points in \mathcal{C}) we can force the doublet to move along any of the four symmetry directions of the magnetic pattern. Hence, the doublet-induced motion of single colloids can potentially be used to arbitrarily

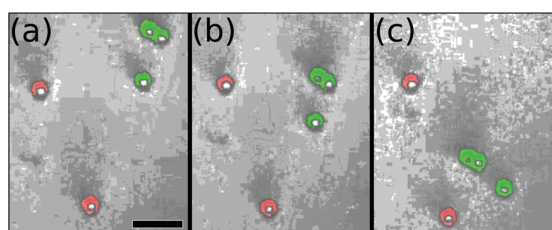


Fig. 5 Time sequence of microscope images showing a doublet (green) moving a singlet (green) out of its way. The other single colloids (red) remain at rest. Scale bar is $10\ \mu\text{m}$. The images correspond to the times (a) $t = 0\ \text{s}$, (b) $t = 2\ \text{s}$, and (c) $t = 4\ \text{s}$. A video clip of the event recorded at twenty frames per second is provided in the ESI† (adfig5.mp4).

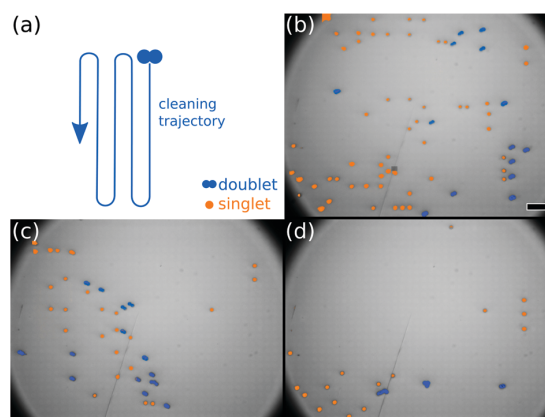


Fig. 6 Surface cleaning. (a) Schematic of the trajectory of a doublet. Sequence of microscope images showing the cleaning of an area from single colloids (orange) by meandering doublets (blue) taken at times $t = 0$ (b), $t = 2\ \text{min}$ (c), and $t = 6\ \text{min}$ (d). The scale bar is $20\ \mu\text{m}$. A video clip of the event is provided in the ESI† (adfig6.mp4).

set the position of the singlets across the pattern. A step in this direction is shown in Fig. 6 where a complex modulation loop is programmed to clean the surface of singlets.

4 Discussion

Our colloidal trains are immersed into a low Reynolds number liquid where the propulsion of shape changing objects is governed by the area enclosed by the loop in shape space of the object.^{14,15} Swimmers are able to move by changing their shape. In contrast, our biomimetic colloidal trains are driven by the shape of the potential created by the pattern and the external field which creates the topological nature of this classical non-adiabatic phenomenon. We have shown in ref. 8, 9, 16–20 that, like other classical topological transport phenomena,^{21–27} there exist similarities with quantum mechanical topological transport.^{28,29}

5 Conclusion

We described the magnetic coupling between well separated colloids that self assemble a colloidal train consisting of magnetically driven colloidal doublets acting as the locomotive of the train and colloidal singlets acting as less powerful carriages. A magnetic pattern below the colloidal train provides two perpendicular sets of periodic railway tracks that can be accessed alternatively and that guide the trains. We showed how we can manipulate the colloidal singlets on those tracks *via* the doublets using magnetic modulation loops that wind around specific directions with a supercritical frequency. We achieve superior coordinated control over a large ensemble of single colloidal particles. Our work adds a new avenue toward the transport of colloidal particles with potential applications on lab on the chip devices and on drug delivery on colloidal carriers.

We demonstrated how long range many-body interactions between the well separated colloidal particles can help sustain

the topological nature of the transport up to higher frequencies of driving. Such speeding up comes in handy for lab-on-the-chip applications such as transporting loads from one place of a chip to another. Whether the doublet-induced motion of the singlets is caused by direct superadiabatic non-equilibrium interparticle interactions³⁰ or mediated by hydrodynamic interactions constitutes the subject of future studies.

Author contributions

MMK, AdE, DdlH, & TMF designed and performed the experiment, and wrote the manuscript with input from all the other authors. MU & FS produced the magnetic film. AT, RH, IK, JG, ArE, DH, & MR performed the fabrication of the micromagnetic domain patterns within the magnetic thin film.

Conflicts of interest

There are no conflicts to declare.

References

- R. Dreyfus, J. Baudry, M. L. Roper, M. Fermigier, H. A. Stone and J. Bibette, Microscopic artificial swimmers, *Nature*, 2005, **437**, 862.
- A. Snezhko, M. Belkin, I. S. Aranson and W. K. Kwok, Self-Assembled Magnetic Surface Swimmers, *Phys. Rev. Lett.*, 2009, **102**, 118103.
- K. J. Solis and J. E. Martin, Chevrons, filaments, spinning clusters and phase coexistence: emergent dynamics of 2- and 3-d particle suspensions driven by multiaxial magnetic fields, *Soft Matter*, 2017, **13**, 5676.
- C. Bechinger, R. Di Leonardo, H. Löwen, C. Reichhardt, G. Volpe and G. Volpe, Active particles in complex and crowded environments, *Rev. Mod. Phys.*, 2016, **88**, 045006.
- F. E. Fish, Kinematics of ducklings swimming in formation - consequences of position, *J. Exp. Zool.*, 1995, **273**, 1.
- A. Snezhko and I. S. Aranson, Magnetic manipulation of self-assembled colloidal asters, *Nat. Matter.*, 2011, **10**, 698.
- N. Casic, N. Quintero, R. Alvarez-Nodarse, F. G. Mertens, L. Jibuti, W. Zimmermann and T. M. Fischer, Propulsion efficiency of a dynamic self-assembled helical ribbon, *Phys. Rev. Lett.*, 2013, **110**, 168302.
- D. de las Heras, J. Loehr, M. Lönne and T. M. Fischer, Topologically protected colloidal transport above a square magnetic lattice, *New J. Phys.*, 2016, **18**, 105009.
- J. Loehr, D. de las Heras, M. Lönne, J. Bugase, A. Jarosz, M. Urbaniak, F. Stobiecki, A. Tomita, R. Huhnstock, I. Koch, A. Ehresmann, D. Holzinger and T. M. Fischer, Lattice symmetries and the topologically protected transport of colloidal particles, *Soft Matter*, 2017, **13**, 5044.
- C. Chappert, H. Bernas, J. Ferré, V. Kottler, J.-P. Jamet, Y. Chen, E. Cambril, T. De-Volder, F. Rousseaux, V. Mathet and H. Launois, Planar patterned magnetic media obtained by ion irradiation, *Science*, 1998, **280**, 1919.
- P. Kuświk, A. Ehresmann, M. Tekielak, B. Szymański, I. Sveklo, P. Mazalski, D. Engel, J. Kisielewski, D. Lengemann, M. Urbaniak, C. Schmidt, A. Maziewski and F. Stobiecki, Colloidal domain lithography for regularly arranged artificial magnetic out-of-plane monodomains in Au/Co/Au layers, *Nanotechnology*, 2011, **22**, 095302.
- R. Adler, A study of locking phenomena in oscillators, *Proc. IRE*, 1946, **34**, 351.
- The drag force on a train of N spheres of radius r scales as $Nr/\ln(N)$. See e.g. J. Happel and H. Brenner, Low Reynolds number hydrodynamics, Martinus Nijhoff Publishers, 1983, p. 156.
- A. Shapere and F. Wilczek, Geometry of self-propulsion at low Reynolds number, *J. Fluid Mech.*, 1989, **198**, 557.
- A. Shapere and F. Wilczek, Efficiency of self-propulsion at low Reynolds number, *J. Fluid Mech.*, 1989, **198**, 587.
- J. Loehr, M. Lönne, A. Ernst, D. de las Heras and T. M. Fischer, Topological protection of multiparticle dissipative transport, *Nat. Commun.*, 2016, **7**, 11745.
- A. M. E. B. Rossi, J. Bugase and Th. M. Fischer, Macroscopic Floquet topological crystalline steel and superconductor pump, *Europhys. Lett.*, 2017, **119**, 40001.
- A. M. E. B. Rossi, J. Bugase, T. Lachner, A. Ernst, D. de las Heras and T. M. Fischer, Hard topological versus soft geometrical magnetic particle transport, *Soft Matter*, 2019, **15**, 8543.
- H. Massana-Cid, A. Ernst, D. de las Heras, A. Jarosz, M. Urbaniak, F. Stobiecki, A. Tomita, R. Huhnstock, I. Koch, A. Ehresmann, D. Holzinger and T. M. Fischer, Edge transport at the boundary between topologically equivalent lattices, *Soft Matter*, 2019, **15**, 1539.
- J. Loehr, D. de las Heras, A. Jarosz, M. Urbaniak, F. Stobiecki, A. Tomita, R. Huhnstock, I. Koch, A. Ehresmann, D. Holzinger and T. M. Fischer, Colloidal topological insulators, *Commun. Phys.*, 2018, **1**, 4.
- M. C. Rechtsman, J. M. Zeuner, Y. Plotnik, Y. Lumer, D. Podolsky, F. Dreisow, S. Nolte, M. Segev and A. Szameit, Photonic Floquet topological insulators, *Nature*, 2013, **496**, 196–200.
- M. Xiao, G. Ma, Z. Yang, P. Sheng, Z. Q. Zhang and C. T. Chan, Geometric phase and band inversion in periodic acoustic systems, *Nat. Phys.*, 2015, **11**, 240.
- A. Murugan and S. Vaikuntanathan, Topologically protected modes in non-equilibrium stochastic systems, *Nat. Commun.*, 2017, **8**, 13881.
- C. L. Kane and T. C. Lubensky, Topological boundary modes in isostatic lattices, *Nat. Phys.*, 2014, **10**, 39.
- J. Paulose, B. G. Chen and V. Vitelli, Topological modes bound to dislocations in mechanical metamaterials, *Nat. Phys.*, 2015, **11**, 153.
- L. M. Nash, D. Kleckner, A. Read, V. Vitelli, A. M. Turner and W. T. M. Irvine, Topological mechanics of gyroscopic metamaterials, *Proc. Natl. Acad. Sci. U. S. A.*, 2015, **112**, 14495.
- S. D. Huber, Topological mechanics, *Nat. Phys.*, 2016, **12**, 621.
- M. Z. Hasan and C. L. Kane, Colloquium: Topological insulators, *Rev. Mod. Phys.*, 2010, **82**, 3045.
- S.-Q. Shen, *Topological insulators: Dirac equation in condensed matters*, Springer Science, and Business Media, 2013.
- M. Schmidt and J. M. Brader, Power functional theory for Brownian dynamics, *J. Chem. Phys.*, 2013, **138**, 214101.

Part III

Summary

Chapter 3

Summary and Outlook

3.1 Summary

This cumulative thesis studies the adiabatic and non-adiabatic transport of colloidal bipeds that walk on top of periodic magnetic patterns. The magnetic patterns are made from magnetic exchange bias films with domains magnetized normal (up and down) to the film plane. Colloidal bipeds are self assembled because of dipolar interactions between single paramagnetic colloidal particles in an external magnetic field. If we perform adiabatic loops of the external field in the control space that is a sphere of all possible external field directions. The long axes of the bipeds are enslaved to the direction of the external field. Therefore the adiabatic control loop in control space is transcribed into a similar loop in the transcription space that is the sphere of the radius of the biped describing the possible biped orientations. Transcription spaces of bipeds of different length are concentric shells packed into the polyglot transcription space that describes the possible orientations of bipeds of arbitrary length. The polyglot transcription space of a square pattern contains periodically spaced fence lines in the equatorial plane for which we can define winding numbers (that are topological invariants) of a loop in a transcription shell of a particular biped lengths. These integer winding numbers depend on the biped length and bipeds of different length are transported by the same loop by a displacement that corresponds to the winding numbers multiplied by the primitive unit vectors. This allows to sort bipeds of different lengths into topological transport classes. We can define transport directions a priori and compute the modulation loop that commands the desired transport to the collections of bipeds of different length. The topological nature of the transport is robust enough to allow the error free simultaneous transport of up to six different biped lengths. For a collection of eleven different biped lengths we could still separate all eleven lengths with the transport albeit no longer error free.

A gauge theory for shape changing swimmers in a low Reynolds number fluid was adapted to our colloidal bipeds. We analyzed the motion of bipeds on a square lattice with non-symmorphic symmetry and on a hexagonal lattice lacking a non-symmorphic symmetry using two gauges. Using the walker gauge that takes the instantaneous center of rotation as an absolute reference point we could decompose the motion into an active component and a passive component. Passive sliding of a foot occurs because the potential minimum of the grounded foot moves as we change the external field. This sliding is always less

than a primitive unit vector. The rest of the motion is an active walking occurring due to a transfer of foothold from one foot to the other. In a hexagonal pattern that lacks a non-symmorphic symmetry fence surfaces come in two different types that are separated by bifurcation lines. A walker starts to limp if the transcribed modulation loop passes through fences of different type. The limping exemplifies by irreversible ratchet jumps that occur on an intrinsic time scale. When the transcribed modulation loop passes through fences of the same type the walking remains adiabatic. For a non-adiabatic modulation there is a competition between magnetic interactions favoring the instantaneous center of rotation to reside in a foot and hydrodynamic interactions favoring the instantaneous center of rotation to reside in the geometric center of the biped. The non-adiabatic motion of the walkers remains topological but only parts of the winding numbers of the transcribed loop are converted into primitive unit vector displacements. Ultimately at very high modulation frequencies the biped stops moving.

Single colloids show only passive motion. There is no active motion of single colloids. The passive motion is especially vulnerable when the modulation is non-adiabatic. Single colloids stall way before the bipeds stop to move. We can reanimate the motion of single colloids by colloidal doublets (bipeds consisting of two single colloids). The more doublets we use the larger the number of single colloids being able to be carried along by the doublets in a train of single colloids being pushed by the doublets. Doublets can force the polymerization addition reaction of two single colloids into one doublet if the single colloids are unwilling of getting pushed along. This way they create a train with more pushing doublets that can again move. The colloidal trains might be useful for carrying along cargo in lab on the chip devices.

My thesis solely dealt with the motion of colloidal bipeds. Dipolar interactions can assemble much more complicated shapes if instead of using only paramagnetic particles one would use a mixture of paramagnetic and diamagnetic particles. Under such circumstances I expect the variety of topological transport phenomena of colloidal assemblies to further increase. It is well possible that very useful phenomena are still waiting to be discovered in this field. My colloidal system in contrast to common electronical systems is dissipative. Recent work on graphene [71, 72] shows that when the electron electron scattering length is short, that electronic systems behave like viscous fluids that can be described by the Navier-Stokes equation. For those systems the analogy to my dissipative colloidal system might be closer as originally expected.

Part IV

References

-
- [1] D. Jongenee, R. Withagen, R. Withagen, F. T. J. M. Zaal; Do children create standardized playgrounds? A study on the gap-crossing affordances of jumping stones *J. Env. Psychology*, **44**, 45-52, (2016)
- [2] Thouless, D. J. Quantization of particle transport *Phys. Rev. B* **27**, 6083-6087 (1983).
- [3] M. Z. Hasan, and C. L. Kane; Colloquium: Topological insulators. *Rev. Mod. Phys.* **82**, 3045-3067 (2010).
- [4] S-Q. Shen; Topological insulators: Dirac equation in condensed matters, *Springer Science, and Business Media* (2013).
- [5] M. J. Rice, and E. J. Mele; Elementary Excitations of a Linearly Conjugated Diatomic Polymer *Phys. Rev. Lett.* **49**, 1455-1459 (1982).
- [6] M. C. Rechtsman, J. M. Zeuner, Y. Plotnik, Y. Lumer, D. Podolsky, F. Dreisow, S. Nolte, M. Segev, and A. Szameit; Photonic Floquet topological insulators *Nature* **496**, 196-200 (2013).
- [7] M. S. Rudner, N. H. Lindner, E. Berg, and M. Levin; Anomalous Edge States and the Bulk-Edge Correspondence for Periodically Driven Two-Dimensional Systems *Phys. Rev. X* **3**, 031005 (2013).
- [8] C. L. Kane, and T. C. Lubensky; Topological boundary modes in isostatic lattices. *Nat. Phys.* **10**, 39-45 (2014).
- [9] J. Paulose, B. G. Chen, and V. Vitelli; Topological modes bound to dislocations in mechanical metamaterials. *Nature Physics* **11**, 153-156 (2015).
- [10] L. M. Nash, D. Kleckner, A. Read, V. Vitelli, Ari M. Turner, and W. T. M. Irvine; Topological mechanics of gyroscopic metamaterials *Proc. Nat. Acad. Sci.* **112**, 14495-14500 (2015).
- [11] M. Xiao, G. Ma, Z. Yang, P. Sheng, Z.Q. Zhang, and C.T. Chan; Geometric phase and band inversion in periodic acoustic systems *Nature Phys.* **11**, 240-244 (2015)
- [12] S. D. Huber; Topological mechanics *Nature Physics* **12**, 621-623 (2016).
- [13] A. Murugan and S. Vaikuntanathan; Topologically protected modes in non-equilibrium stochastic systems *Nat. Comm.* **8**, 13881 (2017).

References

- [14] A. M. E. B. Rossi, J. Bugase, and Th. M. Fischer Macroscopic Floquet topological crystalline steel and superconductor pump *Eur. Phys. Lett.* **119**, 40001 (2017).
- [15] A. M. E. B. Rossi, J. Bugase, T. Lachner, A. Ernst, D. de las Heras, and Th. M. Fischer, Hard topological versus soft geometrical magnetic particle transport, *Soft Matter* **15**, 8543 (2019).
- [16] D. Harland, and N. S. Manton; Rolling Skyrmions and the nuclear spin-orbit force *Nuclear Physics B* **935**, 210-241 (2018)
- [17] J. Loehr, M. Lönne, A. Ernst, D. de las Heras, and Th. M. Fischer, Topological protection of multiparticle dissipative transport. *Nat. Comm.* (2016), **7**, 11745.
- [18] D. de las Heras, J. Loehr, M. Lönne, and Th. M. & Fischer, Topologically protected colloidal transport above a square magnetic lattice. *New J. Phys.* (2016), **18**, 105009.
- [19] J. Loehr, D. de las Heras, M. Lönne, J. Bugase, A. Jarosz, M. Urbaniak, F. Stobiecki, A. Tomita, R. Huhnstock, I. Koch, A. Ehresmann, D. Holzinger, and Th. M. Fischer, Lattice symmetries and the topologically protected transport of colloidal particles. *Soft Matter* (2017), **13**, 5044-5075.
- [20] A. Shapere, and F. Wilczek; Geometry of self-propulsion at low Reynolds number. *Journal of Fluid Mechanics*, **198**, 557-585. (1989)
- [21] A. Shapere, and F. Wilczek; Efficiency of self-propulsion at low Reynolds number. *Journal of Fluid Mechanics*, **198**, 587-599. (1989)
- [22] R. Dreyfus, J. Baudry, M. L. Roper, M. Fermigier, H. A. Stone, and J. Bibette, Microscopic artificial swimmers, *Nature* **437**, 862 (2005).
- [23] A. Snezhko, M. Belkin, I. S. Aranson, and W. K. Kwok, Self-Assembled Magnetic Surface Swimmers, *Phys. Rev. Lett.* **102**, 118103 (2009).
- [24] A. Snezhko, I. S. Aranson, Magnetic manipulation of self-assembled colloidal asters, *Nat. Matter.* **10**, 698 (2011).
- [25] C. Bechinger, R. Di Leonardo, H. Löwen, C. Reichhardt, G. Volpe, and G. Volpe, Active particles in complex and crowded environments, *Rev. Mod. Phys.* **88**, 045006 (2016).
- [26] F. E. Fish, Kinematics of ducklings swimming in formation - consequences of position, *J. Exp Zoology* **273**, 1 (1995).

-
- [27] S. Melle and J. E. Martin, Chain model of a magnetorheological suspension in a rotating field *J. Chem. Phys.* **118**, 9875-9881 (2003).
- [28] N. Casic, N. Quintero, R. Alvarez-Nodarse, F. G. Mertens, L. Jibuti, W. Zimmermann, and T. M. Fischer, Propulsion efficiency of a dynamic self-assembled helical ribbon, *Phys. Rev. Lett.* **110**, 168302 (2013).
- [29] K. J. Solis and J. E. Martin, Chevrons, filaments, spinning clusters and phase coexistence: emergent dynamics of 2- and 3-d particle suspensions driven by multiaxial magnetic fields, *Soft Matter* **13**, 5676 (2017).
- [30] A. Yildiz, M. Tomishige, R. D. Vale, and P. R. Selvin; Kinesin walks hand-over-hand *Science* **303** 676-678. (2004)
- [31] C. L. Asbury; Kinesin: world's tiniest biped *Current Opinion in Cell Biology* **17** 89-97 (2005)
- [32] M. L. Shik, and G. N. Orlovsky; Neurophysiology of locomotor automatism *Physiological Reviews* **56**, 465-501 (1976)
- [33] D. Hamacher, F. Herold, P. Wiegel, D. Hamacher, and L. Schega; Brain activity during walking: A systematic review *Neuroscience and Biobehavioral Reviews* **57** 310-327 (2015)
- [34] P. Holmes, R. J. Full, D. Koditschek, and J. Guckenheimer The Dynamics of Legged Locomotion: Models, Analyses, and Challenges *SIAM Rev.*, **48**, 207-304. (2006)
- [35] W. B. Sherman and N. C. Seeman; A Precisely Controlled DNA Biped Walking Device *Nano Letters* **4**, 1203-1207. (2004)
- [36] Q. Nguyen, H. Ayonga, G. W. Jessy, A. D. Aaron and S. Koushil; 3D Dynamic Walking on Stepping Stones with Control Barrier Functions 2016 IEEE **55TH** CONFERENCE ON DECISION AND CONTROL (CDC) Book Group Author(s):IEEE *Book Series: IEEE Conference on Decision and Control*, 827-834 (2016).
- [37] A. Gottlieb, and G. S. Almasi,. Highly parallel computing. *Redwood City, Calif.: Benjamin/Cummings*. ISBN 978-0-8053-0177-9 (1989).
- [38] D. Chruscinski, and A. Jamiolkowski, Geometric Phases in Classical and Quantum Mechanics *Birkhäuser, Boston, MA, Part of the Progress in Mathematical Physics book series (PMP, volume 36)* ISBN 978-0-8176-8176-0 (2004)
- [39] V. Guillemin, Differential topology *Englewood Cliffs, NJ , Prentice-Hall* (1974)

References

- [40] McDonald, M. P. Spalding G. C. and Dholakia K.; Microfluidic sorting in an optical lattice; *Nature* **426**, 421 (2003).
- [41] Reimann P.; Brownian motors: noisy transport far from equilibrium *Phys. Rep.* **361**, 57-265 (2002).
- [42] Skaug, M. J., Schwemmer, C., Fringes, S., Rawlings, C. D., Knoll, A. W.; Nanofluidic rocking Brownian motors *Science* **359**, 1505-1508 (2018).
- [43] Gopinathan, A. and Grier D. G., Statistically Locked-In Transport through Periodic Potential Landscapes *Phys. Rev. Lett.* **92**, 130602 (2004).
- [44] P. Tierno, and Th. M. Fischer; Excluded volume causes integer and fractional plateaus in colloidal ratchet currents *Phys. Rev. Lett.* **112**, 048302 (2014)
- [45] B. I. Halperin Quantized Hall conductance, current-carrying edge states, and the existence of extended states in a two-dimensional disordered potential *Phys. Rev. B* **25**, 2185-2190 (1982).
- [46] J. Loehr, D. de las Heras, A. Jarosz, M. Urbaniak, F. Stobiecki, A. Tomita, R. Huhnstock, I. Koch, A. Ehresmann, D. Holzinger, and Th. M. Fischer, Colloidal topological insulators, *Comm. Phys.* **1**, 4 (2018).
- [47] H. Massana-Cid, A. Ernst, D. de las Heras, A. Jarosz, M. Urbaniak, F. Stobiecki, A. Tomita, R. Huhnstock, I. Koch, A. Ehresmann, D. Holzinger, and Th. M. Fischer, Edge transport at the boundary between topologically equivalent lattices, *Soft Matter* **15** 1539 (2019).
- [48] DiVincenzo, D. P. Quantum Computation. *Science* **270**, 255-261 (1995).
- [49] Shor, P. W. Polynomial-Time Algorithms for Prime Factorization and Discrete Logarithms on a Quantum Computer. *SIAM J. Comput.* **26**, 1484-1509 (1997).
- [50] Kitaev, A. Y. Fault-tolerant quantum computation by anyons. *Anna Phys (N Y)* **303**, 2-30 (2003).
- [51] Adleman, L. Molecular computation of solutions to combinatorial problems. *Science* **266**, 1021-1024 (1994).
- [52] Lipton, R. J. DNA solution of hard computational problems. *Science* **268**, 542-545 (1995).

-
- [53] Qian, L. & Winfree, E. Scaling Up Digital Circuit Computation with DNA Strand Displacement Cascades. *Science* **332**, 1196-1201 (2011).
- [54] Amir, Y., Ben-Ishay, E., Levner, D., Ittah, S., Abu-Horowitz, A. & Bachlet, I. Universal computing by DNA origami robots in a living animal. *Nature Nanotechnol.* **9**, 353-357 (2014).
- [55] Church G. M., Gao Y. & Kosuri, S. Next-Generation Digital Information Storage in DNA. *Science* **337**, 1628 (2012).
- [56] Rothemund P. W. K. Folding DNA to create nanoscale shapes and patterns. *Nature* **440**, 297-302 (2006).
- [57] Ilievski, F., Mazzeo, A. D., Shepherd, R. F., Chen, X. & Whitesides, G. M. Soft Robotics for Chemists. *Angew. Chem., Int. Ed.* **50**, 1890-1895 (2011).
- [58] Păun, G. Computing with Membranes. *J. Comput. Syst. Sci.* **61**, 108-143 (2000).
- [59] Adamatzky, A., Costello, B. D. L. & Asai, T. Reaction-Diffusion Computer. Elsevier, (2005).
- [60] Prakash, M. & Gershenfeld, N. Microfluidic Bubble Logic. *Science* **315**, 832-835 (2007).
- [61] Kou, S. et al. Fluorescent Molecular Logic Gates Using Microfluidic Devices. *Angew. Chem., Int. Ed.* **47**, 872-876 (2008).
- [62] Phillips, C. L. et al. Digital colloids: reconfigurable clusters as high information density elements. *Soft Matter* **10**, 7468-7479 (2014).
- [63] Cui, J. et al. Nanomagnetic encoding of shape-morphing micromachines. *Nature* **575**, 164-168 (2019).
- [64] <https://codegolf.stackexchange.com/questions/102370/add-a-language-to-a-polyglot>
- [65] M. Schmidt and J. M. Brader, Power functional theory for Brownian dynamics, *J. Chem. Phys.* **138**, 214101 (2013).
- [66] J. Happel and H. Brenner, Low Reynolds number hydrodynamics, Martinus Nijhoff Publishers, (1983).

References

- [67] Julian Bialké, Jonathan T. Siebert, Hartmut Löwen, and Thomas Speck Negative Interfacial Tension in Phase-Separated Active Brownian Particles *Phys. Rev. Lett.* **115**, 098301 (2015).
- [68] C. Chappert, H. Bernas, J. Ferré, V. Kottler, J.-P. Jamet, Y. Chen, E. Cambril, T. De-Volder, F. Rousseaux, V. Mathet, and H. Launois, Planar patterned magnetic media obtained by ion irradiation. *Science* (1998), **280**, 1919-1922.
- [69] P. Kuświk, A. Ehresmann, M. Tekielak, B. Szymański, I. Sveklo, P. Mazalski, D. Engel, J. Kisielewski, D. Lengemann, M. Urbaniak, C. Schmidt, A. Maziewski, and F. Stobiecki; Colloidal domain lithography for regularly arranged artificial magnetic out-of-plane monodomains in Au/Co/Au layers *Nanotechnology* **22**, 095302 (2011)
- [70] R. Adler, A study of locking phenomena in oscillators, Proceedings of the I.R.E. and Waves and Electrons, **34**, 351 (1946).
- [71] A. Principi, G. Vignale, M. Carrega, and M. Polini; Bulk and shear viscosities of the two-dimensional electron liquid in a doped graphene sheet *Phys. Rev. B*, **93**, 125410 (2016)
- [72] A. I. Berdyugin, S. G. Xu, F. M. D. Pellegrino, R. Krishna Kumar, A. Principi, I. Torre, M. Ben Shalom, T. Taniguchi, K. Watanabe, I. V. Grigorieva, M. Polini, A. K. Geim, and D. A. Bandurin; Measuring Hall viscosity of graphene's electron fluid, *Science*, **364**, 162–165, (2019).

Eidesstattliche Versicherung

Hiermit versichere ich an Eides statt, dass ich die vorliegende Arbeit selbstständig verfasst und keine anderen als die von mir angegebenen Quellen und Hilfsmittel verwendet habe.

Zusätzlich erkläre ich hiermit, dass ich keinerlei frühere Promotionsversuche unternommen habe.

Weiterhin erkläre ich, dass ich die Hilfe von gewerblichen Promotionsberatern bzw. -vermittlern oder ähnlichen Dienstleistern weder bisher in Anspruch genommen habe, noch künftig in Anspruch nehmen werde.

Mahla Mirzaee Kakhki

Bayreuth, 3. September 2021